Mechanism of Vein Pattern Formation in *Arabidopsis thaliana* Leaves: Testing the Canalization Hypothesis

by

Mira Amin

Thesis submitted to the
Faculty of Graduate and Postdoctoral Studies
In partial fulfillment of the requirements
For the M.Sc. degree in
Biology

Department of Biology
Faculty of Science
University of Ottawa

Abstract

Several mechanisms have been proposed to explain the process of vein pattern formation in plant tissues. The most widely accepted amongst biologists is the canalization hypothesis, derived from pea root and stem experiments. According to this hypothesis, a signal, thought to be the phytohormone auxin, is transported polarly from cell to cell from the shoot to the root and is canalized progressively into narrow channels of high auxin fluxes that later differentiate to become vascular tissue. In this project, we set out to test whether auxin canalization drives vein pattern formation, using *Arabidopsis thaliana* mutants with increased auxin transport (*max4-1*, *max3-9*, *max2-1* and *max1-1*). We predicted that the mutants would have distinct vein patterns and especially different angles between the primary and secondary veins, compared to the wild type. First rosette leaves of 15 plants per genotype were harvested for analysis each day from 7 to 17 days after sowing, giving a total of eight hundred twenty-five leaf samples to analyze. Venation patterns were extracted and analyzed using custom-made software written with Matlab. Overall, compared with the wild type, mutants with the highest auxin transport (*max4-1* and *max3-9*) had different vein patterns at early developmental stages, confirming a role for auxin transport in vein patterning. However, veins of mutants and wild type connected at similar angles, which is not consistent with the auxin canalization hypothesis, as originally formulated.

Résumé

Plusieurs mécanismes ont été proposés pour expliquer le processus de formation des nervures dans les tissus végétaux. Le plus grandement accepté parmi les biologistes est l'hypothèse de canalisation dérivée à partir des expériences sur les racines et tiges de pois. Selon cette hypothèse, un signal, pouvant être la phytohormone auxine, est transporté polairement de cellule à cellule de la pousse jusqu'à la racine et est canalisé progressivement dans des canaux étroits où le flux d'auxine est haut. Plus tard ces canaux se différencient en tissus vasculaires. Pour ce projet, nous avons décidé de tester si la canalisation conduit à la formation des nervures en utilisant des mutants d'*Arabidopsis thaliana* ayant un transport d'auxine accéléré (*max4-1*, *max3-9*, *max2-1* and *max1-1*). Nous avons prédit que les mutants auraient des motifs de veines distincts et des angles différents en particulier entre les nervures primaires et secondaires par rapport au type sauvage. La première feuille de rosette d'un total de 15 plantes par génotype par jour a été récolté de 7 à 17 jours aprés semis, donnant un total de huit cent vingt-cinq feuilles à analyser. Les réseaux de veines ont été extraits et analysés à l'aide de programmes informatique créés dans notre laboratoire avec Matlab. En général, par rapport au type sauvage, les mutants avec la plus grande capacité de transport d'auxine (*max4-1* et *max3-9*) avaient des motifs de veines différents aux premiers stades de développement, confirmant un rôle pour le transport de l'auxine dans la formation des nervures foliaires. Toutesfois, les veines secondaires des mutants et du type sauvage joignainent les veines primaires à des angles similaires, ce qui n'est pas ce que l'on attend si la canalisation d'auxine, telle que formulée initialement, opère dans les feuilles.

Acknowledgements

First and foremost, I would like to wholeheartedly thank my supervisor, Dr. Anne-Gaëlle Rolland-Lagan for her consistent guidance, encouragement and support during both my undergraduate and graduate research projects.

I wish to acknowledge my supervisory committee members, Dr. John T. Arnason (Professor of Biology) from the University of Ottawa and Dr. Shelley Hepworth (Associate Professor of Biology) from Carleton University for their valuable comments, suggestions and insightful discussions.

I owe gratitude to Dr. Howard Rundle and Dr. Xia Xia for their help and advice with the multivariate analysis. Sincere thanks are extended to Megan Tu and Elizabeth Edmunds for their assistance in measuring and digitizing the many samples.

I would like to salute all lab members, present and past, who made the lab a lively atmosphere to work in, especially my fellow master students Rebecca Assaf, Lauren Remmler and Valerie Tweedle. I also appreciate the friendship and encouragement offered by my colleagues in the Sargent, Bonen, Poulin, Charest, Arnason and Blais labs. It was a privilege as well to interact with other members of the Biology Graduate Student Association and the Department of Biology.

Last but not least, I would like to thank my parents who have been with me every step of the way by supporting and encouraging me in all my endeavors. I gratefully acknowledge funding from the University of Ottawa.

Contents

List of Tables

List of Figures

List of Acronyms

IAA	Indole-3-acetic acid
PAT	Polar Auxin Transport
AUX	Auxin resistant
PIN	PIN FORMED
PGP	Phosphogylcoprotein
SAM	Shoot Apical Meristem
NPA	1-*N*-naphthyl-phthalamic acid
MAX	More AXillary growth
CCD8	CAROTENOID CLEAVAGE DIOXYGENASE 8
CCD7	CAROTENOID CLEAVAGE DIOXYGENASE 7
AXR	Auxin resistant
AFB	Auxin signaling F-box
Col0	Columbia-0
NaOH	Sodium hydroxide
DAS	Days After Sowing

NAA	Naphthalene acetic acid
ANT	AINTEGUMENTA
ICK1	INHIBITOR OF CYCLIN DEPENDENT KINASE1
PID	Protein serine/threonine kinase PINOID
PP2A	Protein phosphatase 2A
GFP	Green fluorescent protein

Chapter 1

Introduction

1.1 Importance of studying the vascular system in plants

The scarcity of food world-wide became severe in the period after the Second World War. In reponse to this global problem the Green Revolution, a technological innovation, was developed at several international agriculture research centers transforming farming practice where the main crops grown were rice, wheat and maize. Described as the father of this broad agricultural movement, Norman Borlaug won the nobel prize for his agricultural techniques of breeding and obtaining high-yielding crop varieties that helped keep pace with population growth. Continuing research is still being done today including efforts to improve crop yield with two major targets, the root and vasculature system, in ways that are economically and environmentally sustainable. The basic research study in

this thesis focuses particularly on understanding the mechanism underlying vein pattern formation in the vegetative leaves of *Arabidopsis thaliana* (L.) Heynh. (Arabidopsis, hereafter), a process that is yet unknown, by conducting quantitative analyses. The contribution of our research along with both the available molecular experimental work and theoretical models of patterning, will hopefully lay the foundation for the applied science that follows.

1.2 Use of Arabidopsis as a model organism for studying vein pattern formation

In order to understand the fundamental principles of plant biology the model plant Arabidopsis, commonly known as mouse-ear cress, is used to study various subjects in plant physiology, molecular genetics and biochemistry. Experimentally, it is easy to grow, small in size and has a short generation time. It has a small genome size (125 megabase) that has been fully sequenced (The Arabidopsis Genome Initiative, (2000)) and is organized into five chromosomes. Arabidopsis is part of the mustard family and is closely related to economically important crops such as canola, cabbage and broccoli. Furthermore, an extensive collection of mutants with different phenotypes are available that are defective in almost every aspect of plant growth and development.

1.3 Anatomy of leaf and vascular system

A leaf consists of a blade (lamina) attached by a petiole (stalk) to the stem of the plant (Figure 1.1). The plant vasculature, a long-distance transport and mechanical support system, allows for efficient exchange of products of absorption and assimilation between the shoot and root. Mature vascular strands are made up of two vascular tissues, known as the phloem and the xylem (Figure 1.2), that are highly regulated and exhibit polarity linked to the adaxial-abaxial (upper-lower) polarity of the leaves (Ye (2002), Ye et al. (2002), Rolland-Lagan et al. (2009)). Products of photosynthesis are translocated along the phloem from mature leaves to areas of growth and storage including the roots while the xylem is the tissue that transports water and minerals from the root system to the aerial parts of the plant. Moreover, different regulatory molecules such as hormones, proteins and RNA use the vascular tissue to regulate growth, developmental and physiological processes (as reviewed by Crawford & Zambryski (1999)). Aside from complex tissues (phloem, xylem and the epidermis (top and bottom outer protective layer - see Figure 1.2)), there are also simple ground tissues. Parenchyma cells (mesophyll) are either tightly packed vertically elongated cells (palisade mesophyll region) or loosely packed rounded cells with some large intracellular spaces (spongy mesophyll) that surround the vein system (Evert (2006)).

The venation of a wild-type strain of Arabidopsis follows a hierarchy (Figure 1.1) reflecting the development of vein formation (Nelson & Dengler (1997); Dengler & Kang (2001); Scarpella & Meijer (2004)). The primary vein (also known as midvein) is formed

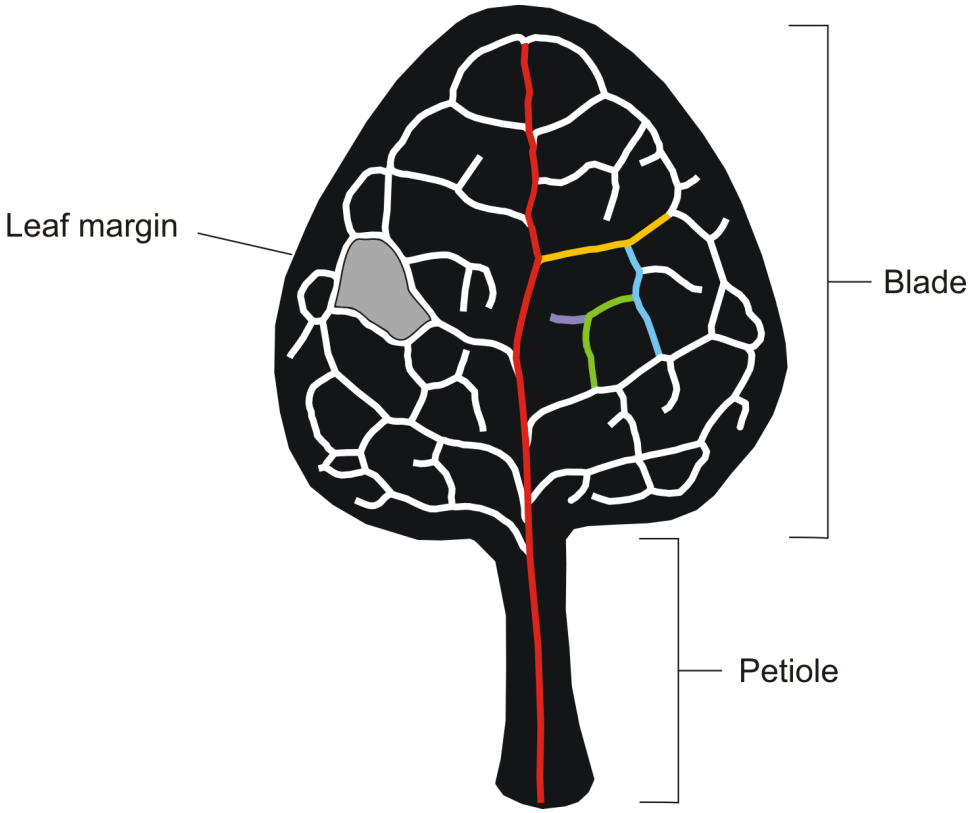

Figure 1.1: Leaf anatomy and hierarchy of leaf veins. The leaf is made of a blade and petiole that attaches the leaf to the plant stem. In dicots, leaf veins are continuous with the stem vasculature. First, the primary vein or midvein (red) is formed at the center of the leaf. Second-order veins (yellow) branch from the primary vein extending towards the margin of the leaf. This process continues, where the third-order veins (blue) form from the secondary veins, the fourth-order (green) veins form from the tertiary veins, until the leaf blade reaches maturity. Higher order veins are formed during the expansion of the leaf blade. These veins either cease in the lamina (free ending veinlets (purple)), or join other veins to form polygonal regions also known as loops or areoles (shaded gray area).

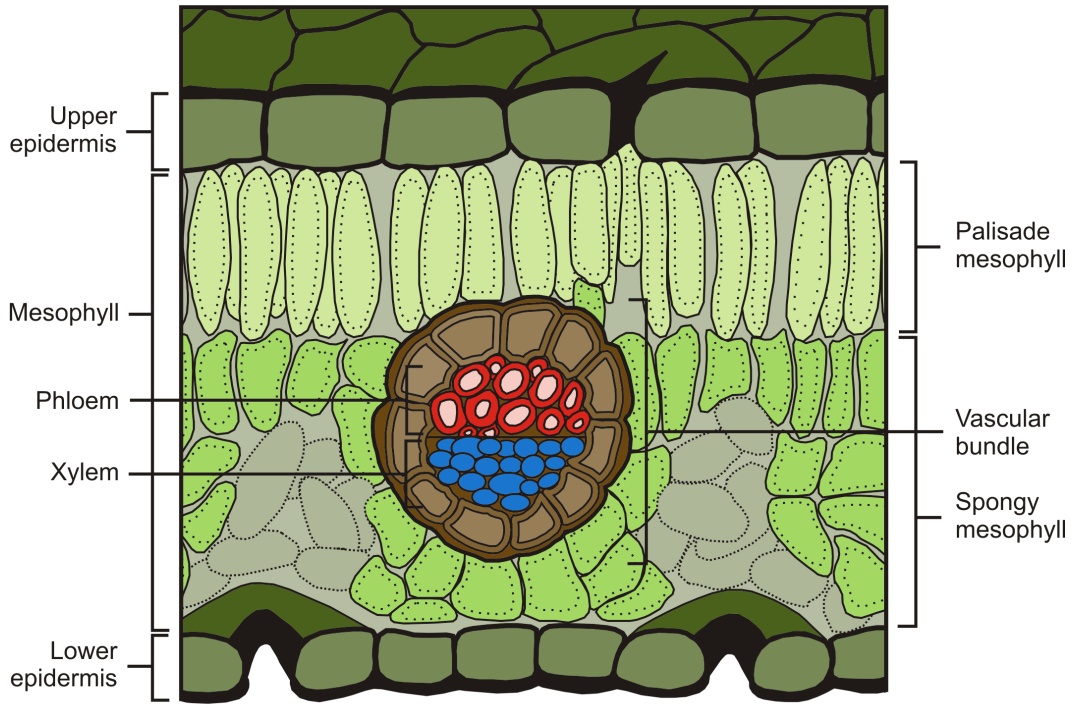

Figure 1.2: Leaf cross section illustrating the types of cells. The epidermis is a continuous layer of cells on the upper and lower surface of the leaf. The photosynthetic parenchyma cells (mesophyll) found between the two layers of the epidermis are composed of a palisade mesophyll (region of tightly packed vertically elongated cells) and a spongy mesophyll (region of loosely packed rounded cells with large intracellular spaces). In the spongy layer of the mesophyll lies the vascular bundle, a conducting tissue composed of the xylem and the phloem. *Image redrawn from BIODIDAC (http://biodidac.bio.uottawa.ca/).*

first acropetally (from base to the tip of the leaf). The midvein then bifurcates, forming the secondary veins. These veins, when connected, form a series of reticulations (polygonal regions) called loops or areoles (Nelson & Dengler (1997); Candela et al. (1999); Mattsson et al. (1999); Sieburth (1999); Dengler & Kang (2001); Kang & Dengler (2004); Scarpella & Meijer (2004)). During leaf expansion, some higher-order veins are formed (Kang & Dengler (2004)), that either cease in the lamina as free ending veinlets or join two connected veins. This process is reiterated many times until the leaf blade reaches maturity and veins of multiple order can be seen (Bohn et al. (2002); Kang & Dengler (2004); Scarpella & Meijer (2004); Scarpella et al. (2006); Wenzel et al. (2007); Sawchuk et al. (2007)).

1.4 Plant growth substances

Auxins. Auxin, the first identified plant hormone, is critical in many physiological processes in plants. The predominant form of auxins in plants is indole-3-acetic acid (IAA) (Figure 1.3). It is the only molecule that stimulates differentiation of the phloem and xylem in addition to inducing vascular strand formation (Sachs (1981)) either by high auxin concentration, high auxin fluxes or a combination of both (Rolland-Lagan & Prusinkiewicz (2005)). Auxin is primarily found in the apical meristem (de Reuille et al. (2006)) and in young leaves (Mattsson et al. (2003)). However the precise site(s) of auxin production in leaves still remains unclear. Evidence based on auxin transport inhibition experiments suggests that auxin is likely to be produced at the leaf margin

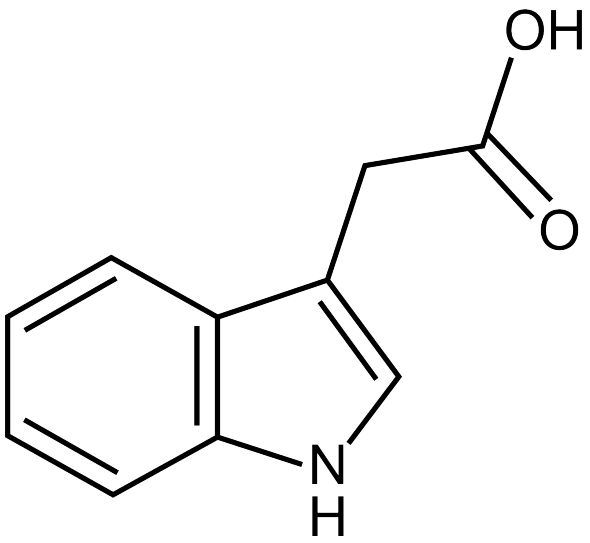

Figure 1.3: Chemical structure of auxin. Indole-3-acetic acid (IAA), a compound made of an aromatic ring and a carboxylic acid group, is the most abundant type of auxin.

(Mattsson et al. (1999)). Yet a study by Aloni *et al.* (2003) proposed that during leaf morphogenesis there are shifts in the sites of auxin production and this is where the control of venation patterning and vein differentiation occurs. Finally, molecular genetic studies have shown the *YUCCA* (*YUC*) genes, that encode flavin monooxygenases, such as YUC1, YUC2, YUC4 and YUC6 in Arabidopsis, play a key role in auxin biosynthesis and plant development (Zhao (2008)). Data revealed the expression of these genes (a) demonstrated that auxin production is spatially and temporally controlled (Cheng et al. (2006, 2007)) and (b) is limited to a small group of cells suggesting that auxin biosynthesis is localized (Cheng et al. (2007)). Notably, in leaves, mutations in all four *YUC* genes displayed fewer vein numbers than the wild type and absence of a continuous circle of vascular strands along the edge of the leaf (Cheng et al. (2006)). This demonstrates that local auxin production by *YUC* genes is essential for proper vein formation.

Auxin transport. Auxin is transported through the phloem and in non-vascular tissues. In the latter case, auxin is transported from cell-to-cell by a process known as polar auxin transport (PAT). Auxin transport follows the chemiosmotic theory originally proposed by Rubery and Sheldrake (1974) (Figure 1.4) and detailed components of the transport machinery have recently been identified (Gälweiler et al. (1998); Palme & Gälweiler (1999); Müller et al. (1998); Friml et al. (2002a,b); Bennett et al. (1996); Yamamoto & Yamamoto (1998); Marchant et al. (1999); Swarup et al. (2001); Yang et al. (2006); Muday & DeLong (2001)). From the acidic extracellular space (pH 5.5), auxin, a weak acid, enters the cell in a protonated form (IAAH) by passive diffusion or in its anionic form (IAA^-) by active co-transport using the influx carrier proteins AUXIN RESISTANT1 (AUX1). In the cytoplasm, the protonated form dissociates into IAA^- and H^+ due to the rise of pH to 7 and can no longer pass through the membrane via diffusion. The anionic form exits the cell via the polarly localized auxin efflux carriers, PIN FORMED (PIN) proteins, and then becomes protonated again once in the apoplast. The PIN protein family consists of eight members, expressed in different parts of the plant, most of which are involved in auxin efflux (PIN1-4, PIN7, PIN8) (Gälweiler et al. (1998); Benková et al. (2003); Reinhardt et al. (2003); Müller et al. (1998); Friml et al. (2002b,a, 2003); Ganguly et al. (2010) and reviewed by Petrásek & Friml (2009)). The direction of auxin transport depends on the asymmetrical localization and tissue-specific expression of PIN transporters at the plasma membrane (Goldsmith (1977); Tanaka et al. (2006); Wisniewska et al. (2006)). It still remains unclear what controls the polar

localization of these proteins, a rate-limiting factor in cellular auxin efflux (Petrásek et al. (2006)). Molecular studies have demonstrated that the presence or absence of PIN polarity regulators such as Ser/Thr protein kinase PINOID (PID) (Christensen et al. (2000); Friml et al. (2004)) and a protein phosphatase 2A (PP2A) (Michniewicz et al. (2007)) influence the position of PIN either towards the apical or basal side of the cell.

The local biosynthesis of auxin and the PIN-dependent transport together produce local auxin maxima and minima that are thought to regulate vascular tissue patterning and differentiation. In the shoot apical meristem (SAM) (Figure 1.5a), PIN proteins in the epidermal layer direct auxin to the site of leaf initiation. As the leaf primordium emerges, PIN proteins (localized basally) direct auxin inward through sub-epidermal tissues (Figure 1.5b) and domains of PIN expression prefigure vein formation (Figure 1.5c) (as reviewed in Rolland-Lagan (2008)). Domains of PIN1 expression initially progress inwards from points of auxin convergence in the leaf margin, which define the future mid-vein and secondary veins. Later domains of PIN expression connect pre-existing veins together (Figure 1.5d). As the leaf continues to grow, the same sequence of events is repeated many times (Figure 1.5e).

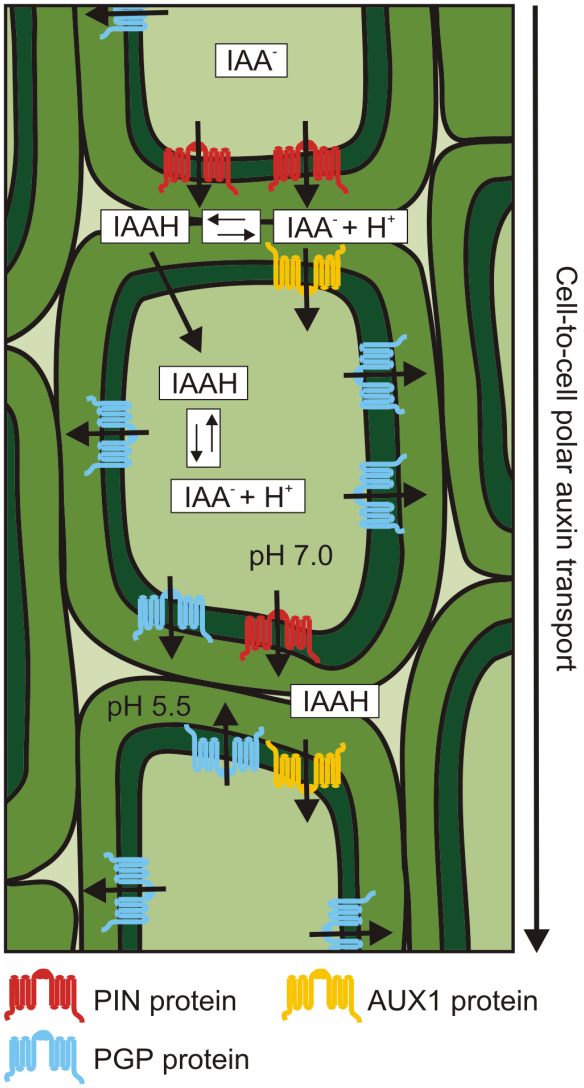

Figure 1.4: Chemiosmotic model for polar, cell-to-cell, auxin transport. Two forms of auxin, anionic (IAA^-) and protonated (IAAH), exist in the cell membrane as well as in the cytoplasm. Movement between compartments of the electrically neutral form occurs by passive diffusion while the auxin ion uses active co-transport of influx carrier proteins AUXIN RESISTANT1 (AUX1) to enter and efflux carrier proteins PIN FORMED1 (PIN1) and phosphogylcoprotein (PGP) (another class of auxin efflux facilitators but with diverse developmental roles (Mravec et al. (2008)) to exit. The dissociation of IAAH is dependent upon the pH gradient across the plasma membrane (from pH 5.5 to pH 7).

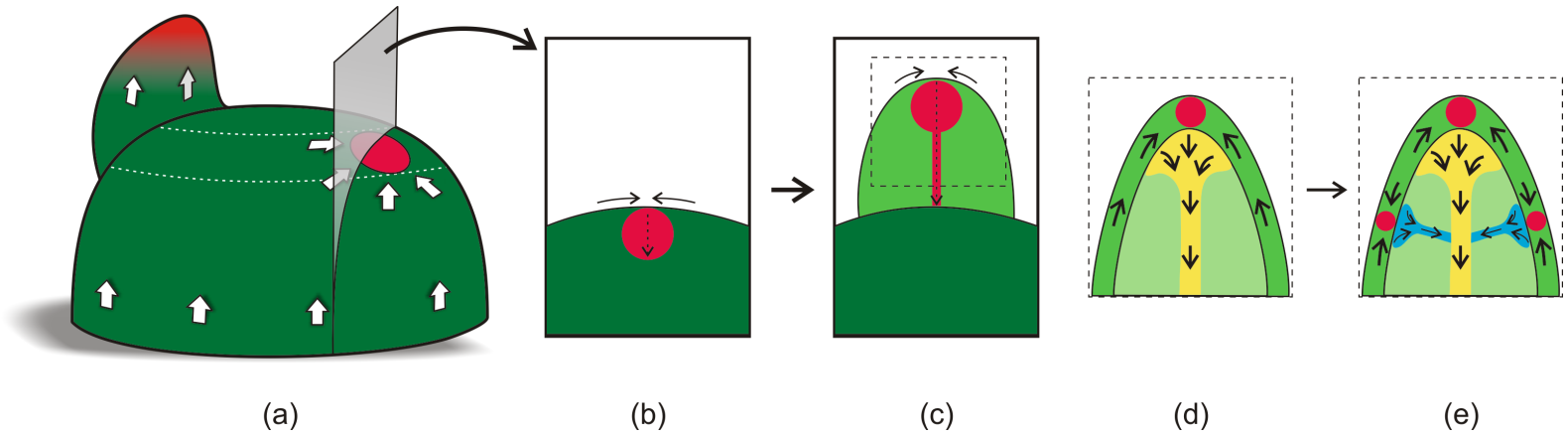

Figure 1.5: Stages of leaf development, vein formation and associated polarities of auxin transport. (a) A three-dimensional view of leaf initiation at the shoot apical meristem (SAM). While an already initiated leaf primodium continues to grow, other leaf primordia are initiated in the peripheral zone of the SAM, delimited by white dotted lines, and corresponds to sites of elevated auxin concentration (shown by a red circle) caused by the convergence points of PIN1 proteins which are localized polarly in the epidermal layer (white arrows). (b) A longitudinal section through the apical meristem. At the convergence point, auxin is directed inwards into internal tissues (black dotted arrow) which then triggers gradually leaf initiation and formation of vascular strands. (c) A small primordium is initiated at the flanks of the SAM (light green) and where auxin is drained through the middle of the primordium to later differentiate into the midvein (yellow) (d). (e) New auxin maxima develop within the leaf margin (shown in dark green) through a process identical to (a) and is correlated with sites of lateral vein formation (shown in blue).

1.5 The canalization hypothesis as a mechanism for vein pattern formation in stems and roots

1.5.1 Experiments with pea (*Pisum sativum*)

A series of experiments executed by Sachs (Sachs (1968, 1969, 1981)) led to the hypothesis that the canalization of auxin flux was capable of inducing vein formation in pea (*Pisum sativum*) stem and root sections. With the application of a lateral auxin source to a stem piece, new vascular strands developed towards pre-exisiting vascular tissue if the latter was unsaturated with auxin (Figure 1.6a). However, when the main vasculature was saturated with auxin (Figure 1.6b), new strands could not form in the vicinity of the pre-existing vascular tissue (did act as a sink for auxin).

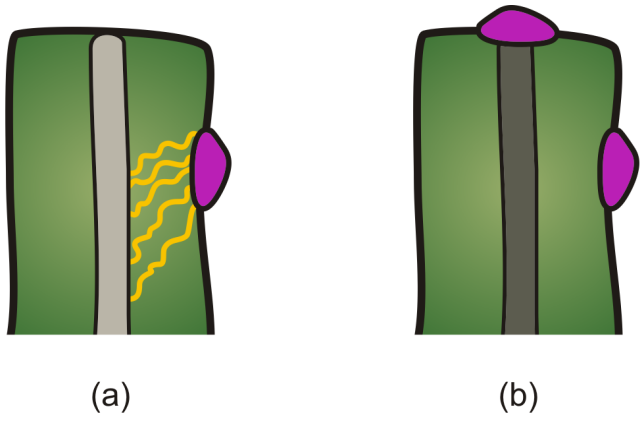

Figure 1.6: Formation of vascular strands in response to local auxin (1% indole acetic acid in lanolin) application in pea (*Pisum sativum*) stems. (a) A lateral source of auxin (pink) initiates the formation of vascular strands (yellow wavy lines) that connect to an existing vascular strand unsaturated with auxin (light gray) (Sachs (1981)). In (b) the main vasculature is saturated (dark gray) by an auxin source and therefore inhibiting formation of veins.

On the basis of these experiments, Sachs proposed that vascular strand formation formed through the canalization of a signal. This hypothesis later became known as the "canalization hypothesis". According to the canalization hypothesis, veins form through a positive feedback process where at first all cells have the same capacity to transport a signal, which is thought to be the phytohormone auxin. An increase of this signal flow in some cells reinforces their capacity to transport the signal even more. These specialized transporting cells channel the signal from the surrounding tissues resulting in a narrow strand with high auxin flux, which later differentiates into vascular tissue. Sachs (1968) also performed supplementary experiments in roots of pea and measured angles that formed between the main vasculature and newly differentiated strands from a lateral auxin source. In this case, xylem differentiation was easier to follow in pea roots compared to the shoot. New xylem strands that formed as a result of a lateral auxin source joined directly to the main vasculature that was not supplied with auxin with an angle of about 70±23°(Figure 1.7a). Two different results were obtained in response to lateral auxin application when the main vasculature was supplied with auxin; (1) auxin-induced xylem strand joined the previously present vasculature at a smaller angle than in the situation of a root of which the main vasculature was unsaturated with auxin with an angle of 26±13°(Figure 1.7b) or in other cases (2) newly formed strands ran parallel to the pre-existing vascular strand (Figure 1.7c). Although research on canalization has not been the main focus of recent studies involving exogenously applied auxin (Sauer et al. (2006); Balla et al. (2011)), investigators were able to replicate Sachs'

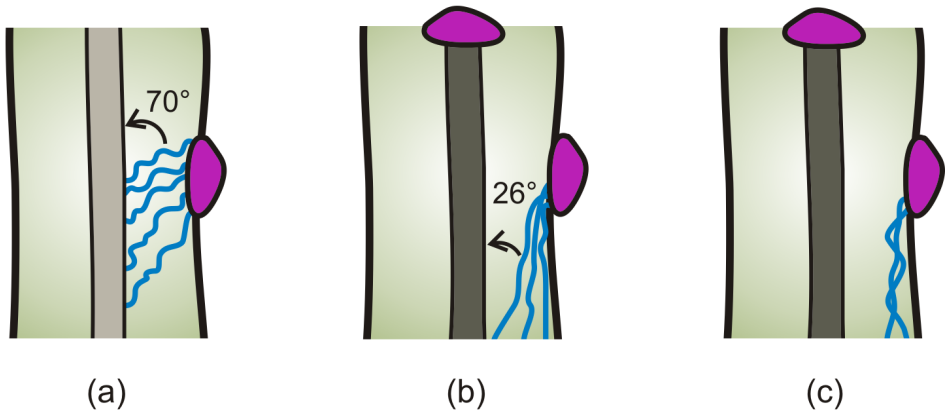

Figure 1.7: Vascular strand formation in response to local auxin (1% indole acetic acid in lanolin) application in pea (*Pisum sativum*) roots. (a) A lateral source of auxin (pink) initiates the formation of vascular strands (blue wavy lines) that join the pre-existing vascular strand unsaturated with auxin (light gray) forming a 70°angle (Sachs (1981)) bigger than in (b). With the main strand saturated with auxin (dark gray) and the presence of a lateral auxin, some roots showed (b) veins connecting lower down the already existing vein at a 26°angle and others (c) showed no joining to the main strand at all.

original experiments by using pea epicotyls (embryonic shoots that are found above the cotyledons) and also evaluate PIN1 expression patterns using immunolocalization techniques. Angle measurements between the primary and secondary veins have been overlooked.

1.5.2 Experiments with Arabidopsis

The induction of vein differentiation by an auxin source was simple to demonstrate with pea stems and roots. Compared with other model systems such as soybean and rice, Arabidopsis roots and stems are very fine and therefore no experiments have been done to test the canalization hypothesis in such species. The question now arises whether the

generalizations reached in the above experiments are applicable to the vascular system of Arabidopsis leaves. As a matter of fact, the concept of canalization has been extended to leaves (Mattsson et al. (1999); Scarpella et al. (2006)). It was shown that domains of PIN expression progressively narrow down to a single strand (Scarpella et al. (2006)) which is consistent with canalization. However it may not be auxin that is drained but another substance. Alternatively, a different mechanism than canalization altogether might control patterns of PIN expression. Moreover, the formation of the leaf vasculature has been considered similar to the mechanism for control of leaf position (phyllotaxis) on a plant stem but on a different shape domain (flat versus cylindrical).

1.6 The canalization hypothesis as a mechanism for vein pattern formation in leaves

Several mechanisms have been proposed to explain vein patterning in leaves (reviewed in Merks et al. (2007)) however the most widely accepted one is auxin canalization. In Arabidopsis leaves, pharmacological treatments with auxin transport inhibitors and mutations in genes affecting auxin polar transport have been shown to alter vein pattern formation. Wild type leaves treated with an artificial auxin transport inhibitor 1-*N*-naphthyl-phthalamic acid (NPA) and leaves of *pin1* mutants should both have higher auxin levels due to poor auxin transport. They could be comparable to Sachs' pea roots where the primary vein was saturated with auxin (Figure 1.7a, b). On the other hand,

accelerated auxin transport mutants (*max* - described later in section 1.6.2) that have been recently isolated should drain auxin faster than in the wild type. This is analogous to pea stems or roots were the main vein was unsaturated with the auxin.

1.6.1 Effects of NPA on vascular development

Leaves treated with NPA showed developmental defects and venation became progressively confined to the edges of the leaf as inhibition doses increased (Mattsson et al. (1999); Sieburth (1999)). This suggested that the leaf margin is the main site of auxin production and when polar auxin transport was blocked, auxin accumulated around the periphery. Our lab attempted to quantify vein patterns of plants treated with this chemical (Stacey Shim and Sareekha Singh, unpublished) but obtained great variability in data. In spite of this, we were still able to assay for general trends over several time points. Compared to the wild type, vascular strands were found to be increased in number along the margin, presence of multiple parallel midveins and vessel differentiation at the base of the leaf was either delayed or incomplete. High vein density was observed with smaller size loops along the margin of the leaf. The inability of auxin to be transported efficiently led to changes in leaf shape and size showing that factors required for continous venation patterning are also imperative for leaf growth (Dengler & Kang (2001)).

1.6.2 The *max* mutants

The shoot system architecture of seed plants is determined by the phyllotaxic arrangement of branches on the stem that develop through axillary bud outgrowth. The buds can remain active or undergo dormancy until outgrowth is triggered. This process is influenced by the prevailing environmental conditions such as the quantity and quality of light as well as the availability of nutrients. Responses to those exogenous and endogenous factors occur through the action of three different plant hormones that are known to be involved in shoot branching; auxin, cytokinin and strigolactone (Ferguson & Beveridge (2009)). The Arabidopsis *max* (*m*ore *ax*illary growth) mutants display increased shoot branching giving a bushy phenotype. Grafting experiments using wild type rootstocks and the branching mutants showed restoration of wild type shoot branching patterns (Turnbull et al. (2002)). This allowed researchers to suggest that a novel transmissible signal, moving acropetally, was indeed acting indirectly to inhibit bud growth. This signal was later shown to be strigolactones, a group of terpenoid lactones (Figure 1.8) derived from carotenoids found in root exudates and act as germination stimulants for seeds of root parasitic plants such as *Striga* and *Orobanche* species (as reviewed in Umehara et al. (2008)). They also act as rhizospheric signaling molecules for forming symbiotic interaction with arbuscular mycorrhizal fungi (Akiyama et al. (2005)).

Strigolactones are synthesized via the MAX pathway. Four genes have been identified; *MAX1*, *MAX2*, *MAX3* and *MAX4*, which are in a single pathway (Figure 1.9). *MAX1*, *MAX3*, and *MAX4* act in strigolactone synthesis while *MAX2* mediates percep-

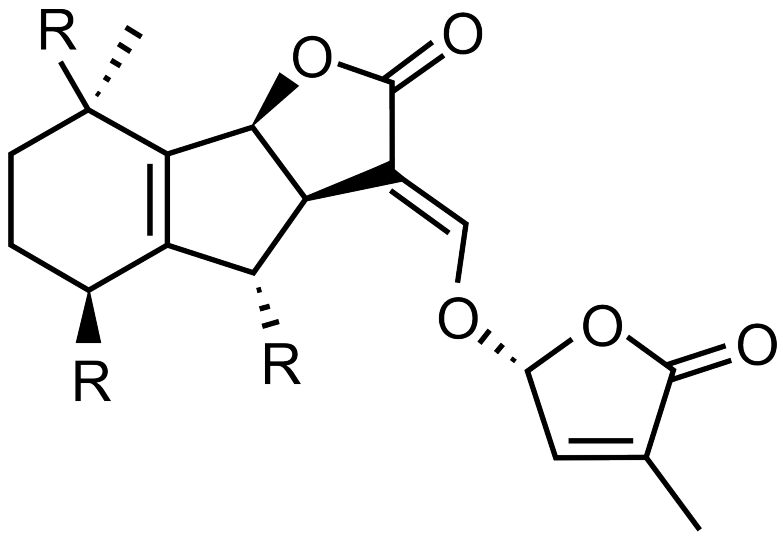

Figure 1.8: General chemical structure of strigolactones, a group of terpenoid lactones.

tion and response to that hormone. Molecular cloning experiments have revealed that *MAX4* encodes for a *CAROTENOID CLEAVAGE DIOXYGENASE8* (*CCD8*) gene (Sorefan et al. (2003)) whereas *MAX3* the *CAROTENOID CLEAVAGE DIOXYGENASE7* (*CCD7*) (Booker et al. (2004)). By contrast, *MAX1* encodes a cytochrome p450 enzyme that acts downstream to convert the carotenoid products of *MAX3* and *MAX4* into branching-inhibiting hormone strigolactone (Booker et al. (2005)). *MAX2* encodes an F-box protein, which is responsible for targeting specific proteins for degradation when activated (Stirnberg et al. (2002)). These mutant alleles have been isolated by either transposon or ethyl methane-sulphonate induced mutations at the *MAX4*, *MAX3*, *MAX2* and *MAX1* loci (Stirnberg et al. (2002); Sorefan et al. (2003); Booker et al. (2004)) and encode prematurely terminated proteins.

The MAX pathway is known to be involved in the regulation of auxin transport

capacity in the stem through effects on the abundance of PIN1 proteins (Bennett et al. (2006)). Absence of the hormonal signal, strigolactone, will result in the inhibition of *PIN* transcription levels and accumulation of auxin in the stem. The buds' ability to grow depends on their ability to export auxin. Since auxin transport capacity is full, this blocks export of auxin from the bud limiting movement along the stem (Figure 1.9). Mutations in the MAX pathway genes results in plants with different auxin transport capacities compared to one another. Transport rates of radio-labeled auxin were measured from stem segments in *max* mutants and wild type (Bennett et al. (2006)). This showed that transport capacity varied from highest to lowest in the different genotypes according to the following order: *max4-1*, *max3-9*, *max2-1*, *max1-1* and Col0.

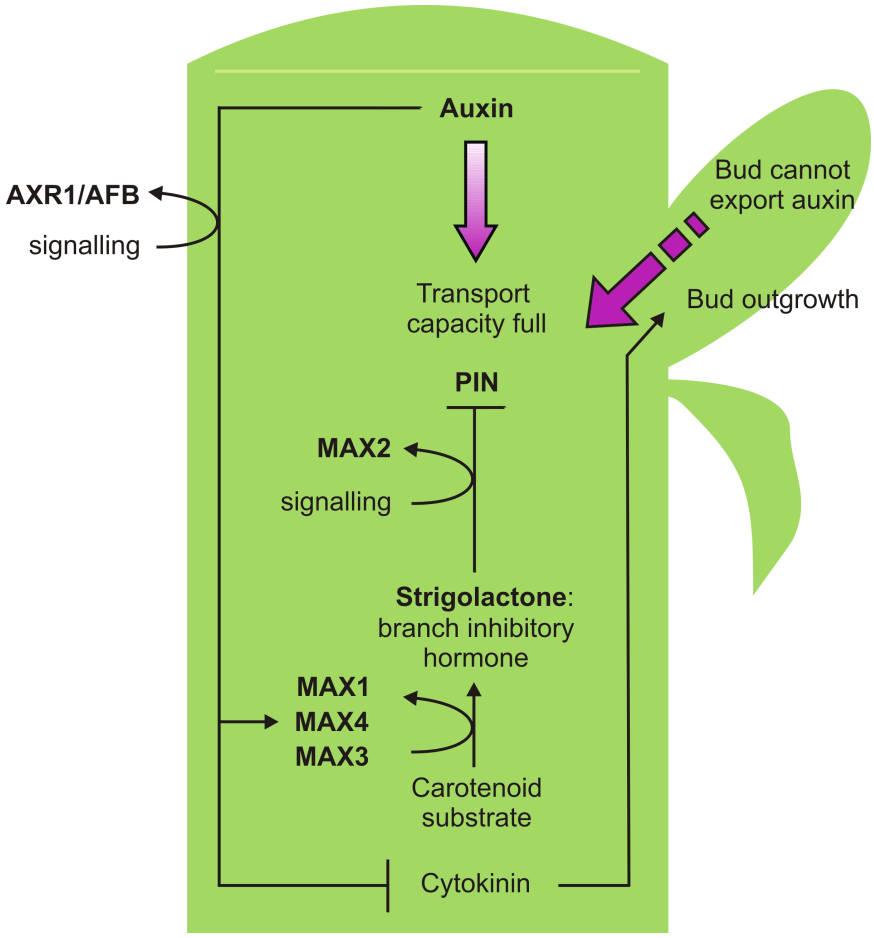

Figure 1.9: Model of the MAX pathway. Auxin is transported from the top to the bottom of the stem (pink arrow) via the polar transport stream. The capacity of the stream to transport auxin is influenced by the MAX pathway where *MAX1*, *MAX4* and *MAX3* (where the two latter encode carotenoid cleavage dioxygenases that are targeted towards the plastid) act to produce the novel branch inhibitory hormone known as strigolactone. This hormone is transported up the plant and detected by *MAX2*-dependent detection and signalling. *PIN* expression is inhibited and therefore auxin transport capacity becomes full in the stem preventing buds from exporting auxin (stripped pink arrow) and being activated. Moreover, the AXR1/AFB pathway monitors auxin concentration in the polar transport stream in order to regulate cytokinin synthesis. Accordingly, a high concentration of auxin will lead to down regulation of cytokinin production which in turn inhibits bud activation. *Redrawn from Ongaro & Leyser (2008).*

Chapter 2

Hypotheses, Predictions and Objectives

2.1 Hypothesis

We hypothesize that in Arabidopsis leaves veins form through the process of auxin canalization.

2.2 Predictions

2.2.1 First prediction

The administration of NPA gave rise to leaves with reduced leaf size, having wider leaf blade shape and higher vein density with smaller sized loops than the wild type. In

contrary to inhibited auxin transport, we predict that mutants with enhanced auxin transport will have the opposite effect. Leaves will be bigger in size, have lower vein density and bigger loops than the wild type and NPA treated plants.

2.2.2 Second prediction

If canalization operates in leaves as it does in stems/roots, then we would expect that in mutants with accelerated auxin transport, newly formed veins join existing veins by taking a shorter path (near to a 90°angle) (Figure 2.1a) than the wild type (Figure 2.1b). These mutants, with less auxin accumulation throughout the leaf, present the same characteristics as Sachs's pea roots system with only the lateral auxin source applied and the main strand unsaturated with auxin. On the contrary, plants exposed with NPA have leaves with numerous parallel vascular strands that correspond to the results attained by Sachs when two auxin sources were provided, one to the main vasculature and the other laterally to the pea roots (Figure 2.1c).

If the three different conditions of auxin transport (fast, normal and slow) are viewed at the cellular level, we would expect for accelerated transport, a continuous cell file that joins directly across since all cells of the midvein are unsaturated (Figure 2.2a). Nevertheless, in the situation of normal transport, the midvein is partially saturated whereby cells found near the top (near the source) have high concentrations of auxin and the cells close to the bottom (close to the sink) have depleting concentrations. Veins formed from the lateral auxin source towards the primary vein will therefore connect

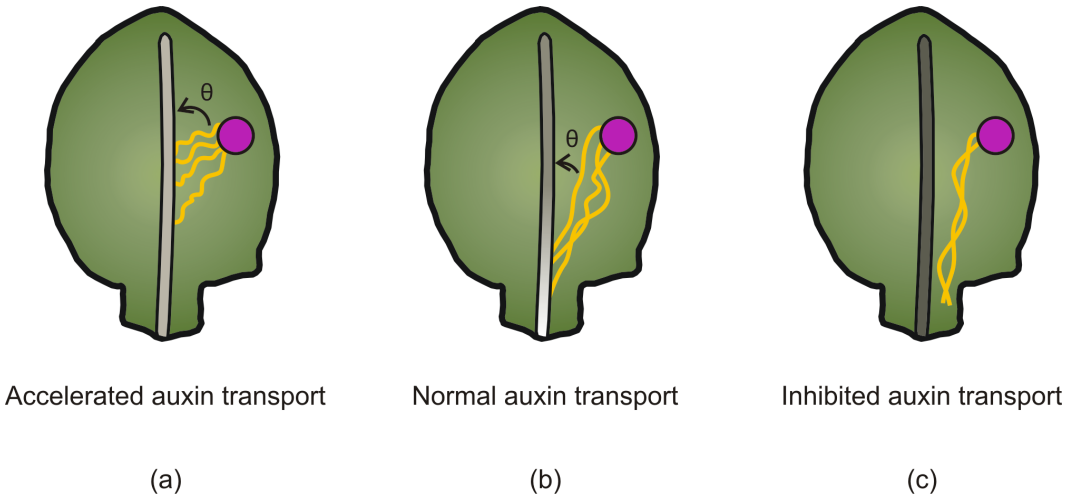

Figure 2.1: Schematic representation of our predictions, based on Sachs' experiments with pea (*Pisum sativum*) stems and roots (Sachs (1968, 1981)), regarding vascular strand formation in Arabidopsis leaves. (a) Mutants with accelerated auxin transport. The existing vascular strand (midvein) is unsaturated with auxin (light gray). New veins formed from a lateral auxin source (pink circle) will be able to join the primary vein directly across at an angle (θ) close to 90°. (b) Normal auxin transport as seen in wild type plants. The main vasculature is moderately unsaturated with auxin (from dark to light gray). Secondary veins will connect (at a smaller angle than (a)) to the bottom of the primary vein where auxin concentration is low. (c) Plants treated with high concentrations of NPA will exhibit strands that do not join the primary vein because the existing vascular cylinder is highly saturated with auxin (dark gray) (Mattsson et al. (1999)).

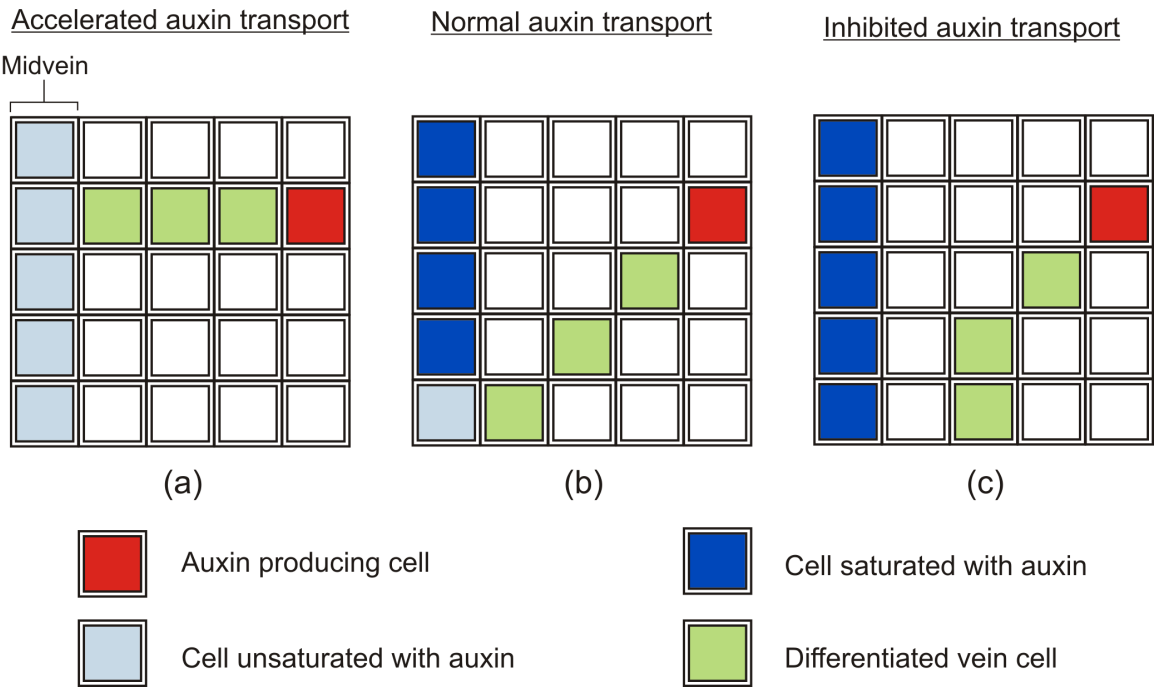

Figure 2.2: Representation of our predictions on vascular strand formation in Arabidopsis leaves at the cellular level. (a) In the accelerated auxin transport mutant, the midvein is composed of cells unsaturated with auxin therfore newly forming veins are able to take the shortest path to connect. (b) In wild type cases, auxin transport is normal and therfore only a few cells at the base of the leaf (near auxin sink) will be unsaturated with auxin. Secondary veins will only be able to join the main vein at a smaller angle. (c) All cells along the midvein of leaves where auxin transport is inhibited are saturated with auxin preventing new veins from adhering.

lower (Figure 2.2b) to cells with low auxin levels. In the case of inhibited transport, the midvein is completely saturated preventing any secondary veins from connecting (Figure 2.2c).

2.3 Objectives

Despite the experimental evidence and theoretical modeling supporting the canalization, it has still not been proven in leaves. The main goal of this study is to test the canalization hypothesis in Arabidopsis leaves by quantifying leaf vein patterns and acquiring measurements of angles formed between the primary and secondary veins of *max* mutants with accelerated auxin transport.

Chapter 3

Methodology

3.1 Plant material

The Arabidopsis ecotype Columbia-0 (Col0) (stock name: CS1092) from the Arabidopsis Information Resource, Carnegie Institution of Washington Department of Plant Biology, Stanford, California was used as a wild-type control to compare with *max* mutants. The following *max* mutants used for this study were received as seeds from Dr. Ottoline Leyser (University of York, United Kingdom): *max1-1*, *max2-1*, *max3-9* and *max4-1* (Figure 3.1 and Figure 3.1) (see Appendix A for a detailed phenotype verification of *max4-1*).

Figure 3.1: The rosette leaves of Arabidopsis *max* mutants (*max4-1*, *max3-9*, *max2-1*, *max1-1*) and wild type (Col0) harvested 17 days after sowing. All scale bars are 2 mm.

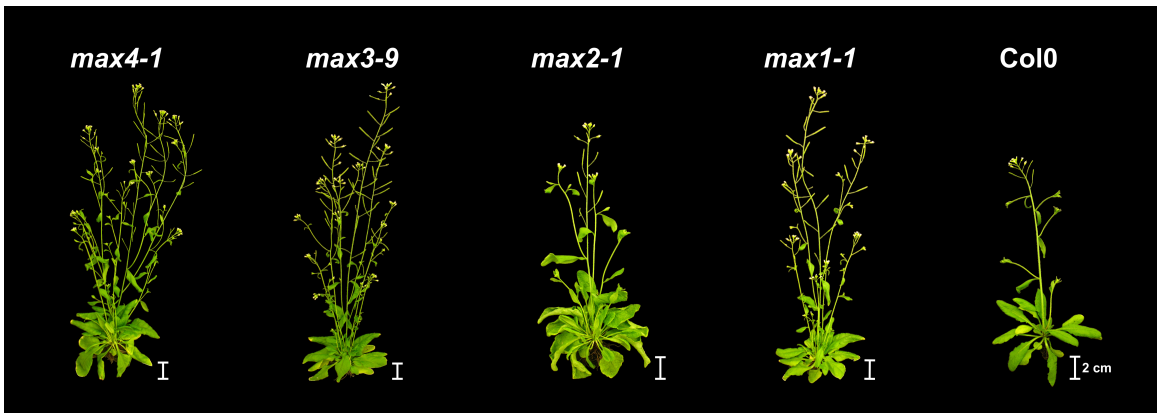

Figure 3.2: The Arabidopsis *max* mutants (*max4-1*, *max3-9*, *max2-1*, *max1-1*) and wild type (Col0) at 35 days after sowing. Plants shown were treated with a fertilizer. All scale bars are 2 cm.

3.2 Growth conditions

Arabidopsis seeds were sterilized and imbibed in distilled water for 4 days at 4°C in the dark. The imbibed seeds were then sown in Premier Pro-mix soil (Premier Horticulture Inc., Rivire-du-Loup, QC, CA) with 25 seeds per pot and grown in an environmentally controlled growth chamber (ATC40, Conviron) at 22°C set at 55% humidity with a 16 hours photoperiod, and a photosynthetic photo flux of 150 μmol $m^{-2}s^{-1}$d.

3.3 Samples and leaf clearing

For each genotype, around 20 to 25 plants were harvested each day from 4 to 20 days after germination. The first two true leaves in Arabidopsis are similar as they emerge nearly simultaneously and are the same size and shape (Tsukaya et al. (2000)). By random selection, one out of the two leaves was chosen and included in the data set. In order to view venation patterns, leaves were cleared following the procedure of Steynen and Schutlz (2003). Eliminating chlorophyll was done by fixing the harvested leaves in a solution of 3:1 ethanol:acetic acid for two hours, then deyhdrating leaves in 70% ethanol for one hour and then into 95% ethanol overnight. The following day, leaves were placed in 5% NaOH for an hour at 60°C in a water bath. Leaves were then mounted on microscope slides in a 50% aqueous glycerol solution and imaged. Only 15 leaves per day were used for further analysis. The extra collected plants were to ensure that there were enough samples for each time point as leaves became very fragile after clearing and tore up easily

while dissecting.

3.4 Microscopy

Leaf pictures of the wild type and mutants were taken under dark field microscopy using a Zeiss V8 Discovery stereomicroscope with an attached Canon Powershot A640 camera.

3.5 Analytical tools

Programs developed in our lab using Matlab software (The Mathworks, Inc. Natwick, MA, USA; http://www.mathworks.com) were used to acquire quantitative information from leaves. This methodology was an object of publication (Rolland-Lagan et al. (2009) - See appendix B for more details) on which I am a co-author. Statistical analyses were conducted using the SPSS software (SPSS Inc., Chicago, IL, USA). Details on statistical tests used for this thesis can be found in the results section.

Chapter 4

Results

Using a method previously developed in our lab (Rolland-Lagan et al. (2009)), we quantified leaf venation patterns. For each time point of the period analyzed, from DAS7 to DAS17, we were able to obtain vein pattern parameters such as blade area, blade shape, vein density, number of loops and number of segments. In addition, spatial results of vein densities and relative loop areas were also collected. To test the canalization hypothesis, we extracted relative angle measurements of the mutants and tested for significance against the wild type. Moreover, angle maps were observed to check for spatial heterogeneties.

In some cases the pattern of the wild type and mutant curves appeared to have similar trends but one was delayed compared to the other. This was due to the fact that some mutants germinated faster than the wild type therefore a recoding was done to standardize the days for comparison. Only *max2-1* and *max3-9* were shifted a day earlier.

Moreover, some exploratory analysis on the data revealed a non normal distribution and therefore non-parametric tests were used throughout this study. One of the drawbacks of performing these types of tests is that they do not allow the use of nested designs.

4.1 Leaf blade area

The mean blade area (square mm) of the first rosette leaves of Arabidopsis increased over time for the wild type and for all four *max* mutants (Figure 4.1a). A Mann-Whitney U Test was performed for each day after sowing (DAS) between both the wild type and the mutant as well as between the different mutant lines to determine if any differences were significant. *max2-1* had significantly larger leaf blades compared to the wild type throughout the whole developmental period analyzed (Mann-Whitney U test, P=<0.05 for each DAS). In contrast, *max4-1* had smaller leaf blade areas (Mann-Whitney U test, P=<0.05 for each DAS) than Col0. As for *max3-9* and *max1-1*, the mean leaf blade areas were significantly smaller than those of the wild type with the exception of several days where there were no statistical differences (*max3-9*: DAS7, DAS9 and DAS15 to DAS17; *max1-1*: DAS8, DAS9 and DAS18) (Mann-Whitney U test, see Appendix C). When compared with *max3-9*, *max4-1* was significantly smaller in leaf size at DAS8 and from DAS11 to DAS17 (Mann-Whitney U test, P=<0.05 for each DAS). From DAS7 to DAS14, both *max3-9* and *max1-1* had similar leaf blade sizes yet at later developmental stages from DAS15 to DAS17 *max3-9* had significantly larger leaves than *max1-1* (Mann-Whitney U test, P=<0.05 for each DAS). In general, *max4-1*, *max3-9* and *max1-1* had

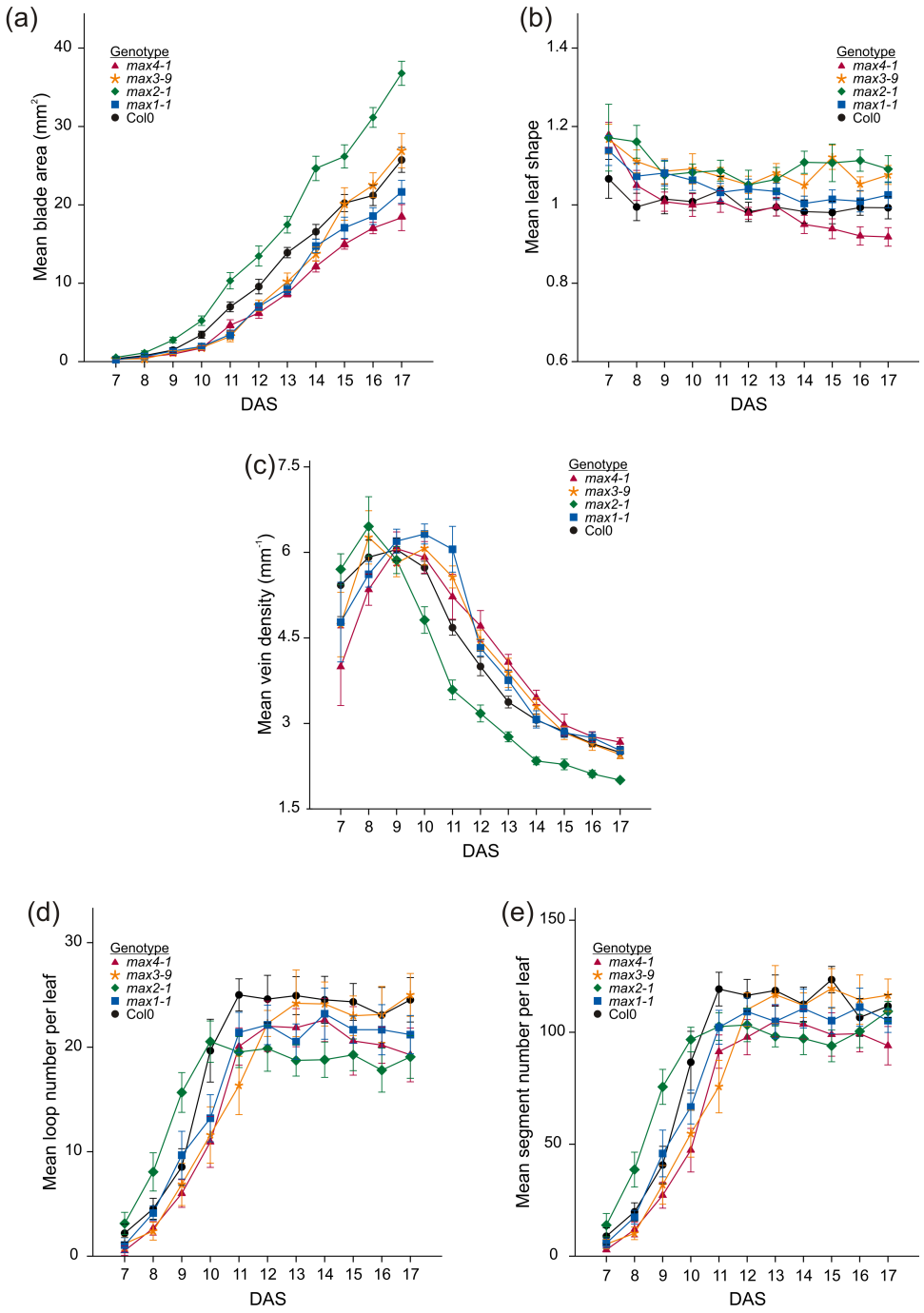

Figure 4.1: Mean leaf size and pattern data from DAS7 to DAS17 for five different genotypes; *max4-1* (red triangle), *max3-9* (orange star), *max2-1* (green diamond), *max1-1* (blue square) and Col0 (black circle). Mean leaf data are shown as a function of developmental stage in DAS (days after sowing) (n=15 leaves per stage). Error bars indicate the standard error of the mean. (a) Mean blade area (mm^2), (b) mean leaf shape, (c) mean vein density (mm^{-1}), (d) mean loop numbers leaf and (e) mean segment numbers per leaf.

the same blade sizes and were all slightly smaller than the wild type (Col0). *max2-1* had a much larger leaf blade area than the wild type and the other three mutants.

4.2 Leaf blade shape

Leaf blade shape was measured as a ratio of the length of the blade to the width of the blade. The mean leaf blade shape for each day and genotype is shown in Figure 4.1b. A non-parametric analysis of variance (Kruskal-Wallis) test was used on leaf blade shape data with day as a factor. A summary of statistical analysis of leaf blade shapes can be found in Figure 4.2.

Mean leaf blade shape for Col0 went from slightly elongated at DAS7 (mean length over width (L/W) ratio=1.07) to round at DAS8 (mean L/W ratio = 0.99) (χ^2=3.882, df=1, P=<0.05). The round shape was maintained throughout the rest of the developmental stages from DAS8 to DAS17 (mean L/W ratio varied between 0.98 and 1.04) (χ^2= 12.225, df= 9, P= 0.201). Similarly, from DAS7 to DAS9, *max4-1* significantly changed leaf shape (χ^2=27.136, df=2, P=<0.05) going from elongated to round (mean L/W ratio decreased from 1.18 to 1.01). From DAS9 to DAS13, the leaf blade shape remained round (mean L/W ratio varied between 0.98 and 1.01) (χ^2=4.688, df=4, P=0.321). Later on, from DAS13 to DAS17, leaf blade shape became significantly wider than long (mean L/W ratio decreased from 1.00 to 0.92) (χ^2= 19.564, df= 4, P=<0.05).

As for *max3-9*, *max2-1* and *max1-1*, all three genotypes were relatively the same shape, being elongated, with minor variations throughout the developmental stages. In

more detail, leaf shape was not significant from DAS7 (mean L/W ratio = 1.17) to DAS8 (mean L/W ratio=1.16) for *max2-1* (χ^2=0.155, df=1, P=0.694) but was significant from DAS8 (mean L/W ratio = 1.16) to DAS9 (mean L/W ratio= 1.08) (χ^2=7.839, df=1, P=<0.05). From DAS7 to DAS9, leaf shape of *max3-9* (mean L/W ratio varied between 1.17 and 1.09) (χ^2=9.638, df=2, P=<0.05) and *max1-1* (mean L/W ratio varied between 1.14 and 1.07) (χ^2=7.334, df=2, P=<0.05) were not significantly different from each other.

This suggests that leaf shape was not different from DAS7 to DAS8 then became less elongated from DAS8 to DAS9 for *max2-1*. As for *max3-9* and *max1-1*, leaf shape started off being elongated to being a little less from DAS7 to DAS9. Leaf blade shape remained unchanged from DAS9 to DAS14 for *max3-9*, from DAS9 to DAS13 for *max1-1* and from DAS9 to DAS17 for *max2-1*.

Towards the last days of the analyzed period, shape varied significantly from DAS14 to DAS17 (mean L/W ratio varied between 1.05 and 1.12) (χ^2=15.142, df=3, P=<0.05) for *max3-9* however was not significantly different from DAS13 to DAS17 for *max1-1* (mean L/W ratio varied between 1.01 and 1.03) (χ^2= 4.571, df= 4, P= 0.334).

4.3 Vein density

The vein density for each leaf was calculated as the total vein length across the leaf divided by the whole leaf area. The mean leaf vein density for each day and genotype is shown in Figure 4.1c. The non-parametric analysis of variance (Kruskal-Wallis) test was

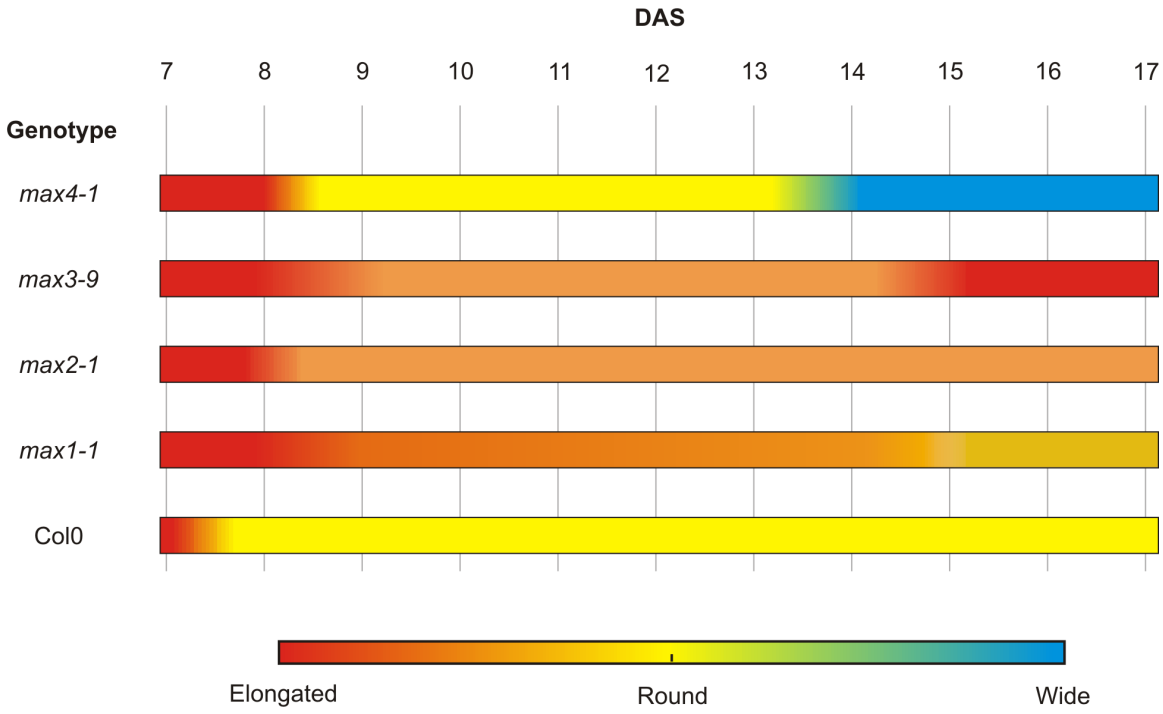

Figure 4.2: Statistical summary of leaf shape for all five genotypes from DAS7 to DAS17. The color bar legend (below the diagram) indicates loop shapes.

used on vein density data with day as a factor. For all genotypes, vein density at first was either constant or increased then remained constant over time and later on decreased. A summary of statistical analysis of vein densities can be found in Figure 4.3.

The test showed that vein density for Col0 did not vary significantly from DAS7 to DAS9 (χ^2=3.717, df=2, P=-.156) but varied significantly from DAS9 to DAS17 (χ^2= 127.555 , df= 8 , P=<0.05) indicating that vein density remained constant from DAS7 to DAS9 then decreased from DAS 9 to DAS17 (Figure 4.1c). Vein density varied significantly from DAS7 to DAS9 for *max4-1* (χ^2=21.960, df=2, P=<0.05), from DAS7 to DAS8 for *max3-9* (χ^2=12.873, df=1, P=<0.05), from DAS 7 to DAS8 for *max2-1*(χ^2=6.091, df= 1, P=<0.05) and from DAS7 to DAS9 for *max1-1* (χ^2= 16.934, df=2, P=<0.05). However vein density did not vary significantly from DAS9 to DAS10 for *max4-1* (χ^2=0.468, df=1, P=0.494), from DAS8 to DAS10 for *max3-9* (χ^2=4.049, df=2 , P=0.132), from DAS8 to DAS9 for *max2-1* (χ^2=3.108, df=1 , P=0.078) and from DAS9 to DAS11 for *max1-1* (χ^2=0.931, df=2, P=0.628). A significant difference in vein density was then observed from DAS10 to DAS17 for *max4-1* and *max3-9* (χ^2= 108.435, df= 7, P=<0.05; χ^2=110.959, df=7, P=<0.05) from DAS9 to DAS17 for *max2-1* and from DAS11 to DAS17 for *max1-1*. This indicates that vein density increased from DAS7 to DAS9 for *max4-1* as well as for *max1-1* and from DAS7 to DAS8 for *max3-9* along with *max2-1* and stayed constant from DAS9 to DAS10 for *max4-1*, from DAS8 to DAS10 for *max3-9*, from DAS8 to DAS9 for *max2-1* and from DAS9 to DAS11 for *max1-1*. Following the stabilization period, vein density of *max4-1*, *max3-9*, *max2-1* and *max1-1*

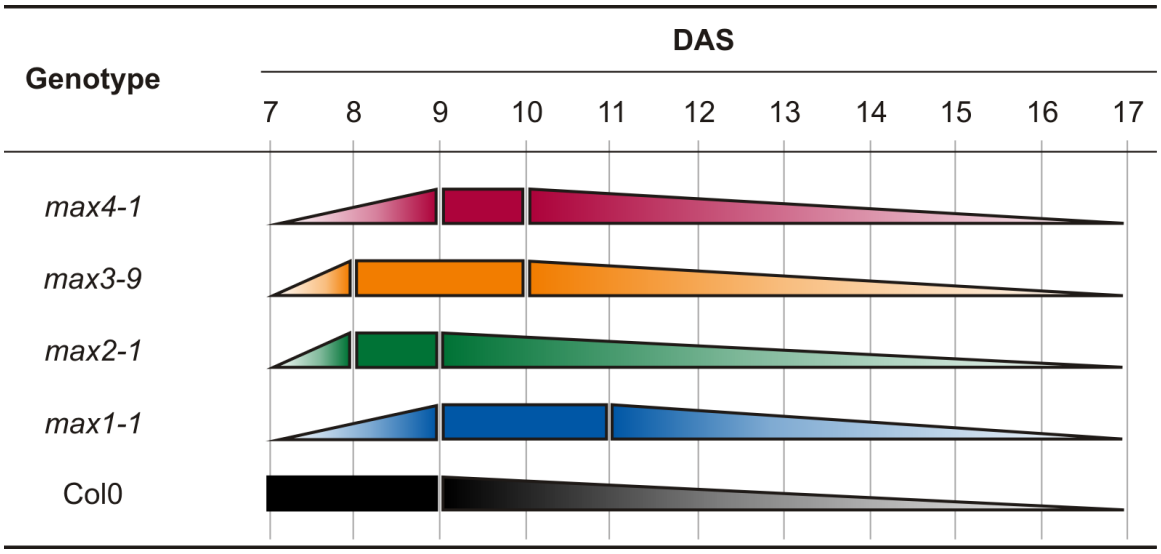

Figure 4.3: Statistical summary of vein density for all five genotypes from DAS7 to DAS17. Example: Vein density of *max4-1* increased significantly from DAS7 to DAS9 then remained constant from DAS9 to DAS10. Later on vein density significant decreased from DAS10 to DAS17. Differences between mutant-mutant and between wild type-mutant are not shown in this representation.

decreased from DAS10 to DAS17, DAS10 to DAS17, DAS9 to DAS17 and DAS11 to DAS17 respectively.

4.4 Spatio-temporal variations in vein density

All plant genotypes exhibited a progressive decrease in vein density from the distal to the proximal part of the leaf between DAS9 and DAS11 for *max2-1*, DAS11 and DAS13 for Col0, *max1-1* as well as *max3-9* and DAS11 and DAS14 for *max4-1* (Figure 4.4). Spatial variation in vein density decreased from DAS 11 (*max2-1*), DAS13 (Col0, *max1-1* as well as *max3-9*) and DAS14 (*max4-1*) onwards then became similar in all parts of the

leaf at DAS 13 for *max2-1*, at DAS15 for Col0, *max1-1* as well as *max3-9* and at DAS16 for *max4-1* till the end of the period analyzed.

4.5 Loop numbers

The mean loop number per leaf for each day for wild type and mutants is shown in Figure 4.1d. The Kruskal-Wallis test was used on loop numbers with day as a factor. A summary of statistical analyses of loop numbers is provided in Figure 4.5.

Loop numbers were significantly different from DAS7 to DAS10 for *max2-1* (χ^2=49.268, df=3, P=<0.05), from DAS7 to DAS11 for Col0 (χ^2=64.902, df=4, P=<0.05), for *max4-1* (χ^2=66.136, df=4, P=<0.05) as well as for *max1-1* (χ^2=66.131, df=4, P=<0.05) and from DAS7 to DAS12 for *max3-9* (χ^2=76.458, df=5, P=<0.05). This means that the number of loops per leaf increased until DAS10 for *max2-1*, DAS11 for the wild type, *max4-1* as well as *max1-1* and until DAS12 for *max3-9*. Loop numbers did not significantly vary from DAS10 to DAS17 for *max2-1* (χ^2=4.961, df=7, P=0.665), from DAS11 to DAS17 for Col0 (χ^2=2.534, df=6, P=0.865), *max4-1* (χ^2=7.829, df=6, P=0.251) as well as *max1-1* (χ^2=4.275, df=6, P=0.639), and from DAS12 to DAS17 for *max3-9* (χ^2=4.438, df=5, P=0.488). The mean loop numbers curves (Figure 4.1d) of *max4-1*, *max3-9* and *max1-1* seem to overlap together and have lower loop numbers than the wild type. A Mann-Whitney U test was performed for each day after sowing (DAS) between the different mutant lines (*max1-1* with *max4-1*, *max1-1* with *max3-9* and *max3-9* with *max4-1*) to determine if any differences were significant. There was no significant

differences between the three mutants throughout the developmental stages except at DAS8 to DAS9 were *max1-1* had a significantly higher loop numbers (Mann-Whitney U test, P=<0.05 for each DAS) than *max3-9* and *max4-1*, DAS11 where once again *max1-1* had a significantly higher loop numbers (Mann-Whitney U test, P=<0.05 for each DAS) than *max3-1*, DAS13 were *max1-1* had a significantly lower loop numbers (Mann-Whitney U test, P=<0.05 for each DAS) than *max3-9* and finally DAS17 were both *max1-1* and *max4-1* had a significantly lower loop numbers (Mann-Whitney U test, P=<0.05 for each DAS) than *max3-9*. A comparison of these three mutants, each with the wild type, showed that *max3-9* and *max1-1* were not significantly different throughout most of the days except at DAS8, DAS10 along with DAS11 for *max3-9* and at DAS10 to DAS11, DAS13, DAS15 as well as DAS17 for *max1-1* that had significantly lower loop numbers (Mann-Whitney U test, P<0.05). On the other hand, the loop numbers of DAS14 (Mann-Whitney U test, P=0.197) and DAS17 (Mann-Whitney, P=0.096) of *max4-1* where not significantly different from the wild type. For the other remaining days, loop numbers of *max4-1* was significantly lower than Col0 (Mann-Whitney U test, P=<0.05). As for *max2-1*, loop numbers at DAS7 (Mann-Whitney U test, P=0.113) and at DAS10 (Mann-Whitney U test, P= 0.242) were not significantly different than Col0. However, in relation to the wild type, loop numbers of *max2-1* was significantly higher from DAS8 to DAS9 and significantly lower from DAS11 to DAS17 (Mann-Whitney U test, P=<0.05).

4.6 Segment numbers

The mean segment numbers per leaf for each day and for each genotype is shown in Figure 4.1e. A Kruskal-Wallis test was performed on segment numbers data with day as a factor. A statistical analyses summary of segment numbers can be found in Figure 4.6.

Segment numbers increased significantly till DAS10 for *max2-1* (χ^2=50.581, df=3, P=<0.05), till DAS11 for Col0 (χ^2=64.740, df=4, P=<0.05), *max4-1* (χ^2=65.684, df=4, P=<0.05) as well as *max1-1* (χ^2=66.501, df=4, P=<0.05) and till DAS12 for *max3-9* (χ^2=77.593, df=5, P=<0.05). Later on, segment numbers for *max4-1* and *max1-1* did not vary significantly from DAS11 to DAS17 (χ^2=8.101, df=6, P=0.231; χ^2= 3.849, df=6, P=0.697 respectively), whereas segment numbers did not vary significantly for *max3-9* from DAS12 to DAS17 (χ^2=2.988, df=5, P=0.702). As for Col0, segment numbers per leaf did not vary significantly from DAS11 to DAS15 (χ^2=7.136, df=4, P=0.129) but decreased from DAS15 to DAS16 (χ^2=8.557, df=1, P=<0.05), then did not significantly change again from DAS16-17 (χ^2=0.992, df=1, P=0.319). For *max2-1*, only DAS10 to DAS16 were considered for analysis as there was an increase in segment numbers towards DAS17. No significant change in segment numbers was observed from DAS10 to DAS16 (χ^2=6.053, df=6, P=0.417). It is important to note that when the number of segments stabilizes the leaf is simply growing and no new veins are forming. Therefore any variations observed in the number of segments in later developmental stages do not fit with the trend which is likely due to sampling bias when harvesting plants.

In order to compare differences in segment numbers between the wild type and mutant as well as between the different mutant lines, a non-parametric Mann-Whitney U Test was performed for each day. Both, *max3-9* and *max1-1* were very similar to the wild type with the exception of segment numbers being significantly lower at DAS8, DAS10 to DAS11 for *max3-9* (Mann-Whitney U test, P=<0.05) and at DAS10 to DAS11, DAS13 as well as DAS15 for *max1-1* (Mann-Whitney U test, P=<0.05). Concerning *max4-1*, segment numbers was significantly lower relative to wild type mostly through all the different developmental stages apart from DAS14 (Mann-Whitney U test, P=0.129) and DAS16 (Mann-Whitney U test, P=0.205). *max2-1* had significantly increased segment numbers compared to Col0 from DAS7 to DAS10 (Mann-Whitney U test, P=<0.05) but then had significantly fewer segments from DAS11 to DAS15 (Mann-Whitney U test, P=<0.05), and was not significantly different from Col0 from DAS16 to DAS17 (Mann-Whitney U test, P=0.299; P=0.693 respectively). When comparing the three following mutant lines together: *max4-1*, *max3-9* and *max1-1*, *max4-1* and *max3-9* are significantly the same with the exception of *max3-9* having higher segment numbers at DAS15 and DAS17 (Mann-Whitney U test, P=< 0.05). For *max1-1*, segment numbers was significantly higher only at earlier days from 7 to 12 compared to both *max4-1* and *max3-9*. With respect to *max2-1*, the other three mutant lines had significantly lower segment numbers per leaf till DAS10 for *max1-1*, till DAS11 for *max3-9* and *max4-1* Mann-Whitney U test, P=<0.05 for each DAS). At later developmental stages, segment numbers did not vary significantly aside from DAS14 to DAS15 (*max1-1*), DAS13 to

DAS15 (*max3-9*) being significantly higher and at DAS17 (*max4-1*) being significantly lower (Mann-Whitney U test, $P<0.05$).

4.7 Relative loop areas

The contour maps data demonstrated clear spatial heterogeneities in loop areas. Loop areas increased from the marginal to the central regions of the leaf blade and remained consistent throughout development from DAS9 onwards as seen in (Rolland-Lagan et al. (2009)). As seen from the above results, the *max* mutants exhibited different leaf sizes compared to the wild type which makes it difficult to analyze certain spatial parameters. It may be that the size of a loop depends on the leaf size, in that for at a given developmental stage there is an optimal loop area. Nevertheless, both parameters may be unrelated if there is the presence of a defined optimal loop size. Therefore, for each day, the relative loop area was calculated as the average loop area of the leaf divided by the whole leaf area as shown in Figure 4.7 (also see maps in Figure 4.9 and Figure 4.10).

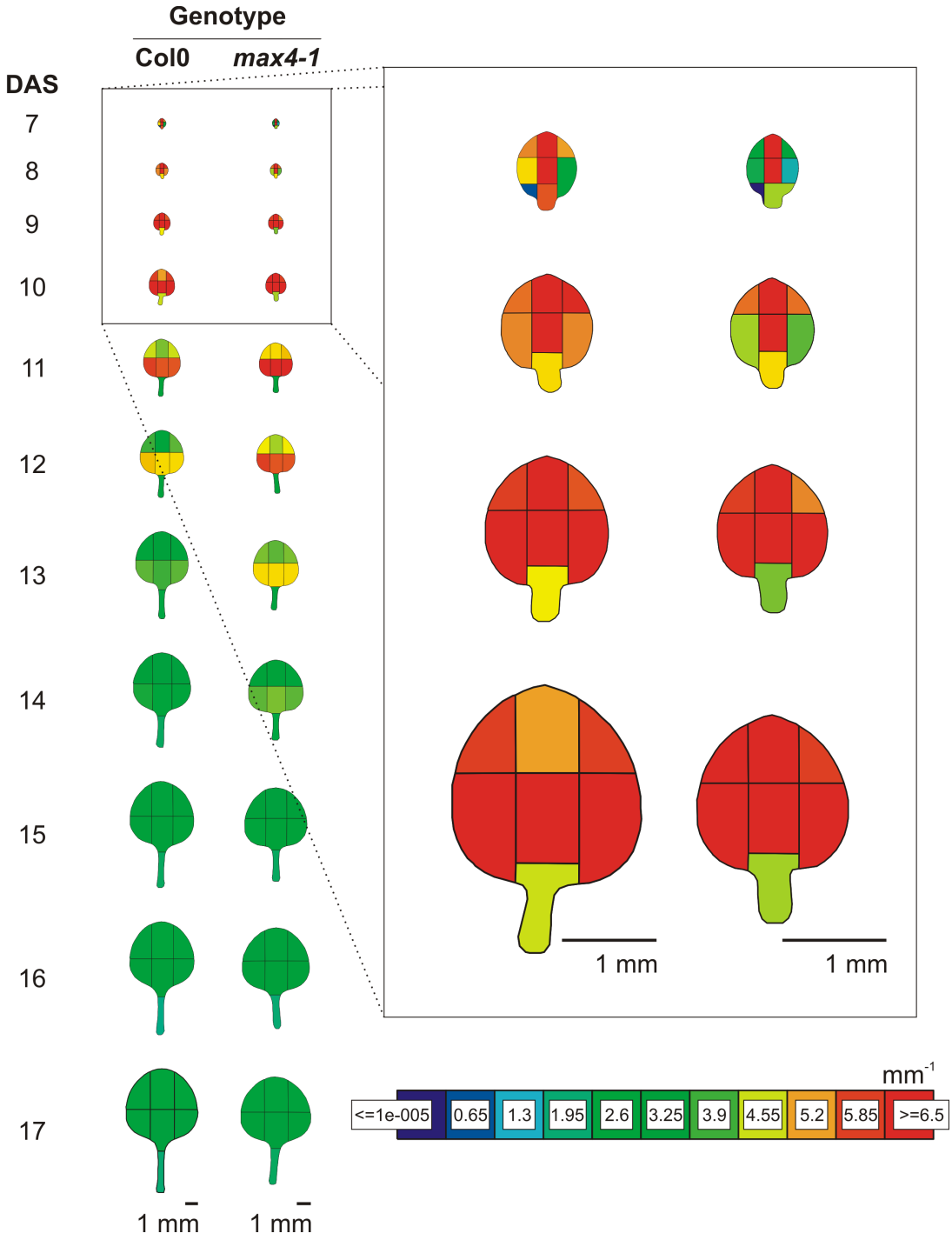

Figure 4.4: Spatial variation in vein density from DAS 7 to DAS17 of Col0 and *max4*. (*Right*) Enlargement at early stages of development from DAS7 to DAS10. Legend for the maps are in mm^{-1}. Other *max* mutants have not been shown as they display similar results to Col0 and *max4-1*.

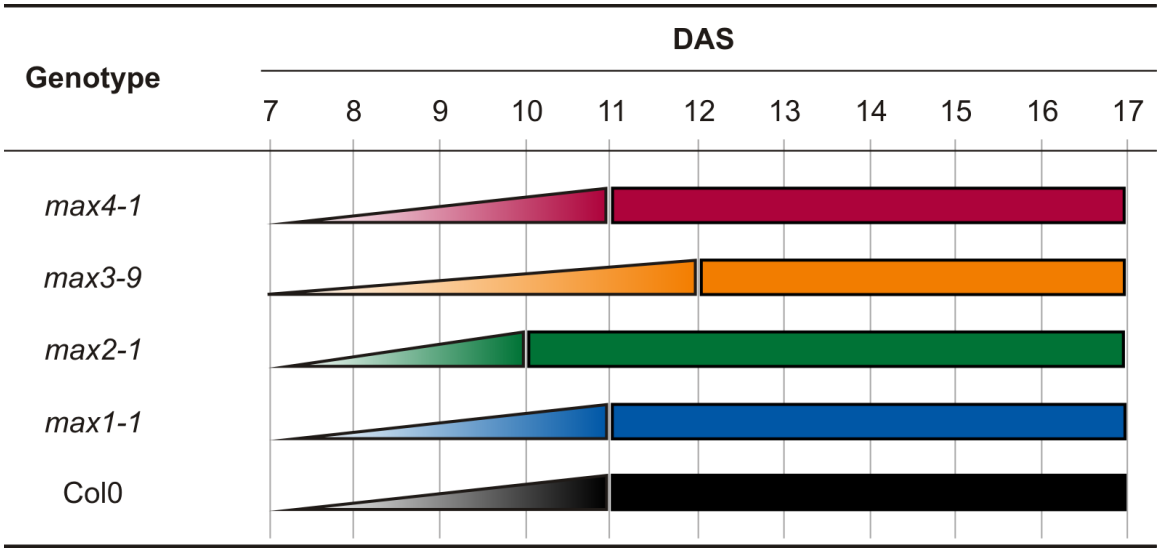

Figure 4.5: Statistical summary of loop numbers for all five genotypes from DAS7 to DAS17. Example: Loop numbers for *max4-1* increased significantly from DAS7 to DAS11 then remained constant from DAS11 to DAS17. Differences between mutant-mutant and between wild type-mutant are not shown in this representation.

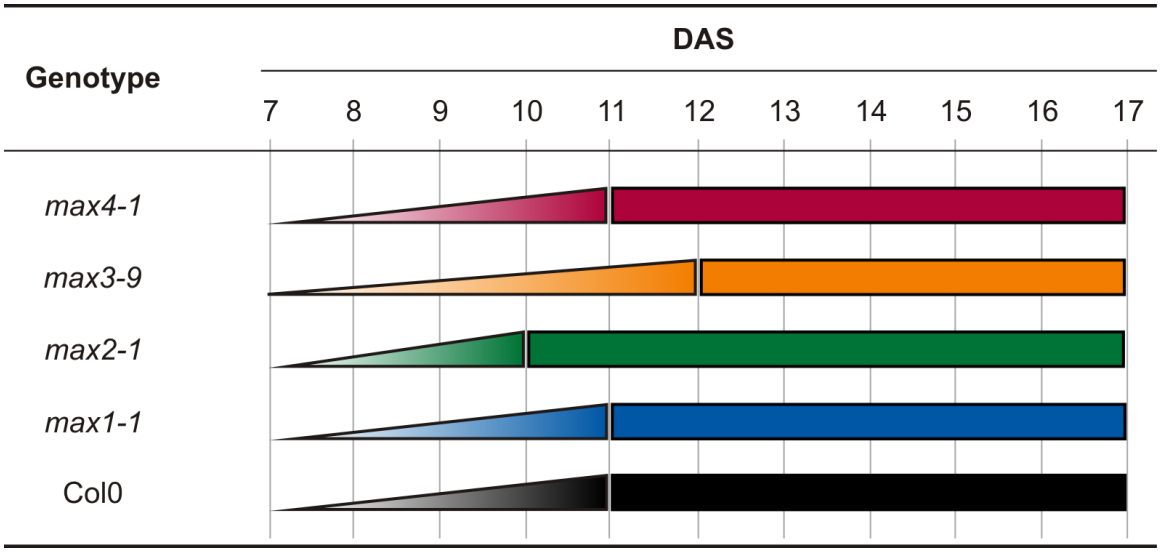

Figure 4.6: Statistical summary of segment numbers for all five genotypes from DAS7 to DAS17. Example: Segment numbers for *max4-1* increased significantly from DAS7 to DAS11 then remained constant from DAS11 to DAS17. Differences between mutant-mutant and between wild type-mutant are not shown in this representation.

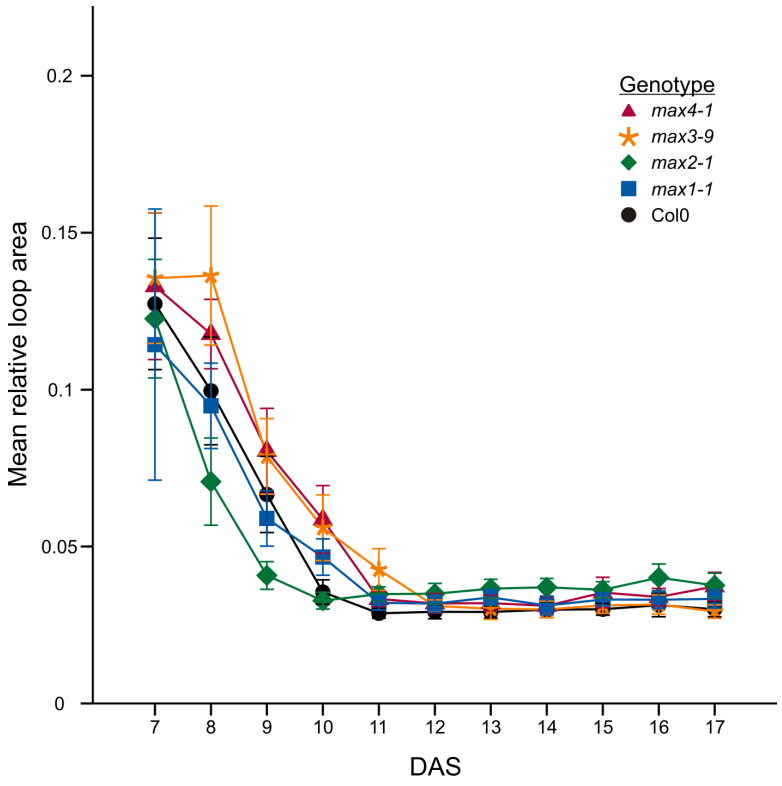

Figure 4.7: Mean relative loop areas from DAS7 to DAS17 for five genotypes; *max4-1* (red triangle), *max3-9* (orange star), *max2-1* (green diamond), *max1-1* (blue square) and Col0 (black circle). Mean leaf data (15 leaves per stage per genotype) are shown as a function of developmental stage in DAS (days after sowing).

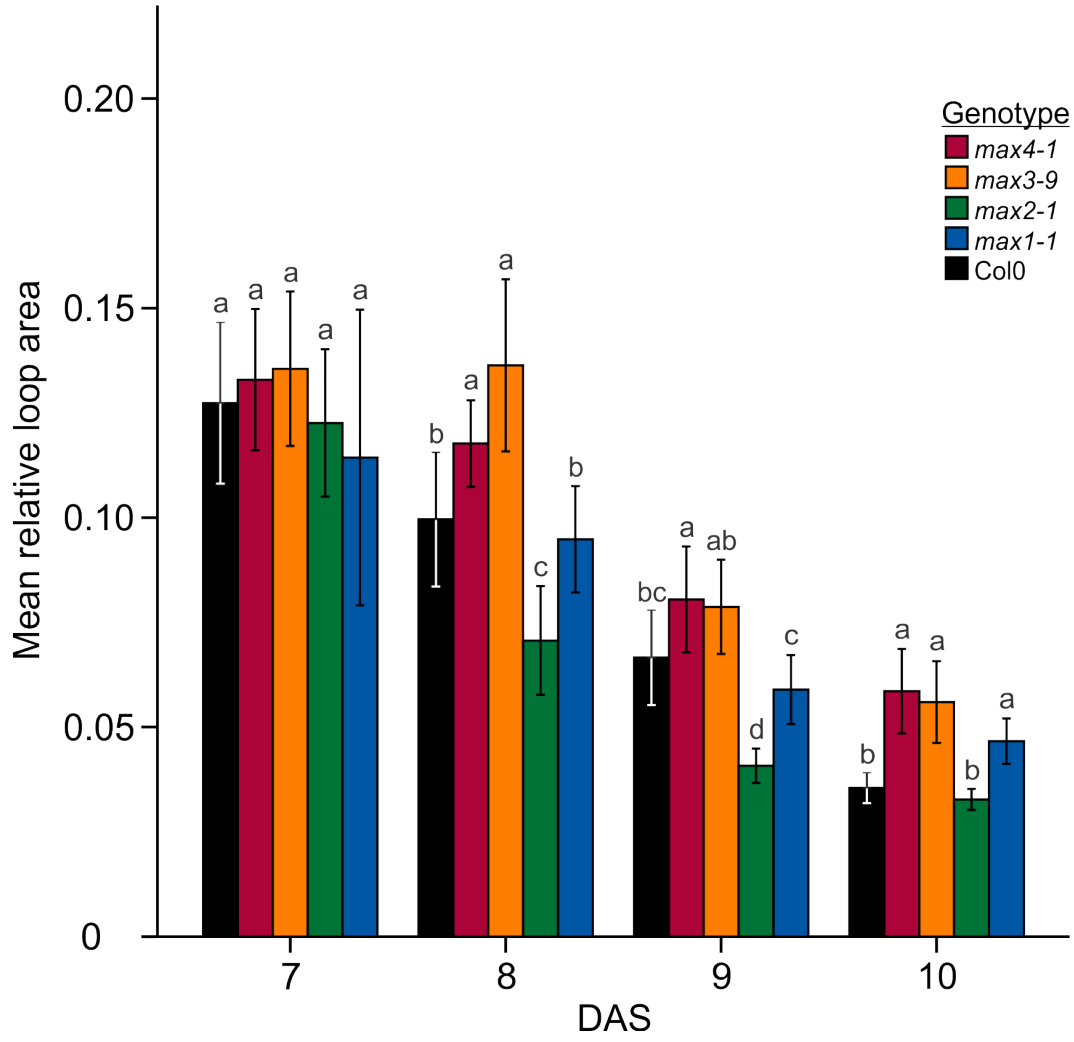

Figure 4.8: Mean relative loop areas from DAS7 to DAS10 for five genotypes; *max4-1*, *max3-9*, *max2-1*, *max1-1* and Col0. Mean leaf data (15 leaves per stage per genotype) are shown as a function of developmental stage in DAS (days after sowing). Asterisks indicate statistcal significance ($P<0.05$).

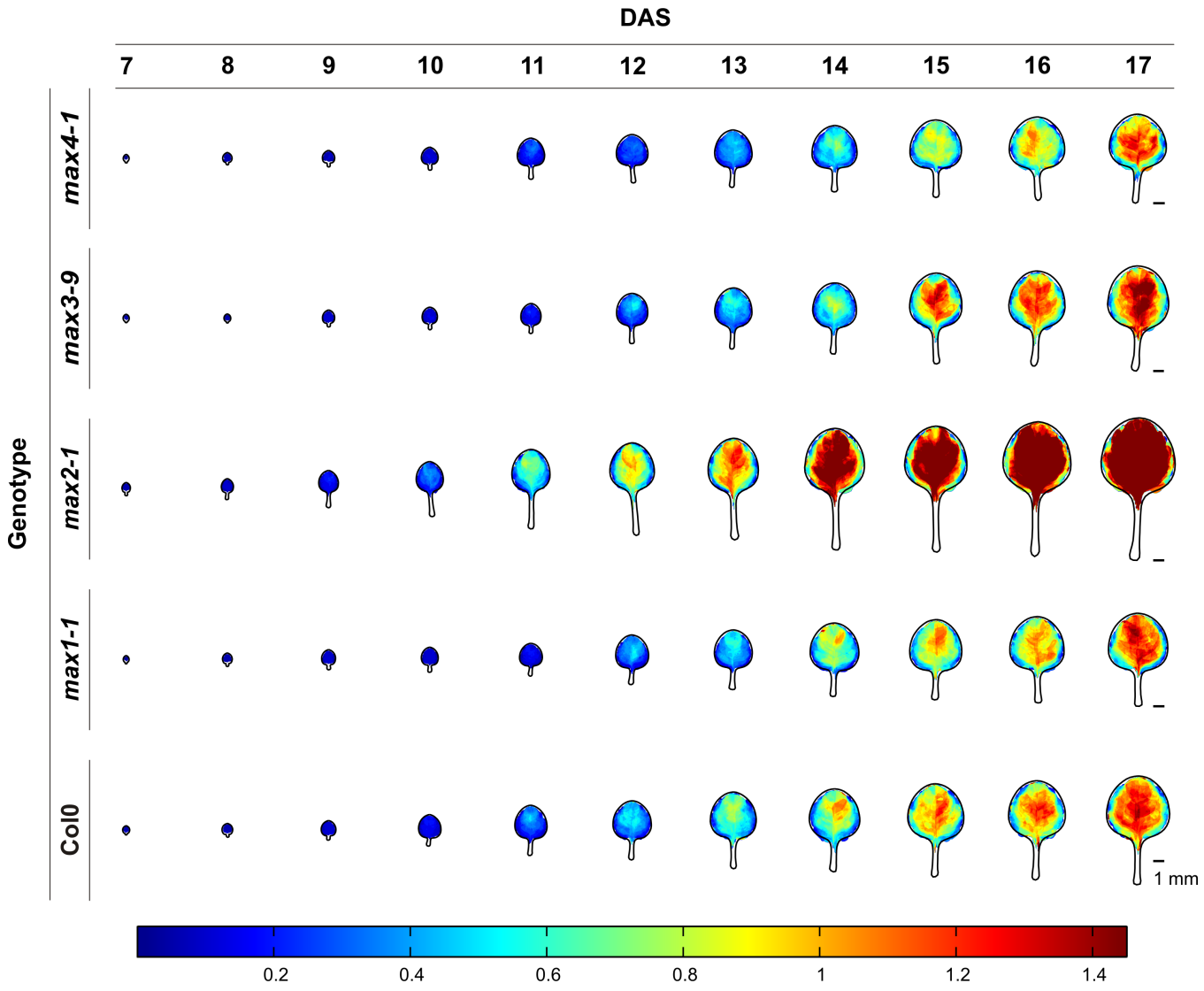

Figure 4.9: Contour maps showing spatial variation of relative loop areas from DAS7 to DAS17 for each genotype. A common color code is given, below the maps, for the whole period analyzed where dark red represents regions with the largest relative loop areas and dark blue the regions with the smallest relative loop areas. Each map is scaled to size with the scale bars indicating the length of 1 mm on the right. For each genotype, 15 leaves per stage.

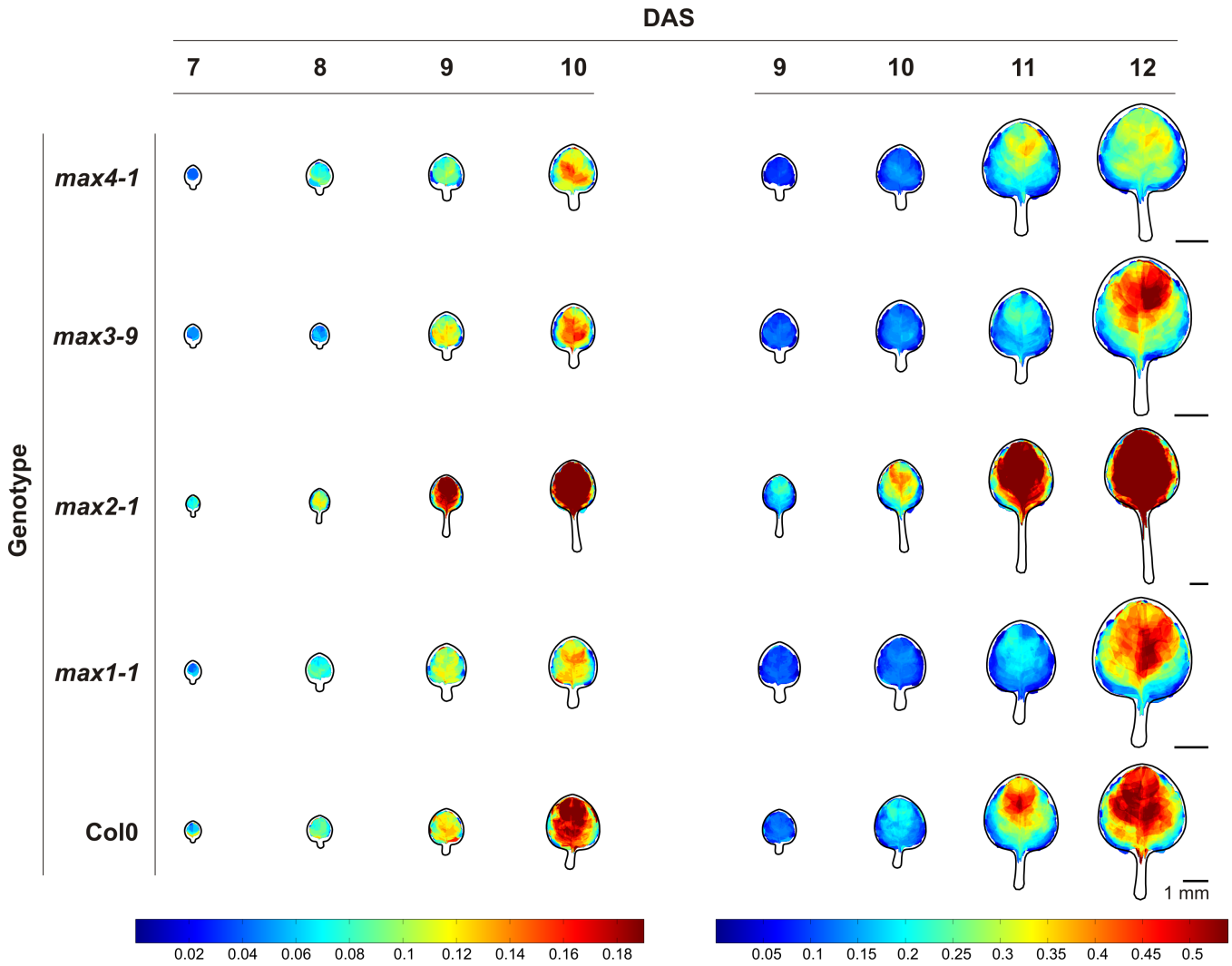

Figure 4.10: Maps showing the spatial variation in relative loop areas, with an adjusted color code (below maps) to reveal spatial heterogeneities at each time point. The stages are separated into 2 groups with overlapping DAS (DAS9 and DAS10). Each map is scaled to size with the scale bars indicating the length of 1mm on the right. For each genotype, 15 leaves per stage.

A non-parametric analysis of variance (Kruskal-Wallis test) on the relative loop areas with day as a factor showed a significant decrease in loop areas from DAS7 to DAS11 for Col0 (χ^2= 60.496, df= 4, P<0.05), *max4-1* (χ^2= 52.085, df= 4, P<0.05) and *max1-1* (χ^2=49.726, df= 4 , P<0.05) before leveling off from DAS11 to DAS17 (χ^2= 2.140, df= 6, P= 0.906; χ^2= 8.387, df= 6, P= 0.211 and χ^2= 4, df= 6, P= 0.677 respectively). However, in *max3-9*, relative loop areas were not significantly different from DAS7 to DAS8 (χ^2= 0.123, df= 1, P=0.725), but a significant decrease in loop areas was observed from DAS8 to DAS12 (χ^2= 56.005, df= 4 , P<0.05), which was later on maintained from DAS12 to DAS17 (χ^2= 3.109, df= 5, P=0.683). As for *max2-1*, relative loop areas significantly decreased from DAS7 to DAS10 (χ^2= 46.409, df= 3, P<0.05) and were not significantly different from DAS10 to DAS17 (χ^2= 10.755, df= 7, P= 0.150).

Differences in relative loop areas (Figure 4.7) were analyzed by carrying out a non-parametric Mann-Whitney U test between the wild type and mutant as well as between the different mutant lines for each day from DAS7 to DAS17 (see Appendix D). The results of the relative loop areas of *max* mutants and wild type for each day are summarized in Table 4.1 based on the statistical results in Appendix D. In general, at early developmental stages, *max4-1* had the largest loop areas followed by *max3-9*, *max1-1*, Col0 and finally *max2-1*. At later developmental stages (after DAS11), *max2-1* caught up and had larger loop areas than the other mutants while Col0 still remained as the plant genotype with the smallest loop areas.

4.8 Angle measurements

Relative angles were measured between the midvein and the secondary veins using a Matlab (The Mathworks Inc., http://www.mathworks.com/) program written by Dr. Rolland-Lagan. For each branching point found along the midvein, three angle measurements were obtained and sorted as small (α_{12}), intermediate (α_{13}) and large (α_{23}) (Figure 4.11) (see Appendix E for more information on the general steps performed by program). The mean of the smaller relative angle for each day is shown in Figure 4.12 where each *max* mutant is compared to the wild type; Figure 4.12a for *max4-1*, Figure 4.12b for *max3-9*, Figure 4.12c for *max2-1* and Figure 4.12d for *max1-1*. A Mann-Whitney U test was conducted in order to prove the prediction that the smallest relative angle of accelerated auxin transport mutants would be bigger than the wild type. The results of the test were in the expected direction for *max3-9* and *max1-1* but not for *max4-1* and *max2-1*. The mean of the smaller relative angle of *max3-9* was significantly higher than Col0 for DAS9, 11, 12, 13, 15 and 16 (Mann-Whitney U test, p>0.05, see Appendix F). Similarly, *max1-1* showed a higher mean of the smaller relative angle at DAS9, 10, 12, 13 and 14 (Mann-Whitney U test, p>0.05, see Appendix F). *max2-1* only had a day, DAS9, where the mean of the smaller relative angle was higher than Col0 while *max4-1* had two days, DAS10 and DAS11 (Mann-Whitney U test, p>0.05, see Appendix F) where this was the case. To verify these results, spatial variations in angles were quantified throughout the period analyzed showing no clear differences (Figure 4.13).

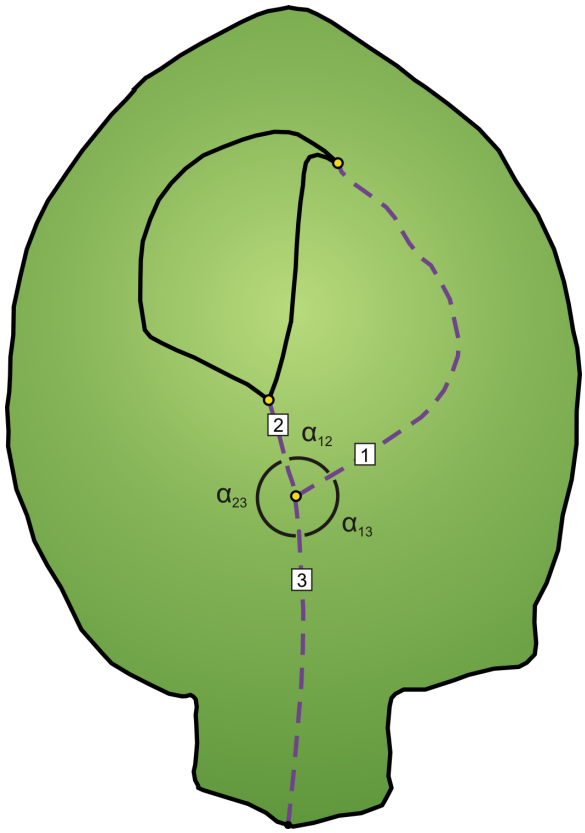

Figure 4.11: Method of calculation of relative angles. At each branching point (yellow circle - junction where three segments (1, 2 and 3) meet) the small (α_{12}), intermediate (α_{13}) and large (α_{23}) relative angles were calculated from absolute angles (See appendix E for detailed method of calculation).

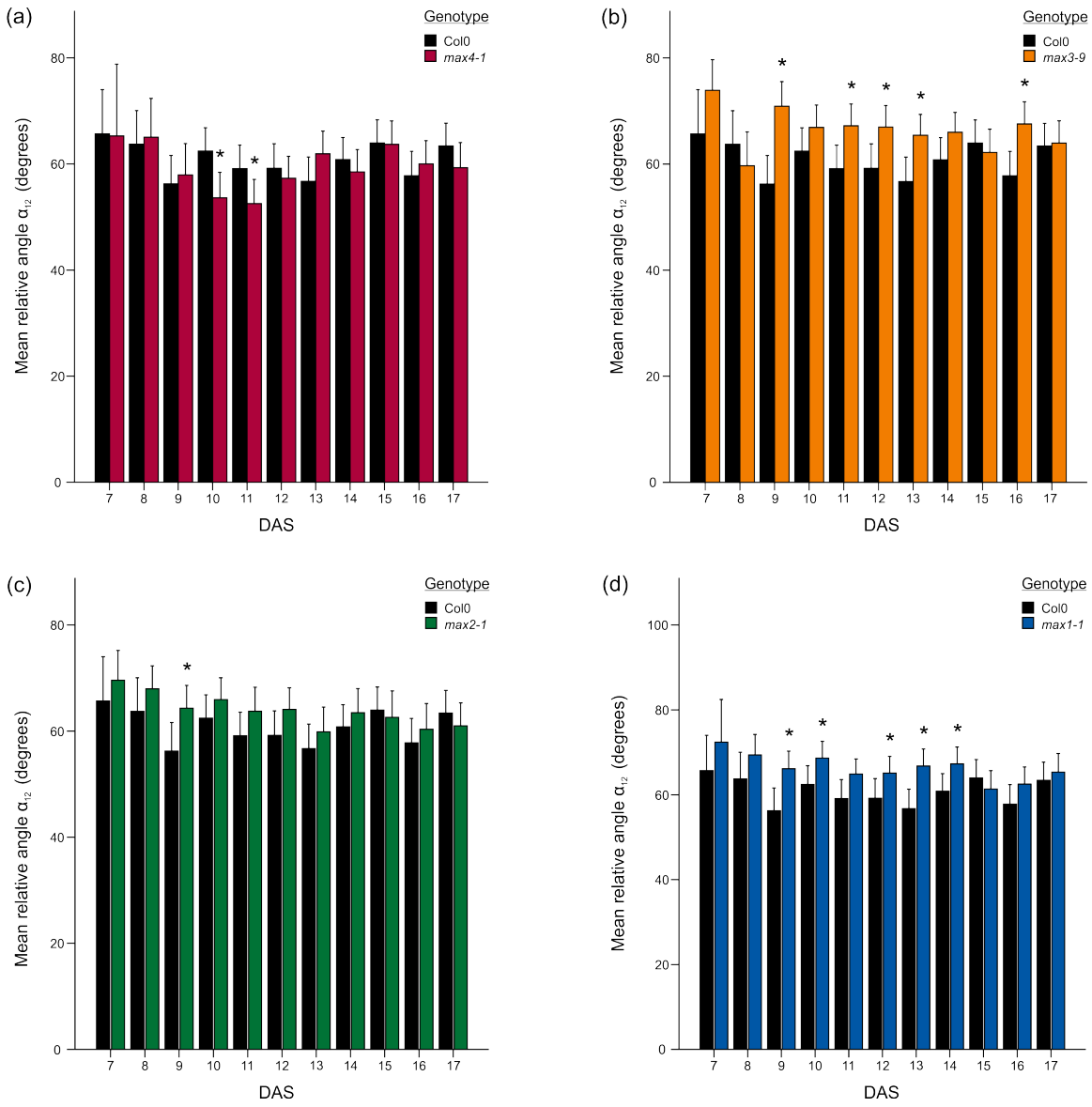

Figure 4.12: Mean relative angles α_{12} (degrees) of (a) *max4-1*, (b) *max3-9*, (c) *max2-1* and (d) *max1-1* each compared to the wild type Col0. Mean angle data measured along the midvein (of 15 leaves per stage per genotype) are shown as a function of developmental stage in DAS. Error bars indicate the standard error of the mean.

Table 4.1: Simplified results of relative loop areas following statistical analysis on wild type and *max* mutants data. For each day, genotypes are ordered from biggest to smallest according to their loop size taking into consideration leaf size. The wild type (Col0) and the *max* mutants (*max4-1*, *max3-9*, *max2-1* and *max1-1*) are marked by different colors to demonstrate qualitatively their auxin transport capacity. The red represents the fastest auxin transport, the orange the second fastest auxin transport, the green shows slower auxin transport, the blue slightly slower than the green and black the slowest.

DAS	Genotypes
7	*max4-1* = *max3-9* = *max2-1* = *max1-1* = Col0
8	*max4-1* = *max3-9* > *max1-1* = Col0 > *max2-1*
9	*max4-1* > *max1-1* = Col0 > *max2-1* *max3-9* = *max4-1* *max3-9* = Col0 *max3-9* > *max2-1* *max3-9* > *max1-1*
10	*max4-1* = *max3-9* = *max1-1* > *max2-1* = Col0
11	*max3-9* > *max4-1* = *max1-1* > Col0 *max2-1* > Col0 *max2-1* = *max4-1* *max2-1* = *max3-9* *max2-1* = *max1-1*
12	*max2-1* > *max3-9* = Col0 *max4-1* = *max3-9* & *max2-1* & *max1-1* *max1-1* = *max3-9* & *max2-1* & Col0
13	*max2-1* > *max4-1* & *max3-9* & Col0 *max1-1* = *max4-1* & *max3-9* & *max2-1* *max1-1* > Col0 *max4-1* = *max3-9* = Col0
14	*max2-1* > *max4-1* = *max3-9* = *max1-1* = Col0
15	*max2-1* > Col0 = *max3-9* *max4-1* & *max1-1* > Col0 *max4-1* = *max3-9* & *max2-1* & *max1-1* *max1-1* = *max2-1* > *max3-9*
16	*max2-1* > *max4-1* = *max3-9* = *max1-1*
17	*max4-1* = *max2-1* = *max1-1* > Col0 = *max3-9*

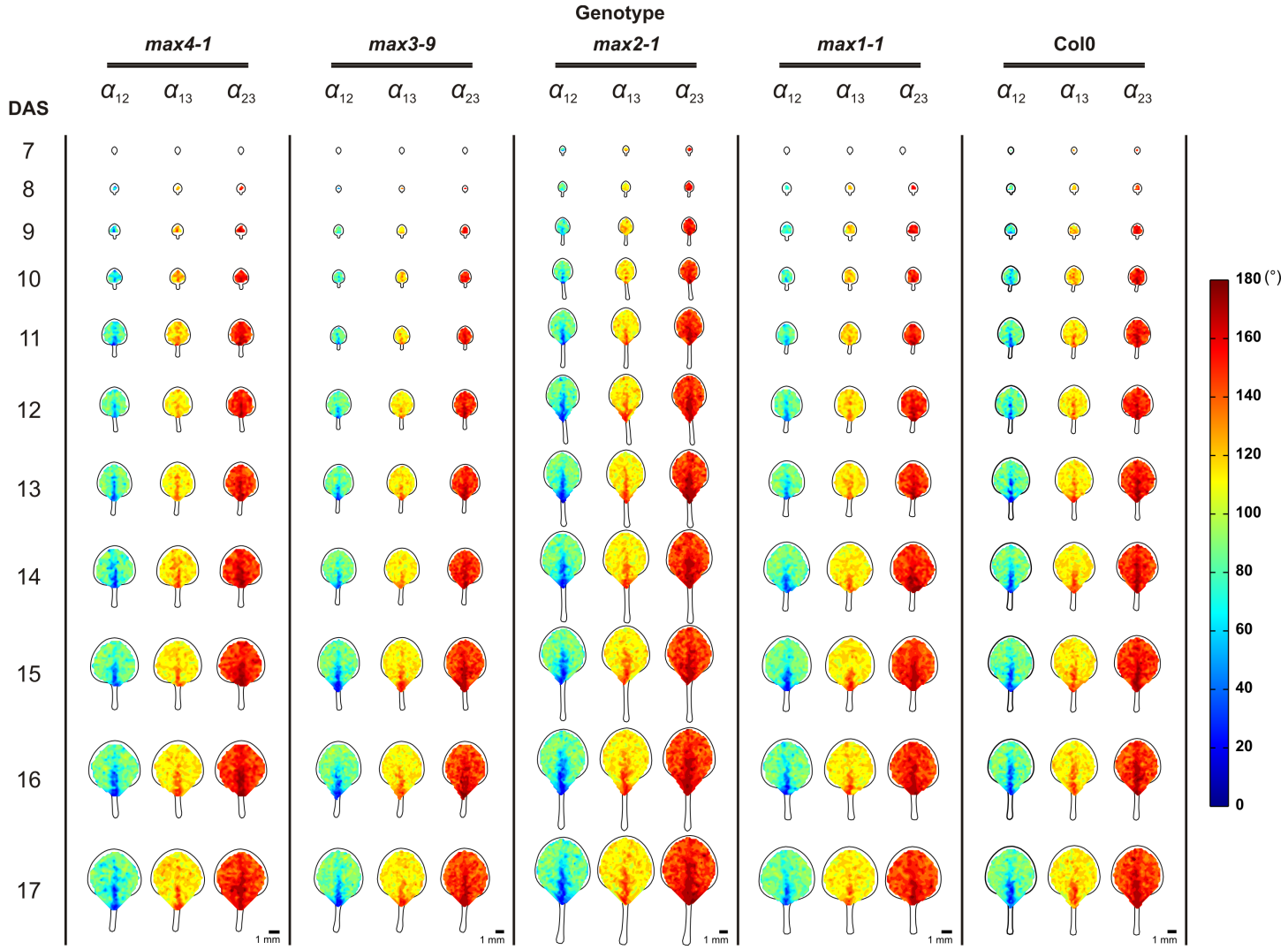

Figure 4.13: Maps showing spatial variation in relative angles (α_{12} - small, α_{13} - intermediate and α_{23} - large) of *max4-1*, *max3-9*, *max2-1*, *max1-1* and Col0 from DAS7 to DAS17 (n=15 leaves per stage). Legend for the maps is displayed to the right. Angles are in degrees.

4.9 Multivariate analysis

A discriminant analysis was conducted to investigate differences between the five genotypes based on the different measured leaf parameters, indicating which parameters contribute most to the group separation. The leaf parameters were area of the blade, shape of leaf blade, loop numbers, segment numbers, vein density, branching point density and free vein ending density. Plant genotypes were Col0, *max4-1*, *max3-9*, *max2-1* and *max1-1*. An evaluation of assumptions of multivariate analysis revealed that only linearity among the pairs of variables within each group was respected and not that of normality. The multivariate analysis was done for each day but only two days (DAS8: early in development and DAS13: later in development) out of seventeen were chosen to first demonstrate how genotypes differed with respect to the measured leaf parameters and second to show the variability that existed throughout the developmental stages.

For DAS8, four discriminant functions were calculated, with a combined $\Lambda = 0.109$, $\chi^2(28) = 150.531$, $p<0.05$. After removal of the first function ($\Lambda = 0.376$, $\chi^2(18) = 66.571$, $p<0.05$), the second function ($\Lambda = 0.662$, $\chi^2(10) = 28.000$, $p<0.05$) and the third ($\Lambda = 0.684$, $\chi^2(4) = 9.946$, $p<0.05$) there was still strong association between groups and variables. The four discriminant functions accounted for 66.6%, 20.8%, 8.3% and 4.3%, respectively, of the variance. The loading matrix of correlations between the variables and discriminant functions, as seen in Table 4.2, suggested that the number of segments, the number of loops and the size of the leaf blade loaded more highly on the first function ($r = -0.725$, $r = -0.638$, $r = -0.538$ respectively) than the second while the shape of the

leaf, the vein density and the free vein ending density loaded more highly on the second function (r= -0.645, r= 0.496, r= 0.484 respectively) than the first. The branching point density loaded fairly evenly onto both functions (r= -0.314 for the first functions and r= 0.235 for the second). As shown in Figure 3.13a, the first discriminant function maximally separates *max2-1* from the other four groups. The second discriminant function discriminated *max3-9* from Col0, *max4-1* and *max1-1*, with *max2-1* falling between these groups.

Table 4.2: DAS08 Loading matrix

	Function	
Pattern parameters	1	2
Segment number	-.725	-.109
Loop number	-.638	-.131
Blade area	-.538	-.346
Leaf shape	-.399	-.645
Free vein ending density	-.032	.484
Vein density	-.209	.496
Branching point density	-.314	.235

For DAS13, four discriminant functions were also calculated, with a combined Λ= 0.031, $\chi^2(28)$= 235.192, p<0.05. After removal of the first function (Λ=0.235, $\chi^2(18)$=98.611, p<0.05), the second function (Λ=0.473, $\chi^2(10)$=50.911, p<0.05) and the third (Λ=0.759, $\chi^2(4)$=18.760, p<0.05) there was still strong association between the groups and variables. The four discriminant functions accounted for 76.9%, 12.1%, 7.2% and 3.8%, respectively, of the between group-variability. In Table 4.3, the loading matrix of correlations between the variables and discriminant functions demonstrated that the leaf

blade size, the vein density, the branching point density as well as the free vein ending density loaded more highly on the first function (r=0.836, r=-0.628, r=-0.535, r=-0.421 respectively) than on the second. On the other hand, the leaf shape, leaf blade area and the number of loops loaded highly on the second function (r=0.572, r=-0.420, r=-0.414). The discriminant function plot (Figure 3.13b) showed that the first function discriminated *max2-1* from Col0 and from the remaining other three groups together (*max4-1*, *max3-9*, *max1-1*). The second discriminant function segregated Col0 from *max2-1*, *max3-9* and *max1-1* with *max4-1* falling between these groups.

Table 4.3: DAS13 Loading matrix

	Function	
Pattern parameters	1	2
Blade area	.836	-.420
Vein density	-.628	.117
Branching point density	-.535	.200
Free vein ending density	-.421	.308
Segment number	-.079	-.307
Leaf shape	.112	.572
Loop number	-.117	-.414

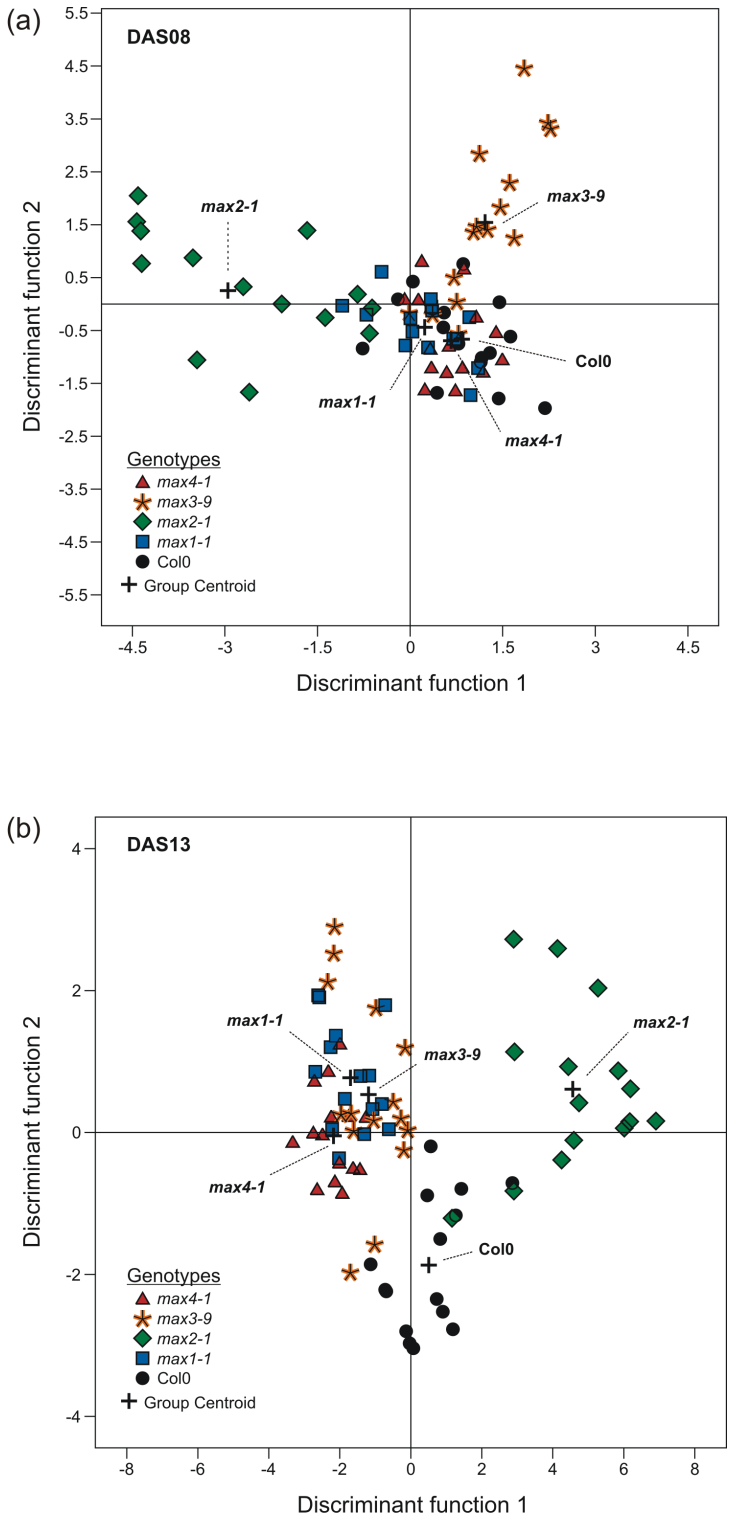

Figure 4.14: Discriminant function analysis of five plant genotypes (*max4-1*, *max3-9*, *max2-1*, *max1-1* and Col0) at (a) DAS8 and (b) DAS13 based on different measured leaf parameters such as leaf area, shape of leaf blade, loop numbers, segment numbers, vein density, branching point density and free vein ending density.

Chapter 5

Discussion

Despite the accumulating data on genes implicated in vein pattern formation, the mechanism controlling when and where veins form remains unknown. The pioneering work of Sachs (1969) on vein pattern formation involved pea stems and roots while today many experimental and theoretical studies focus on leaves. Yet, does the process of vein patterning occur similarly in pea stems and roots as in Arabidopsis leaves? In this present study, we used quantitative methods previously developed in the lab to test whether canalization, a mechanism for vein pattern formation originally proposed by Sachs, is likely to drive leaf vein formation.

The canalization hypothesis, initially formulated from the notion that veins are induced by the flow of auxin through a tissue (Sachs (1969)), assumes that there is a positive feedback regulation where the ability of cells to transport auxin is reinforced, and that the flux of auxin through cells promotes vein differentiation (Sachs (1981)). If

indeed the canalization process is the mechanism by which veins form, we expect with our accelerated auxin transport mutants (main vein unsaturated due to fast auxin flow) to observe angle measurements that are bigger than samples with fairly saturated primary midvein such as the wild type (since compared to the mutants, newly forming veins are attracted lower down the midvein where auxin concentration is believed to be low).

The comparaison of leaf pattern parameters (such as the leaf size, leaf shape, vein density, loop number, segment number and relative loop areas) of mutants with enhanced auxin transport and of the wild type show that proper transport of auxin is required for normal leaf development. On the other hand, angle meaurements between the primary and secondary veins of mutants and wild type are similar and therefore our results are not consistent with an auxin canalization process identical to the one proposed by Sachs in pea stems and roots.

5.1 Effect of accelerated auxin transport on leaf development

5.1.1 Leaf size

The mean blade area (mm^2) of *max4-1*, *max3-9*, *max2-1*, *max1-1* and Col0 increased over time. The *max4-1*, *max3-9* and *max1-1*, with higher auxin transport capacity than the wild type, had slightly smaller leaf blade areas than Col0. However, *max2-1* had bigger leaves than all four plant types (Figure 4.1). Knowing that plants grown in the

presence of an auxin transport inhibitor led to smaller sized leaves (due to high auxin concentration in the surroundings), we predicted that the wild type would also have smaller blade areas than the *max* mutants because of slower auxin transport. Therefore, we expected *max4-1*, to have the largest leaf areas followed by *max3-9*, *max2-1*, *max1-1* and finally Col0 with the smallest leaf sizes. Our results showed partial contradiction with the above predictions in that *max4-1*, *max3-9* and *max1-1* had smaller leaves than Col0 while *max2-1* had larger leaf sizes than all genotypes.

The role of the growth-regulating substance, auxin, in leaf expansion is still poorly understood. Multiple studies on leaf growth of various plant species report conflicting results when leaf auxin content is increased above endogenous levels. Tissue growth is observed in excised interveinal strips from growing tobacco (*Nicotiana tabacum* L. cv Xanthi) leaves incubated in α-naphthalene acetic (NAA) or IAA (Keller & Van Volkenburgh (1997); Keller & E (1998)) and in intact young leaves or cut out leaf discs from bean (*Phaseolus vulgaris*) plants applied with auxins (Lippincott & Lippincott (1971); Hayes & Lippincott (1976); Hayes (1977)). In both cases, the leaves exhibit increased growth on one surface side causing curvature. However, in transgenic plants overproducing auxin such as the Arabidopsis *superroot1* and *superroot2* mutants (Boerjan et al. (1995); Ljung et al. (2001)) and petunia (*Petunia hybrida*), the increase in auxin concentration leads to smaller and narrower leaves than the wild type (Klee et al. (1987)). For both of these latter studies, auxin is superabundant throughout the plant and therefore the observed outcome of leaf growth may be due to other auxin-induced changes to

whole-plant development. A study by Keller and others (2004) investigated the effects of localized aqueous auxin application on leaf blade expansion of intact common bean and Arabidopsis plants. Common beans exposed to naturally occurring auxin (IAA) or the synthetic form (NAA), have reduced leaf sizes as a result of slower expansion than normal. Inhibition of auxin transport (NPA) to the petiole of intact plants results in smaller leaf sizes compared to the control due to high endogenous auxin levels present within the leaf.

Our quantitative data on leaf size possibly follows a dose dependent trend (Figure 5.1a). The effect of different concentrations of exogenous auxins on tobacco cells results in a bell-shaped curve where at very low and very high concentrations, cell division is decreased (Campanoni & Nick (2005)). This typical curve for many auxin responses is also seen in Arabidopsis roots where high concentrations of auxin inhibits cell expansion (Evans et al. (1994)). Since *max* mutants transport auxin at a faster rate compared to the wild type, we can expect that auxin is less available in the tissue (because it is transported away from the leaf faster), leading to the formation of smaller leaves. Conversely, plants in the presence of the auxin transport inhibitor, NPA, have stunted leaf morphology (Sieburth (1999)) due to higher than normal levels of auxin which leads to toxic side effects such as inhibition of growth (Mattsson et al. (1999)). Our data shows that the wild type with normal auxin transport does not lead to the largest leaf size (Figure 5.1b) but instead the accelerated auxin transport mutant *max2-1* as confirmed by Shen and others (2007) (See Figure 1 in Supplemental data). Further tests on auxin levels present

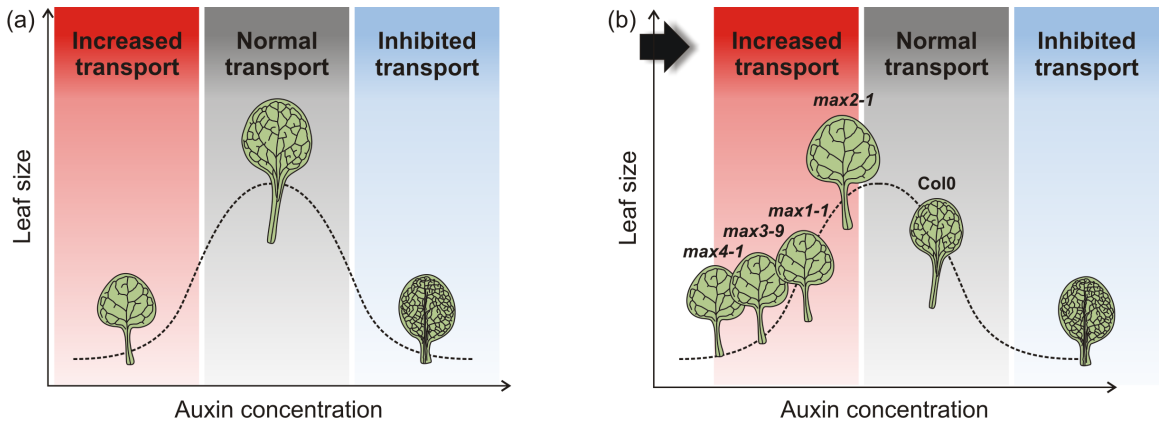

Figure 5.1: Schematic representations showing the effect of different auxin transport capacities on growth of Arabidopsis leaves. This follows a bell-shaped dose-response curve. (a) At low and high concentrations leaf size is small and at medium concentration leaf area is bigger. Mutants with increased auxin transport (red shaded area) have lower auxin levels compared to the wild type (gray shaded area). On the contrary, artificially impaired plants treated with NPA (blue shaded area) have high levels of auxin due to the accumulation of this phytohormone. From the auxin response model in (a) it is expected that *max* mutants will have smaller leaf blade area compared to the wild type. (b) Consistent with our predictions, *max4-1*, *max3-9* and *max1-1* are slightly smaller in leaf size compared to the wild. However *max2-1* has larger leaf area than both Col0 and the other three *max* mutants. These results could be explained by a possible shift to the right (black arrow) of the different plant types along the bell shaped curve.

in leaves of each plant genotype would validate this predicted model. Moreover, a closer look at the cellular level between each plant genotype could clarify whether (1) there is an increase in cell proliferation or a decrease in cell expansion or (2) a compensation mechanism occurs whereby (a) a decrease in cell number below a threshold triggers an increase in cell volume or (b) an increase in cell volume is compensated by a decrease in cell number.

5.1.2 Leaf shape

Observations of leaf blade shapes from images of wild type and mutants show no major differences. However, after plotting curve lines and conducting statistical tests there are slight variations in leaf morphology. The mutants that have an elongated leaf shape are *max1-1*, *max3-9* and *max2-1* with the latter being more elongated than the other two. Throughout most of the developmental stages, the leaf shape of the wild type is round. As for *max4-1*, leaf shape in early stages of development is similar to Col0 but later became wider. We had predicted that *max* mutants would be more elongated than the wild type. Surprisingly, the mutant with the most accelerated auxin transport, *max4-1*, did not coincide with our predictions.

Leaf size and leaf shape are both regulated by genetic, developmental and environmental factors (Tsukaya & Horiguchi (2005)); however, leaf size is determined by the overall amount of growth while leaf shape is defined by differential growth. During early stages of development of the leaf primordia (primary morphogenesis) cell division predominates while in later developmental stages, the leaf reaches the final shape and size (secondary morphogenesis) by both cell division and cell expansion with the latter mostly prevailing. The direction in which these two processes occur is also significant in establishing the final shape of the leaf. Changes in leaf shape could happen, due to variations in growth, along three axes: proximal/distal (from the base to the tip of the leaf blade as seen in *max3-9*, *max2-1* and *max1-1*), medial/lateral (from the midrib to the edge of the leaf blade as seen for *max4-1*) and adaxial/abaxial (from the upper surface of the

leaf towards the under side).

There are a few possible reasons that could justify why *max2-1* has the most elongated leaf blade while *max4-1* is wider than the wild type.

Firstly, the rationale behind small variations seen in leaf shape between the wild type and *max* mutants could be that cell expansion follows, just like cell proliferation, an auxin dose-response curve where at low and high concentrations cell elongation is inhibited (Evans et al. (1994)).

Secondly, adjustment of the final leaf shape, taking place during the last stages of leaf development, can be further modified based on environmental conditions. As reviewed by Volkenburgh (1999), light is one among many factors that contribute to leaf expansion. Perhaps the reason *max2-1* has a more elongated leaf morphology and larger lamina area than the other plant types analyzed relies on the fact that the *MAX2* gene functions also in light signaling (Shen et al. (2007)).

Thirdly, the elongated shape of most *max* mutants at early developmental stages is comparable to the results obtained with the transgenic Arabidopsis line over-expressing the *PIN1* gene under the caulifower mosaic virus 35S promoter when analyzed relative to its wild type L*er* (Landsberg *erecta*, stock name: CS24596) (Mira Amin, unpublished data). Auxin transport is also increased in this line due to the ubiquitous expression of PIN1 proteins in the cells of the whole plant. Future work would require collecting quantitative measurements on leaf shape to verify whether these trends (slightly elongated to similar shape as the wild type) are general across other mutants with accelerated auxin

transport.

5.1.3 Vein density, loop and segment number

The process of vein patterning occurs in three distinct phases. Timing of these phases varied between genotypes (Figure 5.2). In the first phase vein density was either constant or increased and then became constant. This "patterning phase", indicated that vein formation proceeded while the leaf was still growing. In the second phase, vein density started to decrease and at the same time loop numbers and segment numbers were still continuing to increase. In this "transition phase", vein patterns continued to form but at a slower rate. Patterning therefore slowed down overall with regard to growth. Finally, in the "growth phase", the vein pattern simply enlarged as the leaf carried on growing. Analysis on vein density was therefore concentrated on earlier days of development (first and second phase) when veins were still being formed.

In contrast to the vein density of leaves exposed to NPA, we expected that the *max* mutants with faster auxin transport would have a lower vein density compared to the wild type. Visually, trends showed that all mutants with the exception of *max2-1* had lower vein density at early developmental stages and higher vein density than Col0 at later days. Statistically, *max4-1* and *max3-9* had lower densities than Col0 in the first few days and *max2-1* and *max1-1* were similar to the wild type. Across the days, there were no major differences in vein density observed between genotypes. Nonetheless the small increase in vein density of *max4-1* and *max3-9* demonstrated veins formed faster

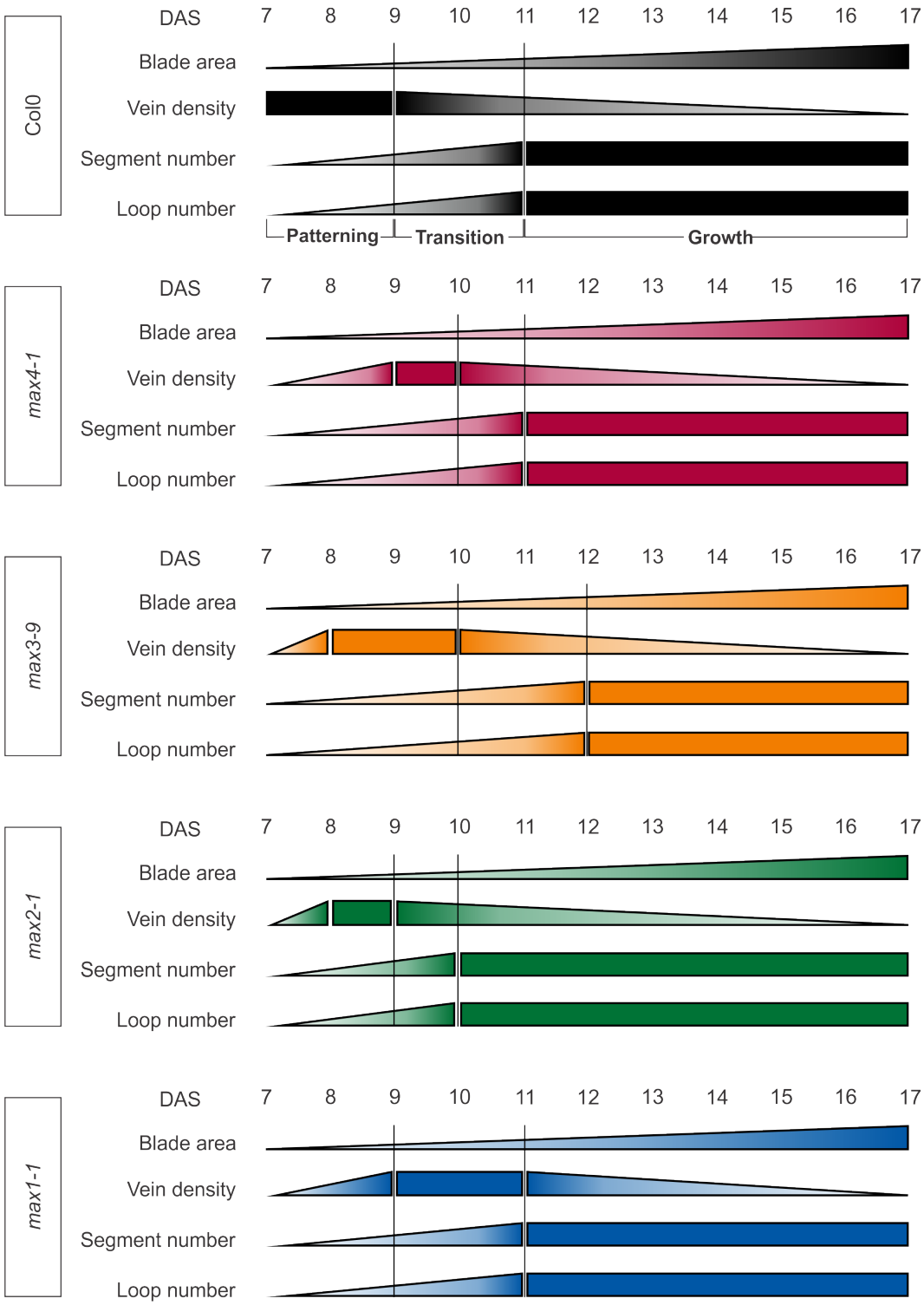

Figure 5.2: Relative timing of patterning and growth for all five genotypes: *max4-1*, *max3-9*, *max2-1* and *max1-1* from DAS7 to DAS17. Patterning occurs in first phase while the leaf is growing for example from DAS7 to DAS9 for *max4-1*. The second phase is characterized by patterning slowing down relative to growth and the third phase is growth only.

than the wild type. Vein density decreased in later days for all *max* mutants and wild type and this is explained by the growth phase where patterning has halted and the leaf was simply expanding. The *max4-1*, *max3-9* and *max1-1* in later days had higher vein density compared to the wild type possibly because the patterning rate was faster. Additionally, the formation of late free ending veins or reconnecting veins can alter the vein density of the original pattern that has already been established from the beginning (Scarpella & Meijer (2004); McKown & Dengler (2009)).

Vein pattern formation is also tightly linked to cell proliferation (Kang et al. (2007)). As previously discussed, the greater leaf size seen in the *max2-1* mutant, conceivably because of faster growth than the wild type, is justified by the auxin-dependent dose bell-shaped curve. Kang and co-workers (2007), used Arabidopsis leaves with genetically modified cell proliferation patterns to study the role of cell proliferation during vein order formation. Gain- and loss-of-function of genes that modulate cell proliferation in leaves, ANT (AINTEGUMENTA) and ICK1(INHIBITOR OF CYCLIN DEPENDENT KINASE1), were examined and compared to the wild type. The increase of cell division in developing organs (*35S::ANT*) is accompanied by a slight increase in the number of secondary veins and in the number of branching points relative to the wild type. On the other hand, with reduced cell proliferation (*ant-1* and *35S::ICK1*) fewer secondary veins formed and a significant decrease in the number of branching points is observed. Hence, an elevated number of branching points implies an increase in the number of vein segments leading to the formation of more loops as demonstrated by *max2-1*. These

findings certainly suggest that the formation of vein patterns along with cell division and expansion involves many factors in coordinating all three processes together (Dengler & Kang (2001); Hu et al. (2003); Beemster et al. (2006); Kang et al. (2007)).

5.1.4 Relative loop areas

The different leaf sizes among genotypes made it difficult to directly compare differences in areolar areas. For this reason, relative loop areas were calculated to facilitate the analysis. Little research has been conducted to test the relationship between auxin and loop sizes. One study only compared estimated loop areas of different grass species (monocots) (Ueno et al. (2006)). However, with dicots (Arabidopsis), several researchers showed that leaves oversupplied with auxin (whether by exogenous local application or using transport inhibitors), have smaller loops relative to the wild type because the space between auxin convergence points in the epidermal layer is reduced (Mattsson et al. (1999); Sieburth (1999); Scarpella et al. (2006)). In *max* mutants, auxin transport capacity is higher than the wild type and for this reason no substantial amounts of auxin accumulation occurs in the leaves as with pharmacologically treated plants. Our expectations are confirmed as *max4-1*, the mutant with the most increased transport of auxin (with *max3-9* closely following), have in general larger relative loop areas than *max2-1*, *max1-1* and Col0. Leaf growth of *max2-1* is much more advanced than all other genotypes and this may have affected the rate of loop formation and subdivision. In comparison with the other genotypes, the smaller relative loop areas of *max2-1* may

be associated with increased speed of vein patterning and growth of leaf tissue. It is also interesting to note that the relative loop area curves of *max* mutants are either separated from or overlapping with one another according to the position at which the *MAX* genes are found in the biosynthetic pathway. More precisely, mutations in the MAX genes at the *MAX4*, *MAX3* and *MAX1* (involved in strigolactone synthesis) loci have higher relative loop area values than leaves with an altered MAX2 locus, responsible in mediating perception. Plants with a modified *MAX4* or a *MAX3* gene (the only two members of the CCD family) have higher auxin transport capacity than the other genotypes and also have similar relative loop sizes. The *max1-1* mutant shows smaller relative loop areas than *max4-1* and *max3-9* being that the *MAX1* gene, which encodes a cytochrome P450 family member, acts downstream of *MAX4/3* (Booker et al. (2005)).

5.1.5 Variability of data

It is evident from leaf pattern parameter plots (Figure 4.1) that all genotypes follow similar trends however considering the shape of the curves it appeared that lines were shifted a little, either to the left or to the right of the wild type. On this account, comparing mutants requires to have a developmental series of data rather than performing single day analyses between mutant-mutant and mutant-wild type. From one time point it is possible to find, for example, that vein density is higher in a genotype than in another when in fact this is only true for a very limited developmental period. To further verify these observations, a discriminant function analysis is used to visualize the separation

of the different plant genotypes in multidimensional space according to the variation of different leaf parameters for a given day. As expected, plant groups in DAS08 cluster together differently than in DAS13. The formation of vein patterns in leaves happens *de novo* and the position and timing of initiation of the first procambial strand is largely unpredictable (Scarpella & Meijer (2004)). This inherent variability in leaves entails the usage of multiple individual samples to be analyzed for each day. Therefore, it is insufficient to make any qualitative or/and quantitative deductions based on individual samples nor is it highly favorable to use many sacrificed plants for a single developmental stage. A more effective way to characterize the highly variable vein pattern networks is by tracking the same leaf over time for multiple samples (Rebecca Assaf, unpublished).

5.2 Canalization hypothesis in leaves

The majority of angles measured between the primary and secondary veins are not significantly different between mutant and wild type. Moreover, spatial maps indicate the formation of smaller angles between the midvein and the secondary veins at the center-base of the leaf for all genotypes with no other differences throughout the leaf blade. Based on Sachs' experiments, we predicted that secondary veins of *max* mutant leaves would join the primary vein at a larger angle than the wild type, if the formation of veins occurred through canalization. Although graphs showing vein angles suggested that our prediction was correct, statistical analysis shows that the angles at which veins connect are not significantly different between wild type and mutants for the majority of the days

analyzed.

5.2.1 Higher auxin transport capacity in veins does not affect the angle at which primary and secondary veins connect

In light of the fact that *max* mutants' secondary veins did not connect to the midvein at a larger angle than the wild type, one could argue that the differences in auxin transport capacities (Bennett et al. (2006)) may have not been sufficient to be reflected in differences between angles. Also, the smaller relative angles at the center-base of the leaf lamina are considerably smaller than the ones found across the whole leaf blade for the wild type as well as the mutant. This observation could be explained by the fact that growth around the blade-petiole area is anisotropic, as confirmed by the spatial maps (data not shown), where loop shapes at the distal end of the leaf are more isodiametric and more elongated at the proximal end.

Angles could reflect physical forces within the tissue as proposed by Bohn and others (2002). These authors theorize that each segment at a node pulls with a force in the direction of the segment, with a magnitude relative to the radius of the segment. The thicker the vein, the stronger the force. The angles between vein segments is also directly related to the radii. If segments are of equal radii, angles are of 120°. In the case of one very thin and two thick segments, the angle between the two thick veins is approximately 180°. To test if our data fits with the force model, vein thickness was visually examined, as the quantification of radii is beyond the scope of this thesis. Essentially, all vein

segments have similar radii throughout the leaf blade with the exception of the primary vein which appears to become thicker towards the base. Angles in the leaf lamina were not of 120°. A circumferential stretch (perpendicular force) of the midvein at the base of leaf lamina is, most probably, created by the flow of water and minerals via the xylem from the roots to the leaves by capillarity, osmosis and transpirational pull. It is possible that the midvein becomes thinner at the tip as water content is reduced due to evapotranspiration via stomata.

5.2.2 A potential mechanism explaining vein pattern formation involves biochemical and biomechanical properties

If veins in leaves do not develop by the simple drainage of auxin into narrow strands, they could possibly form by a combination of biochemical and mechanical processes. The first model of vein formation was formalized by Mitchison (1981) with two possible mechanisms: polar transport and facilitated diffusion. The movement of auxin from one cell to another is simulated in a two-dimensional rectangular grid cells of unit area. In Mitchison's polar transport model, through a feedback mechanism, the permeability of the plasma membrane increases, by the recruitment of either pumps or channels, based on high levels of auxin flux. As for the second model, auxin diffuses from one cell to another in any direction with a diffusion constant that increases with the flux. Thereafter, different canalization models such as those proposed by Rolland-Lagan and Prusinkiewicz (2005), Runions (2005), Fujita and Mochizuki (2006), Dimitrov and Zucker

(2006), Feugier and Iwasaa (2006) and Kramer (2009) have relied on available molecular data. These models are largely qualitative and have not been thoroughly tested against experimental data. In fact, quantitative results have been scarce in the literature up until the development of appropriate quantification methods (Rolland-Lagan et al. (2009); Price et al. (2011)) to allow for extraction of pattern data in two dimensions from leaf images. Taking our data into account, alternative models aside from canalization should also be considered.

A distinct type of model of vein morphogenesis was proposed which involves reaction-diffusion (Turing (1952)), a mechanism that requires the interaction of two substances (A and B). In the postulated reaction-diffusion model of vein patterning, A and B are regulated auto-catalytically and diffuse at different rates, to give rise to spatial patterns (Meinhardt (1976, 1984)). A local high concentration of a morphogen, known as an activator (A), was suggested to initiate vein differentiation in exposed cells. The increase in concentration of this substance is generated by a strong feedback on its own production rate. At the same time, A controls the production of the second substance B, termed inhibitor which diffuses in the surrounding area and down-regulates the activator. Accordingly, once the activator reaches its maximum level, a shift to the adjacent cell occurs allowing it to differentiate into a vein. To date, there has been no experimental proof showing the interaction of two chemicals to form veins in leaves.

The process by which veins form has not only been a questionable matter for developmental biologists but also for physicists. Biological growth is not entirely governed by

genetic factors but also by laws of physics. Couder and colleagues (Couder et al. (2002)), demonstrated that patterns with a net-like structure, like those found in leaf veins, can be obtained by observing cracks in a drying gel (made out of concentrated colloidal suspensions of latex particles in water) depending on the variation of gel thickness and the manner in which it desiccates. The discrete patterns produced from gel cracks, formed as the material shrinks, resembles tightly the intricately connected networks in leaves where tissue is stretched. From this, the researchers proposed that vein formation in leaves occurs in a tensorial field and put forward a hypothesis that the application of a compressive stress exceeding a certain threshold value on mesophyll cells will initiate the differentiation process that will allow them to become procambium. Based on this theory, Laguna and others (2008) devised a numerical model that generates patterns qualitatively similar to venation patterns of leaves and also demonstrated comparable statistical properties. They considered the mesophyll as an elastic layer with a highly non-linear behavior that was described using free energy in terms of an elastic field. In contrast to both of the above studies, Corson and others (2009), developed a model whereby mechanical forces drive the rearrangement of veins to form the networks. The majority of these theoretical mechanical models have not implemented much of the biochemical mechanisms of plant tissue growth. Using the current available molecular data and mechanical stress patterns known in plant tissues, we were able to put together a hypothetical mechanism to explain the formation of veins.

There is a plethora of information available on the mechanics as well as the chemical

aspects of plant cells (as outlined above, in the Introduction and Appendix G) that could not be entirely covered in this thesis. Nevertheless, we propose a possible mechanism that could explain the formation of vein patterns. It is described as follows:

(1) Consider a cell within a tissue initially composed only of undifferentiated ground meristem cells.

(2) Unequal growth around this meristemic cell could cause the neighboring cells to apply stronger mechanical forces in one direction compared to the other leading, for example, to a horizontal compression (Figure 5.3a).

(3) As a result of different mechanical forces and/or hormonal activities:

(a) Ground meristem cells could become either mesophyll or procambial cells (Sawchuk et al. (2008)).

(b) Expansion dispersed over the cell surface (polar diffuse growth) manifests as a consequence of non randomly arranged (partially affected by the impact of mechanical compression) cellulose microfibrils and microtubules (Figure 5.3b).

(4) PIN1 distribution and the orientation of the microtubule array are affected by mechanical forces (Figure 5.3c) experienced by the cell during expansion (Heisler et al. (2010); Feraru et al. (2011)).

(5) Finally, subsequent events of cell differentiation continue to happen (Figure 5.3d).

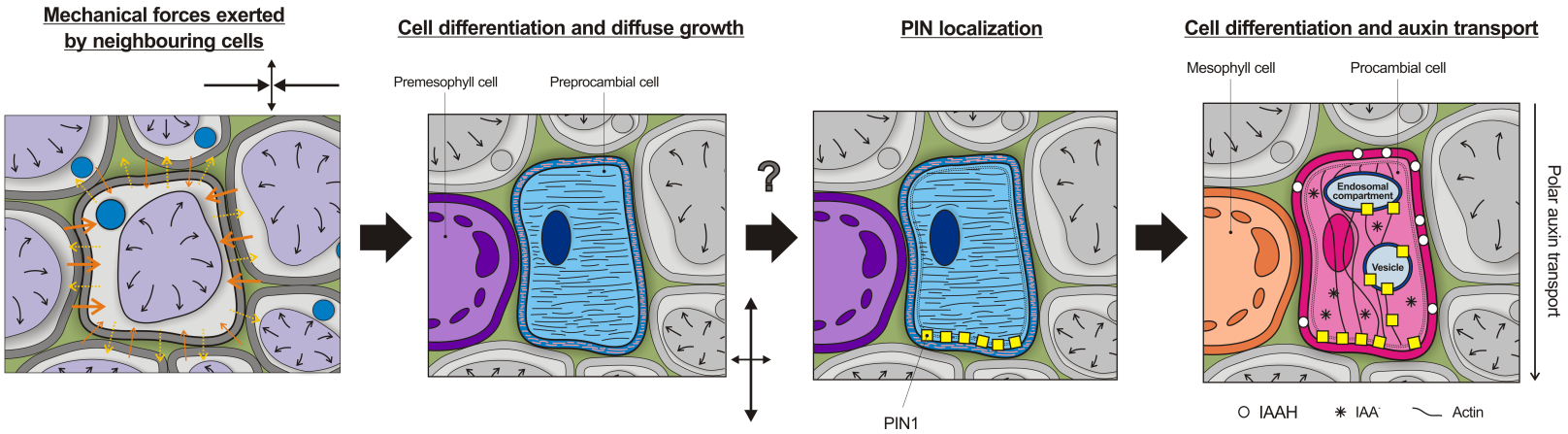

Figure 5.3: Proposed mechanism to explain vein pattern formation integrating biochemical and biomechanical properties. (a) Some of the neighbouring cells of a given ground meristem cell (middle) may exert stronger mechanical forces due to differences in tissue growth throughout the leaf leading to a horizontal compression of the cell (arrows). (b) As a result of compression, randomly organized microtubules (black segments) and cellulose microfibrils (pink segments) become arranged parallel to one another but transverse to the axis of growth (arrows) allowing the cell to elongate. A number of ground meristem cells will transition into an intermediate irreversible stage of cell differentiation either into a premesophyll (purple) or a preprocambial (blue) cell possibly caused by a hormone or mechanical forces. (c) PIN1 localization depends indirectly on the orientation of microtubule array. PIN1 proteins will be confined to an anticlinal wall that is parallel to the microtubules. (d) The cell will continue to differentiate into mesophyll (orange) and procambial (pink) and auxin is being exported by PIN1 proteins that cycle along actin filaments between an endosomal compartment, vesicle and the plasma membrane.

5.2.3 Proposed bio-mechanical and -chemical mechanism could possibly account for vein patterns observed with NPA treated plants

The mechanism of auxin transport inhibitors is still elusive. It is believed that NPA interferes with the cycling of PIN proteins and disrupts polar auxin transport (Geldner et al. (2001)). Consequently, high levels of auxin accumulate within the cells due to the improper localization of PIN proteins to the basal plasma membranes. The few studies that have investigated the effect of NPA on vein pattern formation (Sieburth (1999); Mattsson et al. (1999); O'Donnell et al. (2004); Wenzel et al. (2008)) have mainly concentrated on analyzing results at the whole leaf as well at the genetic level but not much has been researched at the cellular scale. Future experimental work would include quantifying physical cell parameters and testing whether these parameters will vary according to different auxin concentration within the cell. The formation of veins could in some way involve a feed back loop between mechanical forces and auxin.

Chapter 6

Conclusion

6.1 Main findings

The main goal of this thesis was to confirm that veins in leaves of Arabidopsis form in the same manner as they develop in pea stems and roots by canalization. Many investigators in the field have based their research on leaf venation patterns solely on Sachs hypothesized mechanism using stems and roots dating back to the late 1980s not knowing whether it is also applicable to leaves. Sections of pea roots with the main vein full of auxin resulted in some secondary veins being repulsed from forming in vicinity and some forming but joining much lower down the midvein. On the contrary, primary veins unsaturated with auxin allowed newly forming veins to connect directly across taking a shorter path. We imitated identical experimental conditions in leaves by using mutants with accelerated auxin transport representing the pea root sections that had

unsaturated primary veins. We expected that if the canalization hypothesis does in fact occur in leaves, then secondary veins would connect at a larger angle in *max* mutants than wild type. Our quantitative analysis at the tissue level disproved our prediction putting forth the assumption that perhaps leaf veins develop by means of specific biochemical and biomechanical processes. Finally, exploiting *max* mutants to test the hypothesis has also shed some light on the role of auxin in vascular strand formation.

6.2 Contribution and Future directions

Quantifying vein networks of leaves in plants is an important advancement in understanding the mechanism of vein pattern formation, the function of genes implicated in this process and the impact of different environmental conditions. A new non-invasive method has been developed by our lab (Assaf and Rolland-Lagan, unpublished) to study growth and vein patterning simultaneously. This procedure consists of imaging a set of leaves at successive time points and retrieving three dimensional surface data as well as vein pattern parameters by using transgenic lines with fluorescent vasculature. To further corroborate our results, we could adopt this approach by employing Arabidopsis transgenic lines with early markers, for example PIN1:GFP (Scarpella et al. (2006)), to measure angles between the primary and secondary veins at very primitive stages of development.

The classical experiments performed by Sachs in the 1980's using pea epicotyls have recently been reproduced (Sauer et al. (2006); Balla et al. (2011)). However, identical

experiments undertaken with Arabidopsis hypocotyls were reported to be unsuccessful partly because of the small size of the model organism. Here we attempted to test the canalization hypothesis in leaves. A more in-depth experiment to be explored in the future, is to examine the patterns of vein formation *in vivo* through time-lapse imaging (as mentioned above) while applying a lateral auxin source to intact leaves of wild type, accelerated as well as inhibited auxin transport mutants and compare the results with those obtained by Sachs in pea stems and roots.

Ultimately, the aim of studying the molecular and genetic aspects of leaf vein patterns is to be able to bio-engineer crops in order to obtain higher yields faster and also able to tolerate different environmental conditions.

Bibliography

Akiyama, K., Matsuzaki, K.-i., & Hayashi, H. (2005). Plant sesquiterpenes induce hyphal branching in arbuscular mycorrhizal fungi. *Nature*, *435*(7043), 824–7.

Alberts, B., Johnson, A., Lewis, J., Raff, M., Roberts, K., & Walter, P. (2002). *Molecular biology of the cell*. New York: Garland Science, 4th ed.

Aloni, R., Schwalm, K., Langhans, M., & Ullrich, C. I. (2003). Gradual shifts in sites of free-auxin production during leaf-primordium development and their role in vascular differentiation and leaf morphogenesis in arabidopsis. *Planta*, *216*(5), 841–53.

Balla, J., Kalousek, P., Reinöhl, V., Friml, J., & Procházka, S. (2011). Competitive canalization of pin-dependent auxin flow from axillary buds controls pea bud outgrowth. *Plant J*, *65*(4), 571–7.

Baskin, T. I. (2001). On the alignment of cellulose microfibrils by cortical microtubules: a review and a model. *Protoplasma*, *215*(1-4), 150–71.

Beemster, G. T. S., Vercruysse, S., De Veylder, L., Kuiper, M., & Inzé, D. (2006). The arabidopsis leaf as a model system for investigating the role of cell cycle regulation in organ growth. *J Plant Res*, *119*(1), 43–50.

Benková, E., Michniewicz, M., Sauer, M., Teichmann, T., Seifertová, D., Jürgens, G., & Friml, J. (2003). Local, efflux-dependent auxin gradients as a common module for plant organ formation. *Cell*, *115*(5), 591–602.

Bennett, M. J., Marchant, A., Green, H. G., May, S. T., Ward, S. P., Millner, P. A., Walker, A. R., Schulz, B., & Feldmann, K. A. (1996). Arabidopsis aux1 gene: a permease-like regulator of root gravitropism. *Science*, *273*(5277), 948–50.

Bennett, T., Sieberer, T., Willett, B., Booker, J., Luschnig, C., & Leyser, O. (2006). The arabidopsis max pathway controls shoot branching by regulating auxin transport. *Curr Biol*, *16*(6), 553–63.

Boerjan, W., Cervera, M. T., Delarue, M., Beeckman, T., Dewitte, W., Bellini, C., Caboche, M., Van Onckelen, H., Van Montagu, M., & Inzé, D. (1995). Superroot,

a recessive mutation in arabidopsis, confers auxin overproduction. *Plant Cell*, *7*(9), 1405–19.

Bohn, S., Andreotti, B., Douady, S., Munzinger, J., & Couder, Y. (2002). Constitutive property of the local organization of leaf venation networks. *Phys Rev E Stat Nonlin Soft Matter Phys*, *65*(6 Pt 1), 061914.

Booker, J., Auldridge, M., Wills, S., McCarty, D., Klee, H., & Leyser, O. (2004). Max3/ccd7 is a carotenoid cleavage dioxygenase required for the synthesis of a novel plant signaling molecule. *Curr Biol*, *14*(14), 1232–8.

Booker, J., Sieberer, T., Wright, W., Williamson, L., Willett, B., Stirnberg, P., Turnbull, C., Srinivasan, M., Goddard, P., & Leyser, O. (2005). Max1 encodes a cytochrome p450 family member that acts downstream of max3/4 to produce a carotenoid-derived branch-inhibiting hormone. *Dev Cell*, *8*(3), 443–9.

Campanoni, P., & Nick, P. (2005). Auxin-dependent cell division and cell elongation. 1-naphthaleneacetic acid and 2,4-dichlorophenoxyacetic acid activate different pathways. *Plant Physiol*, *137*, 939–948.

Candela, H., Martínez-Laborda, A., & Micol, J. L. (1999). Venation pattern formation in arabidopsis thaliana vegetative leaves. *Dev Biol*, *205*(1), 205–16.

Cheng, Y., Dai, X., & Zhao, Y. (2006). Auxin biosynthesis by the yucca flavin monooxygenases controls the formation of floral organs and vascular tissues in arabidopsis. *Genes & Development*, *20*(13), 1790–1799.

Cheng, Y., Dai, X., & Zhao, Y. (2007). Auxin synthesized by the yucca flavin monooxygenases is essential for embryogenesis and leaf formation in arabidopsis. *Plant Cell*, *19*(8), 2430–2439.

Christensen, S. K., Dagenais, N., Chory, J., & Weigel, D. (2000). Regulation of auxin response by the protein kinase pinoid. *Cell*, *100*(4), 469–78.

Cleary, A. L., & Hardham, A. R. (1993). Pressure induced reorientation of cortical microtubules in epidermal cells of lolium rigidum leaves. *Plant Cell Physiol*, *34*(7), 1003–1008.

Corson, F., Adda-Bedia, M., & Boudaoud, A. (2009). In silico leaf venation networks: growth and reorganization driven by mechanical forces. *J Theor Biol*, *259*(3), 440–8.

Cosgrove, D. J. (1997). Relaxation in a high-stress environment: the molecular bases of extensible cell walls and cell enlargement. *Plant Cell*, *9*(7), 1031–41.

Couder, Y., Pauchard, L., Allain, C., Adda-Bedia, M., & Douady, S. (2002). The leaf venation as formed in a tensorial field. *Eur. Phys. J. B*, *28*, 135–138.

Crawford, K. M., & Zambryski, P. C. (1999). Phloem transport: Are you chaperoned? *Curr Biol*, *9*(8), R281–5.

de Reuille, P. B., Bohn-Courseau, I., Ljung, K., Morin, H., Carraro, N., Godin, C., & Traas, J. (2006). Computer simulations reveal properties of the cell-cell signaling network at the shoot apex in arabidopsis. *Proc Natl Acad Sci U S A*, *103*(5), 1627–32.

Dengler, N., & Kang, J. (2001). Vascular patterning and leaf shape. *Curr Opin Plant Biol*, *4*(1), 50–6.

Dimitrov, P., & Zucker, S. W. (2006). A constant production hypothesis guides leaf venation patterning. *Proc Natl Acad Sci U S A*, *103*(24), 9363–8.

Evans, M., Ishikawa, H., & Estelle, M. (1994). Responses of arabidopsis roots to auxin studied with high temporal resolution - comparison of wild-type and auxin-response mutants. *Planta*, *194*(2), 215–222.

Evert, R. F. (2006). *Esau's plant anatomy*. John Wiley & Sons, Inc., 3rd ed.

Feraru, E., Feraru, M. I., Kleine-Vehn, J., Martinière, A., Mouille, G., Vanneste, S., Vernhettes, S., Runions, J., & Friml, J. (2011). Pin polarity maintenance by the cell wall in arabidopsis. *Curr Biol*, *21*(4), 338–43.

Ferguson, B. J., & Beveridge, C. A. (2009). Roles for auxin, cytokinin, and strigolactone in regulating shoot branching. *Plant Physiol*, *149*(4), 1929–44.

Feugier, F. G., & Iwasa, Y. (2006). How canalization can make loops: A new model of reticulated leaf vascular pattern formation. *Journal of Theoretical Biology*, *243*(2), 235–244.

Friml, J., Benková, E., Blilou, I., Wisniewska, J., Hamann, T., Ljung, K., Woody, S., Sandberg, G., Scheres, B., Jürgens, G., & Palme, K. (2002a). Atpin4 mediates sink-driven auxin gradients and root patterning in arabidopsis. *Cell*, *108*(5), 661–73.

Friml, J., Vieten, A., Sauer, M., Weijers, D., Schwarz, H., Hamann, T., Offringa, R., & Jürgens, G. (2003). Efflux-dependent auxin gradients establish the apical-basal axis of arabidopsis. *Nature*, *426*(6963), 147–53.

Friml, J., Wiśniewska, J., Benková, E., Mendgen, K., & Palme, K. (2002b). Lateral relocation of auxin efflux regulator pin3 mediates tropism in arabidopsis. *Nature*, *415*(6873), 806–9.

Friml, J., Yang, X., Michniewicz, M., Weijers, D., Quint, A., Tietz, O., Benjamins, R., Ouwerkerk, P. B. F., Ljung, K., Sandberg, G., Hooykaas, P. J. J., Palme, K., & Offringa, R. (2004). A pinoid-dependent binary switch in apical-basal pin polar targeting directs auxin efflux. *Science*, *306*(5697), 862–5.

Fujita, H., & Mochizuki, A. (2006). The origin of the diversity of leaf venation pattern. *Dev Dyn*, *235*(10), 2710–21.

Gälweiler, L., Guan, C., Müller, A., Wisman, E., Mendgen, K., Yephremov, A., & Palme, K. (1998). Regulation of polar auxin transport by atpin1 in arabidopsis vascular tissue. *Science*, *282*(5397), 2226–30.

Ganguly, A., Lee, S. H., Cho, M., Lee, O. R., Yoo, H., & Cho, H.-T. (2010). Differential auxin-transporting activities of pin-formed proteins in arabidopsis root hair cells. *Plant Physiol*, *153*(3), 1046–61.

Geldner, N., Friml, J., Stierhof, Y. D., Jürgens, G., & Palme, K. (2001). Auxin transport inhibitors block pin1 cycling and vesicle trafficking. *Nature*, *413*(6854), 425–8.

Goldsmith, M. H. M. (1977). The polar transport of auxin. *Annual Review of Plant Biology*, *28*, 439–478.

Hayes, A. B. (1977). Developmental aspects of leaf blade hyponasty. *Botanical Gazette*, *138*(1), 52–55.

Hayes, A. B., & Lippincott, J. A. (1976). Growth and gravitational response in the development of leaf blade hyponasty. *American Journal of Botany*, *63*(4), 383–387.

Heisler, M. G., Hamant, O., Krupinski, P., Uyttewaal, M., Ohno, C., Jönsson, H., Traas, J., & Meyerowitz, E. M. (2010). Alignment between pin1 polarity and microtubule orientation in the shoot apical meristem reveals a tight coupling between morphogenesis and auxin transport. *PLoS Biol*, *8*(10), e1000516.

Hu, Y., Xie, Q., & Chua, N.-H. (2003). The arabidopsis auxin-inducible gene argos controls lateral organ size. *Plant Cell*, *15*(9), 1951–61.

Kang, J., & Dengler, N. (2004). Vein pattern development in adult leaves of arabidopsis thaliana. *International Journal of Plant Sciences*, *165*(2), 231–242.

Kang, J., Mizukami, Y., Wang, H., Fowke, L., & Dengler, N. G. (2007). Modification of cell proliferation patterns alters leaf vein architecture in arabidopsis thaliana. *Planta*, *226*(5), 1207–18.

Keller, & E, V. V. (1998). Evidence that auxin-induced growth of tobacco leaf tissues does not involve cell wall acidification. *Plant Physiol*, *118*(2), 557–64.

Keller, C. P., & Van Volkenburgh, E. (1997). Auxin-induced epinasty of tobacco leaf tissues (a nonethylene-mediated response). *Plant Physiol*, *113*(2), 603–610.

Klee, H. J., Horsch, R. B., Hinchee, M. A., Hein, M. B., & Hoffmann, N. L. (1987). The effects of overproduction of two agrobacterium tumefaciens t-dna auxin biosynthetic gene products in transgenic petunia plants. *Genes Dev*, *1*, 86–96.

Kramer, E. M. (2009). Auxin-regulated cell polarity: an inside job? *Trends Plant Sci*, *14*(5), 242–7.

Laguna, M. F., Bohn, S., & Jagla, E. A. (2008). The role of elastic stresses on leaf venation morphogenesis. *PLoS Comput Biol*, *4*(4), e1000055.

Lippincott, B. B., & Lippincott, J. A. (1971). Auxin-induced hyponasty of the leaf blade of philaseolus vulgaris. *American Journal of Botany*, *58*(9), 817–826.

Ljung, K., Bhalerao, R. P., & Sandberg, G. (2001). Sites and homeostatic control of auxin biosynthesis in arabidopsis during vegetative growth. *Plant J*, *28*(4), 465–74.

Marchant, A., Kargul, J., May, S. T., Muller, P., Delbarre, A., Perrot-Rechenmann, C., & Bennett, M. J. (1999). Aux1 regulates root gravitropism in arabidopsis by facilitating auxin uptake within root apical tissues. *EMBO J*, *18*(8), 2066–73.

Mattsson, J., Ckurshumova, W., & Berleth, T. (2003). Auxin signaling in arabidopsis leaf vascular development. *Plant Physiol*, *131*(3), 1327–39.

Mattsson, J., Sung, Z., & Berleth, T. (1999). Responses of plant vascular systems to auxin transport inhibition. *Development*, *126*(13), 2979–2991.

McKown, A. D., & Dengler, N. G. (2009). Shifts in leaf vein density through accelerated vein formation in c4 flaveria (asteraceae). *Ann Bot*, *104*(6), 1085–98.

Meinhardt, H. (1976). Morphogenesis of lines and nets. *Differentiation*, *6*(2), 117–23.

Meinhardt, H. (1984). *Models of pattern formation and their application to plant development*, chap. 1, (pp. 1–30). Cambridge University Press.

Merks, R. M. H., Van de Peer, Y., Inzé, D., & Beemster, G. T. S. (2007). Canalization without flux sensors: a traveling-wave hypothesis. *Trends Plant Sci*, *12*(9), 384–90.

Michniewicz, M., Zago, M. K., Abas, L., Weijers, D., Schweighofer, A., Meskiene, I., Heisler, M. G., Ohno, C., Zhang, J., Huang, F., Schwab, R., Weigel, D., Meyerowitz, E. M., Luschnig, C., Offringa, R., & Friml, J. (2007). Antagonistic regulation of pin phosphorylation by pp2a and pinoid directs auxin flux. *Cell*, *130*(6), 1044–56.

Mitchison, G. J. (1981). The polar transport of auxin and vein patterns in plants. *Phil. Trans. R. Soc. Lond. B*, *295*, 461–471.

Mravec, J., Kubes, M., Bielach, A., Gaykova, V., Petrásek, J., Skůpa, P., Chand, S., Benková, E., Zazímalová, E., & Friml, J. (2008). Interaction of pin and pgp transport mechanisms in auxin distribution-dependent development. *Development*, *135*(20), 3345–54.

Muday, G. K., & DeLong, A. (2001). Polar auxin transport: controlling where and how much. *Trends Plant Sci*, *6*(11), 535–42.

Müller, A., Guan, C., Gälweiler, L., Tänzler, P., Huijser, P., Marchant, A., Parry, G., Bennett, M., Wisman, E., & Palme, K. (1998). Atpin2 defines a locus of arabidopsis for root gravitropism control. *EMBO J*, *17*(23), 6903–11.

Nelson, T., & Dengler, N. (1997). Leaf vascular pattern formation. *Plant Cell*, *9*(7), 1121–1135.

O'Donnell, B. M., Garrido, P., Kersey, S., & Ghoshroy, S. (2004). Structural alteration of arabidopsis thaliana leaf vasculature and restricted virus systemic movement in response to auxin transport inhibition. *Microscopy and Microanalysis*, *10*, 220–221.

Ongaro, V., & Leyser, O. (2008). Hormonal control of shoot branching. *J Exp Bot*, *59*(1), 67–74.

Palme, K., & Gälweiler, L. (1999). Pin-pointing the molecular basis of auxin transport. *Curr Opin Plant Biol*, *2*(5), 375–81.

Petrásek, J., & Friml, J. (2009). Auxin transport routes in plant development. *Development*, *136*(16), 2675–88.

Petrásek, J., Mravec, J., Bouchard, R., Blakeslee, J. J., Abas, M., Seifertová, D., Wisniewska, J., Tadele, Z., Kubes, M., Covanová, M., Dhonukshe, P., Skupa, P., Benková, E., Perry, L., Krecek, P., Lee, O. R., Fink, G. R., Geisler, M., Murphy, A. S., Luschnig, C., Zazímalová, E., & Friml, J. (2006). Pin proteins perform a rate-limiting function in cellular auxin efflux. *Science*, *312*(5775), 914–8.

Price, C. A., Symonova, O., Mileyko, Y., Hilley, T., & Weitz, J. S. (2011). Leaf extraction and analysis framework graphical user interface: segmenting and analyzing the structure of leaf veins and areoles. *Plant Physiol*, *155*(1), 236–45.

Reinhardt, D., Pesce, E.-R., Stieger, P., Mandel, T., Baltensperger, K., Bennett, M., Traas, J., Friml, J., & Kuhlemeier, C. (2003). Regulation of phyllotaxis by polar auxin transport. *Nature*, *426*(6964), 255–60.

Rolland-Lagan, A.-G. (2008). Vein patterning in growing leaves: axes and polarities. *Curr Opin Genet Dev*, *18*(4), 348–53.

Rolland-Lagan, A.-G., Amin, M., & Pakulska, M. (2009). Quantifying leaf venation patterns: two-dimensional maps. *Plant J*, *57*(1), 195–205.

Rolland-Lagan, A.-G., & Prusinkiewicz, P. (2005). Reviewing models of auxin canalization in the context of leaf vein pattern formation in arabidopsis. *Plant J*, *44*(5), 854–65.

Rubery, P. H., & Sheldrake, A. R. (1974). Carrier-mediated auxin transport. *Planta*, *88*, 101–121.

Runions, A., Fuhrer, M., Lane, B., Federl, P., Rolland-Lagan, A., & Prusinkiewicz, P. (2005). Modeling and visualization of leaf venation patterns. *Acm Transactions On Graphics*, *24*(3), 702–711.

Sachs, T. (1968). On the determination of the pattern of vascular tissue in peas. *Annals of Botany*, *32*, 781–790.

Sachs, T. (1969). Polarity and the induction of organized vascular tissues. *Annals of Botany*, *33*(2), 263–275.

Sachs, T. (1981). The control of the patterned differentiation of vascular tissues. *Advances in Botanical Research*, *9*, 151–262.

Sauer, M., Balla, J., Luschnig, C., Wisniewska, J., Reinöhl, V., Friml, J., & Benková, E. (2006). Canalization of auxin flow by aux/iaa-arf-dependent feedback regulation of pin polarity. *Genes Dev*, *20*(20), 2902–11.

Sawchuk, M. G., Donner, T. J., Head, P., & Scarpella, E. (2008). Unique and overlapping expression patterns among members of photosynthesis-associated nuclear gene families in arabidopsis. *Plant Physiol*, *148*(4), 1908–24.

Sawchuk, M. G., Head, P., Donner, T. J., & Scarpella, E. (2007). Time-lapse imaging of arabidopsis leaf development shows dynamic patterns of procambium formation. *New Phytol*, *176*(3), 560–71.

Scarpella, E., Marcos, D., Friml, J., & Berleth, T. (2006). Control of leaf vascular patterning by polar auxin transport. *Genes Dev*, *20*(8), 1015–27.

Scarpella, E., & Meijer, A. (2004). Pattern formation in the vascular system of monocot and dicot plant species. *New Phytologist*, *164*(2), 209–242.

Shen, H., Luong, P., & Huq, E. (2007). The f-box protein max2 functions as a positive regulator of photomorphogenesis in arabidopsis. *Plant Physiol*, *145*(4), 1471–83.

Shi, L., Wang, B., Gong, W., Zhang, Y., Zhu, L., & Yang, X. (2011). Actin filaments and microtubules of arabidopsis suspension cells show different responses to changing turgor pressure. *Biochem Biophys Res Commun*, *405*(4), 632–7.

Sieburth, L. E. (1999). Auxin is required for leaf vein pattern in arabidopsis. *Plant Physiol*, *121*(4), 1179–90.

Sorefan, K., Booker, J., Haurogné, K., Goussot, M., Bainbridge, K., Foo, E., Chatfield, S., Ward, S., Beveridge, C., Rameau, C., & Leyser, O. (2003). Max4 and rms1 are orthologous dioxygenase-like genes that regulate shoot branching in arabidopsis and pea. *Genes Dev*, *17*(12), 1469–74.

Steynen, Q. J., & Schultz, E. A. (2003). The forked genes are essential for distal vein meeting in arabidopsis. *Development*, *130*(19), 4695–708.

Stirnberg, P., van De Sande, K., & Leyser, H. M. O. (2002). Max1 and max2 control shoot lateral branching in arabidopsis. *Development*, *129*(5), 1131–41.

Swarup, R., Friml, J., Marchant, A., Ljung, K., Sandberg, G., Palme, K., & Bennett, M. (2001). Localization of the auxin permease aux1 suggests two functionally distinct hormone transport pathways operate in the arabidopsis root apex. *Genes Dev*, *15*(20), 2648–53.

Taiz, L., & Zeiger, E. (2006). *Plant physiology*. Sinauer Associates, Inc.

Tanaka, H., Dhonukshe, P., Brewer, P. B., & Friml, J. (2006). Spatiotemporal asymmetric auxin distribution: a means to coordinate plant development. *Cell Mol Life Sci*, *63*(23), 2738–54.

The Arabidopsis Genome Initiative. (2000). Analysis of the genome sequence of the flowering plant arabidopsis thaliana. *Nature*, *408*(6814), 796–815.

Tsukaya, H., & Horiguchi, G. (2005). [leaf morphogenesis]. *Tanpakushitsu Kakusan Koso*, *50*(6 Suppl), 627–32.

Tsukaya, H., Shoda, K., Kim, G. T., & Uchimiya, H. (2000). Heteroblasty in arabidopsis thaliana (l.) heynh. *Planta*, *210*(4), 536–42.

Turing, A. (1952). The chemical basis of morphogenesis. *Philosophical Transactions of the Royal Society of London Series B-Biological Sciences*, *237*(641), 37–72.

Turnbull, C. G. N., Booker, J. P., & Leyser, H. M. O. (2002). Micrografting techniques for testing long-distance signalling in arabidopsis. *Plant J*, *32*(2), 255–62.

Ueno, O., Kawano, Y., Wakayama, M., & Takeda, T. (2006). Leaf vascular systems in c(3) and c(4) grasses: a two-dimensional analysis. *Ann Bot*, *97*(4), 611–21.

Umehara, M., Hanada, A., Yoshida, S., Akiyama, K., Arite, T., Takeda-Kamiya, N., Magome, H., Kamiya, Y., Shirasu, K., Yoneyama, K., Kyozuka, J., & Yamaguchi, S. (2008). Inhibition of shoot branching by new terpenoid plant hormones. *Nature*, *455*(7210), 195–200.

Volkenburgh, E. V. (1999). Leaf expansion - and integrating plant behaviour. *Plant Cell Environ*, *22*(12), 1463–1473.

Wenzel, C. L., Hester, Q., & Mattsson, J. (2008). Identification of genes expressed in vascular tissues using npa-induced vascular overgrowth in arabidopsis. *Plant Cell Physiol*, *49*(3), 457–68.

Wenzel, C. L., Schuetz, M., Yu, Q., & Mattsson, J. (2007). Dynamics of monopteros and pin-formed1 expression during leaf vein pattern formation in arabidopsis thaliana. *Plant J*, *49*(3), 387–98.

Wisniewska, J., Xu, J., Seifertová, D., Brewer, P. B., Ruzicka, K., Blilou, I., Rouquié, D., Benková, E., Scheres, B., & Friml, J. (2006). Polar pin localization directs auxin flow in plants. *Science*, *312*(5775), 883.

Wymer, C. L., Wymer, S. A., Cosgrove, D. J., & Cyr, R. J. (1996). Plant cell growth responds to external forces and the response requires intact microtubules. *Plant Physiol*, *110*, 425–430.

Yamamoto, M., & Yamamoto, K. T. (1998). Differential effects of 1-naphthaleneacetic acid, indole-3-acetic acid and 2,4-dichlorophenoxyacetic acid on the gravitropic response of roots in an auxin-resistant mutant of arabidopsis, aux1. *Plant Cell Physiol*, *39*(6), 660–4.

Yang, Y., Hammes, U. Z., Taylor, C. G., Schachtman, D. P., & Nielsen, E. (2006). High-affinity auxin transport by the aux1 influx carrier protein. *Curr Biol*, *16*(11), 1123–7.

Ye, Z. (2002). Vascular tissue differentiation and pattern formation in plants. *Annual Review of Plant Biology*, *53*, 183–202.

Ye, Z., Freshour, G., Hahn, M., Burk, D., & Zhong, R. (2002). Vascular development in arabidopsis. *International Review of Cytology - a Survey of Cell Biology, Vol 220*, *220*, 225–256.

Zhao, Y. (2008). The role of local biosynthesis of auxin and cytokinin in plant development. *Current Opinion In Plant Biology*, *11*(1), 16–22.

Appendix A - The *max* mutant phenotype

The phenotype analysis done by Elizabeth Edmunds (a previous honours student in the Rolland-Lagan lab) showed that the *max4-1* (n=6), compared to the wild type (n=9), had a significantly larger number of rosette branches (Figure 1a and Figure 2a) (Mann-Whitney U test, $P<0.05$, n=15, SE=75.21) and rosette leaves (Figure 1b, c and Figure 2b) (Mann-Whitney U test, emphP<0.05, b=15m SE=83.94). These results demonstrate clearly that the *max* mutant bushy phenotype mutation (Ongaro & Leyser (2008)) was present. Moreover the increase number of rosette leaves suggests that the MAX pathway is not solely involved in regulating hormone distribution to the branches but also to leaves and perhaps maybe altering vein patterns.

Figure 1: Branching phenotype of wild type (Col0) Arabidopsis and *max4-1* mutant. (a) *Left.* Whole plant of Col0, n=5. *Right.* Whole plant of *max4-1* mutant, n=4. Close-up photo of (b) Col0 and (c) *max4-1* primary stem and rosette leaves. Notice the characteristic bushy phenotype of *max4-1* on the right. *Images taken by Elizabeth Edmunds.*

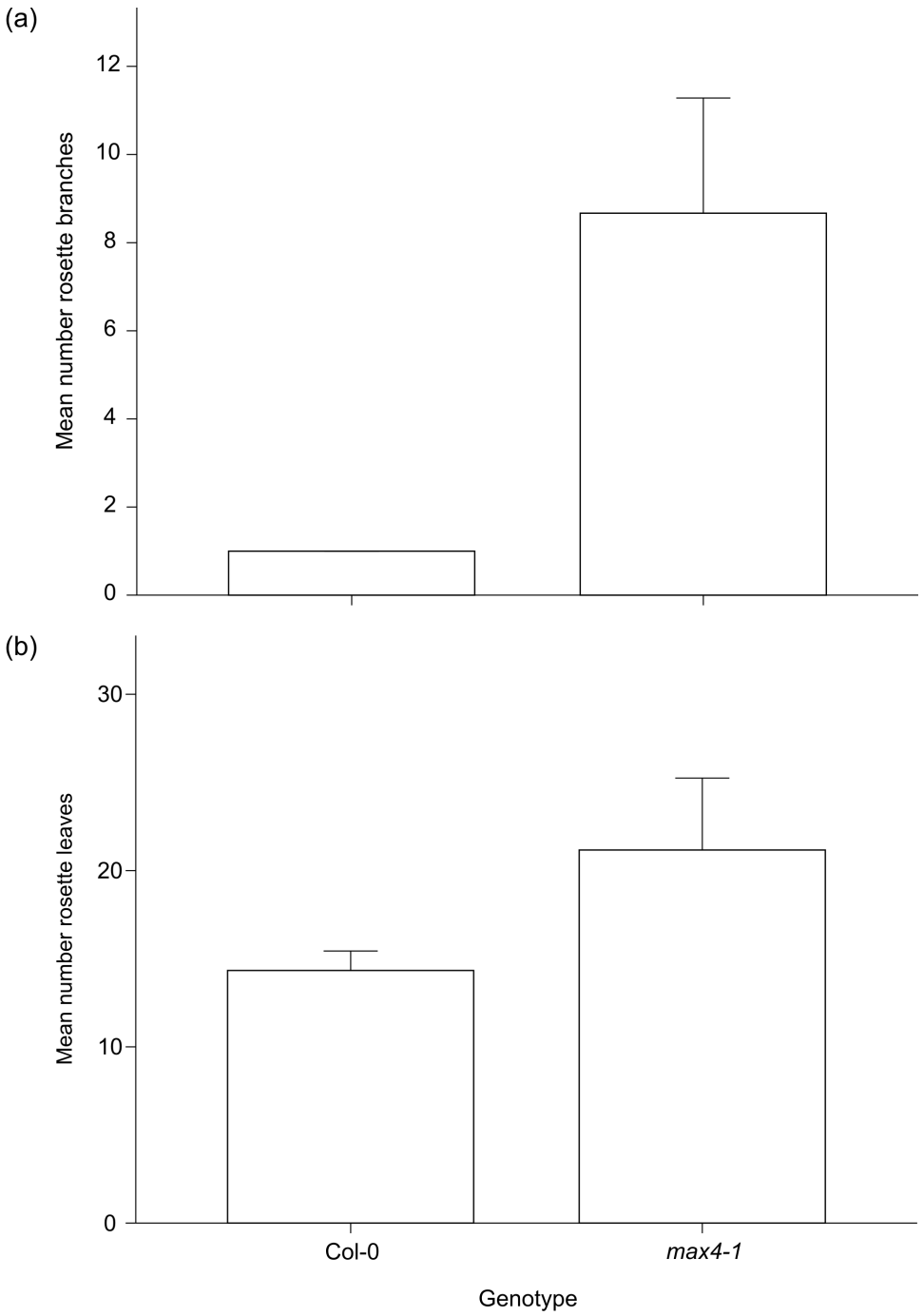

Figure 2: Mean number of rosette branches (a) and rosette leaves (b) of Col0 (n=9) and *max4-1* (n=6). Error bars indicate the standard error of the mean. *Graphs generated by Elizabeth Edmunds.*

Appendix B - Methodology: Image analysis and pattern extraction

(**1**) A written Matlab® user interface program was used to measure and record leaf parameters such as the length, width and area of the blade and petiole. Three points were marked (one at the tip and two at the base of the blade) in order to have all leaves analyzed in a common orientation. Finally the whole leaf area was measured (Figure 3).
(**2**) A second written Matlab® user interface program was developed to digitize vein segments. Veins were not traced in one continuous line but rather by segments from one node to another (Figure 4). These segments are made up of many points that are recorded in a matrix containing all vein segments on a leaf.
(**3**) A network topology (Figure 5a) was acquired and all free ending and branching points were tagged. From the known topology and the segment positions, loops were identified and given a color depending on their size (Figure 5b). Extraction of whole leaf parameters could then be obtained; leaf blade area, leaf shape, vein density, loop numbers, segment numbers, branching points and free ending veins.
(**4**) Temporal analysis allowed us to see variation in vein pattern parameters with each time point but spatial analysis demonstrated variation with regard to the position on the leaf. To retrieve information on spatial variation in pattern parameters, the mean pattern data across several samples were used. For each group of leaves harvested (15 leaves) on the same day, we calculated the average leaf shape, and warped all leaf shapes and venation patterns for that day to the average shape. Example: At each point of the leaf surface the mean area of loops overlapping that point is calculated. Other spatial parameters can also be extracted such as loop number, loop area, loop shape, loop subdivision and vein density. Contour maps are used to visualize the spatial differences.

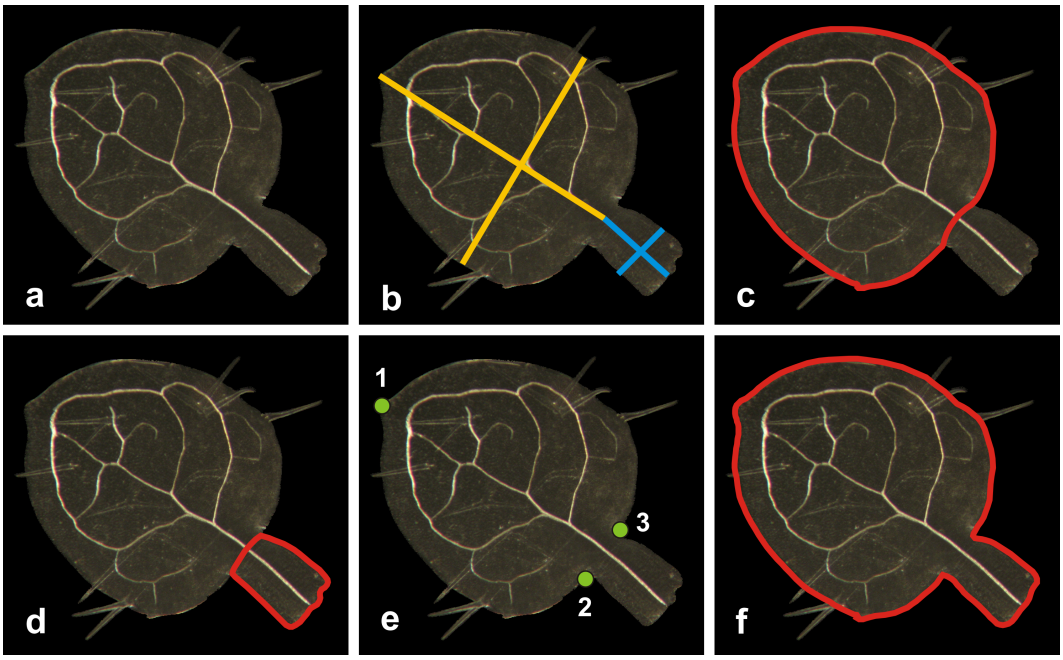

Figure 3: A Matlab® user interface was developed to measure and record leaf parameters from leaf images (see Rolland-Lagan et al. (2009)) (a). The length and width (yellow lines) of the leaf blade and petiole (blue lines) are measured (b) followed by the area (c and d). (e) Three points are marked to have all leaves oriented in one common direction. (f) Lastly, the whole leaf area is measured.

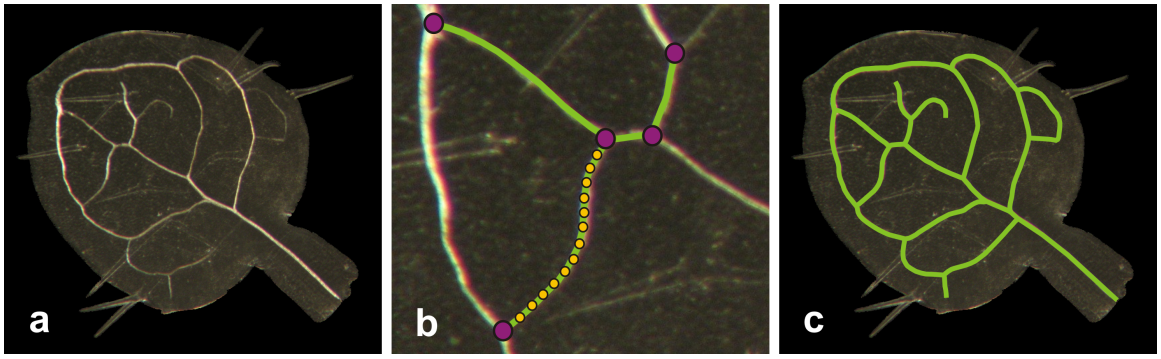

Figure 4: A second Matlab® user interface was written to trace vein segments from leaf images (see Rolland-Lagan et al. (2009)) (a). A region is selected for zooming in order to digitize veins correctly. (b) Veins were not drawn as a continuous line but rather as segments (green line) from one branching point (purple circles) to another. There are points (yellow circles) along the segments that were recorded in a matrix that contains all vein segments of the leaf. (c) Process in (b) was repeated multiple times until all vein segments have been traced.

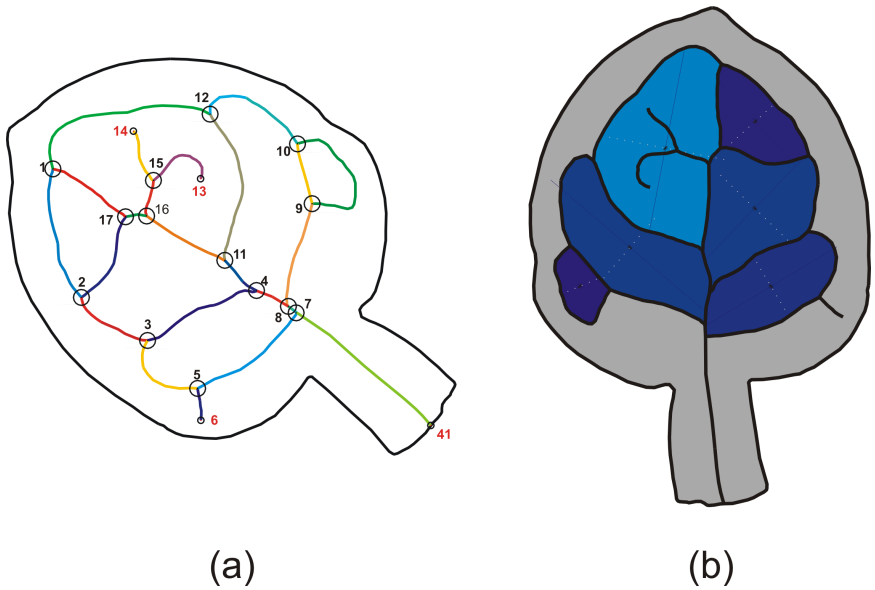

Figure 5: Extraction of segment and loop parameters from network topology. (a) Using the network topology, segments, branching points and free vein endings were identified and recoded in a matrix. (b) Loops were were also identified and color-coded with shades of blue according to their area.

Appendix C - Statistical table of Mann-Whitney U test on leaf blade area

Genotype grouping	DAS	Mann-Whitney U	Z	*P*-value
Col0 & *max4-1*	7	64	-2.013	.044
	8	55	-2.385	.017
	9	50	-2.592	.010
	10	9	-4.293	.000
	11	16	-4.003	.000
	12	9	-4.293	.000
	13	0	-4.666	.000
	14	8	-4.334	.000
	15	3	-4.542	.000
	16	10	-4.252	.000
	17	10	-4.252	.000
Col0 & *max3-9*	7	98	-0.601	.548
	8	16	-4.003	.017
	9	78	-1.431	.010
	10	10	-4.252	.000
	11	2	-4.583	.000
	12	33	-3.298	.000
	13	11	-4.210	.000
	14	28	-3.505	.000
	15	87	-1.058	.000
	16	82	-1.265	.000
	17	112	-0.021	.000
Col0 & *max2-1*	7	43	-2.883	.004
	8	48	-2.675	.007
	9	16	-4.003	.000
	10	24	-3.671	.000
	11	11	-4.210	.000
	12	22	-4.754	.000
	13	19	-4.878	.000
	14	0	-4.666	.000
	15	6	-4.417	.000
	16	0	-4.666	.000
	17	0	-4.666	.000
Col0 & *max1-1*	7	65	-1.970	.049
	8	68	-1.846	.065
	9	92	-0.850	.010

Genotype grouping	DAS	Mann-Whitney U	Z	*P*-value
	10	13	-4.127	.000
	11	6	-4.417	.000
	12	24	-3.671	.000
	13	1	-4.625	.000
	14	54	-2.426	.000
	15	39	-3.049	.000
	16	49	-2.634	.000
	17	32	-3.339	.000
max4-1 & *max1-1*	7	104	-0.353	.724
	8	74	-1.597	.110
	9	62	-2.095	.036
	10	88	-1.016	.310
	11	51	-2.551	.011
	12	55	-2.385	.017
	13	83	-1.224	.021
	14	25	-3.629	.000
	15	57	-2.302	.021
	16	69	-1.804	.071
	17	51	-2.551	.011
max3-9 & *max1-1*	7	78	-1.431	.152
	8	16	-4.003	.000
	9	87	-1.058	.290
	10	98	-0.601	.548
	11	95	-0.721	.468
	12	111	-0.062	.950
	13	70	-1.763	.078
	14	75	-1.555	.120
	15	51	-2.551	.011
	16	37	-3.132	.002
	17	18	-3.920	.000

Appendix D - Statistical table of Mann-Whitney U test on relative loop areas

DAS	Genotype 1	Genotype 2	Mann-Whitney U	Z	*P*-value
7	Col0	*max4-1*	29	-.345	.730
		max3-9	59	-.372	.710
		max2-1	94	-.161	.872
		max1-1	38	-.594	.552
	max4-1	*max2-1*	31	-.567	.570
		max1-1	12	-.893	.372
	max3-9	*max2-1*	61	-.777	.437
		max1-1	24	-1.073	.283
	max2-1	*max1-1*	44	-.599	.549
8	Col0	*max4-1*	55	-2.385	.017
		max3-9	48	-2.488	.013
		max2-1	45	-2.800	.005
		max1-1	110	-.104	.917
	max4-1	*max2-1*	19	-3.878	.000
		max1-1	54	-2.426	.015
	max2-1	*max1-1*	54	-2.426	.015
9	Col0	*max4-1*	69	-1.804	.071
		max3-9	78	-1.431	.152
		max2-1	17	-3.961	.000
		max1-1	98	-.601	.548
	max4-1	*max3-9*	109	-.145	.885
		max2-1	4	-4.500	.000
		max1-1	54	-2.426	.015
	max3-9	*max2-1*	13	-4.127	.000
		max1-1	54	-2.426	.015
	max2-1	*max1-1*	29	-3.463	.001

DAS	Genotype 1	Genotype 2	Mann-Whitney U	Z	*P*-value
10	Col0	*max4-1*	26	-3.588	.000
		max3-9	36	-3.173	.002
		max2-1	74	-1.597	.110
		max1-1	34	-3.256	.001
	max4-1	*max3-9*	103	-.394	.694
		max2-1	13	-4.127	.000
		max1-1	67	-1.887	.059
	max3-9	*max2-1*	14	-4.086	.000
		max1-1	86	-1.141	.254
	max2-1	*max1-1*	24	-3.671	.000
11	Col0	*max4-1*	38	-3.090	.002
		max3-9	13	-4.127	.000
		max2-1	30	-3.422	.001
		max1-1	62	-2.095	.036
	max4-1	*max3-9*	57	-2.302	.021
		max1-1	95	-.726	.468
	max3-9	*max1-1*	42	-2.924	.003
	max2-1	*max1-1*	71	-1.721	.085
12	Col0	*max4-1*	85	-1.141	.254
		max3-9	81	-1.307	.191
		max2-1	46	-2.758	.006
		max1-1	86	-1.099	.272
	max4-1	*max3-9*	104	-.353	.724
		max2-1	78	-1.431	.152
		max1-1	112	-.21	.983
	max3-9	*max2-1*	57	-2.302	.021
		max1-1	107	-0.228	.820
	max2-1	*max1-1*	80	-1.348	.178
13	Col0	*max4-1*	70	-1.763	.078
		max3-9	101	-.477	.633
		max2-1	18	-3.920	.000
		max1-1	46	-2.758	.006
	max4-1	*max3-9*	93	-.809	.419
		max2-1	56	-2.344	.019
		max1-1	83	-1.224	.221
	max3-9	*max2-1*	50	-2.592	.010
		max1-1	72	-1.680	.093
	max2-1	*max1-1*	87	-1.058	.290

DAS	Genotype 1	Genotype 2	Mann-Whitney U	Z	*P*-value
14	Col0	*max4-1*	96	-.684	.494
		max3-9	112	-.021	.983
		max2-1	36	-3.173	.002
		max1-1	95	-.726	.468
	max4-1	*max3-9*	97	-.643	.520
		max2-1	40	-3.007	.003
		max1-1	112	-.021	.983
	max3-9	*max2-1*	36	-3.173	.002
		max1-1	99	-.560	.576
	max2-1	*max1-1*	44	-2.841	.004
15	Col0	*max4-1*	65	-1.970	.049
		max3-9	103	-.394	.694
		max2-1	27	-3.546	.000
		max1-1	56	-2.344	.019
	max4-1	*max3-9*	76	-1.514	.130
		max2-1	99	-.560	.576
		max1-1	103	-.394	.694
	max3-9	*max2-1*	48	-2.675	.007
		max1-1	69	-1.804	.071
	max2-1	*max1-1*	67	-1.887	.059
16	Col0	*max4-1*	82	-1.265	.206
		max3-9	100	-.518	.604
		max2-1	43	-2.883	.004
		max1-1	84	-1.182	.237
	max4-1	*max3-9*	88	-1.016	.310
		max2-1	56	-2.344	.019
		max1-1	112	-.021	.983
	max3-9	*max2-1*	46	-2.758	.006
		max1-1	99	-.560	.576
	max2-1	*max1-1*	56	-2.344	.019
17	Col0	*max4-1*	48	-2.675	.007
		max3-9	102	-.436	.633
		max1-1	64	-2.012	.044
	max4-1	*max3-9*	40	-3.007	.003
		max2-1	104	-.353	.724
		max1-1	80	-1.348	.178
	max3-9	*max2-1*	27	-3.546	.000
		max1-1	58	-2.261	.024
	max2-1	*max1-1*	70	-1.763	.078

Appendix E - Angle measurement extraction

Custom programs were written by Dr. Rolland-Lagan (University of Ottawa) using Matlab® to obtain angle measurements found between the midvein and secondary veins from leaf images. A second program was made to display the spatial angle data. Here are a few general steps that were performed by the programs:
(**i**) From the image analysis and pattern extraction programs (Rolland-Lagan et al. (2009)), we were able to record segment parameters as well as the number and position of branching points using the topology of the network and coordinates of points along each vein segment. Such recorded data were loaded and used to acquire angle measurements along the midvein and throughout the leaf blade.
(**ii**) Points along each vein were recorded in a matrix S that represented all vein segments on the leaf and another matrix B contained only branching point coordinates. Using the latter, the program was able to identify in the S matrix which coordinates were branching points.
(**iii**) Branching points that were found along the midvein had to be differentiated from those found throughout the leaf blade. Since this study did not follow individual leaves through time-lapsing imaging, it is difficult to know exactly which is the primary vein from which formed secondary veins.Therefore, the user was given the choice to select one out of four methods that best identified the midvein.
(**iv**) In order to determine which 3 segments were connected to one particular branching point, the program identified which points had the same x and y coordinates.
(**v**) To avoid any inaccuracies in angle measurements of bent veins at the junction, lines from the first to the third point coordinates on vein segments were created to be used for the calculations (see Figure 6.2).
(**vi**) To calculate the relative angles α_{12}, α_{13} and α_{23} (Figure 4.11) at each branching point, the absolute values were first obtained using the following equation:

$$(\alpha \tan 2(y_2 - y_1, x_2 - x_1)) * \tfrac{180}{\pi}$$

Absolute angle ϕ_1 was measured from a defined horizontal line to segment 1, ϕ_2 from the horizontal line to segment 2 and ϕ_3 from the horizontal line to segment 3. Both α_{12} and α_{23} were then calculated:

$$\alpha_{12} = \phi_2 \text{ - } \phi_1$$
$$\alpha_{23} = \phi_3 \text{ - } \phi_2$$

Knowing that the Euclidean geometry requires the sum of all angles between segments at a node to be 360°, the relative angle α_{13} was calculated as follows:

$$\alpha_{13} = 360 \text{ - } (\alpha_{12} + \alpha_{23})$$

For each plant type, an excel file was generated containing information for each day of the period analyzed the leaf number, the relative angles and their corresponding

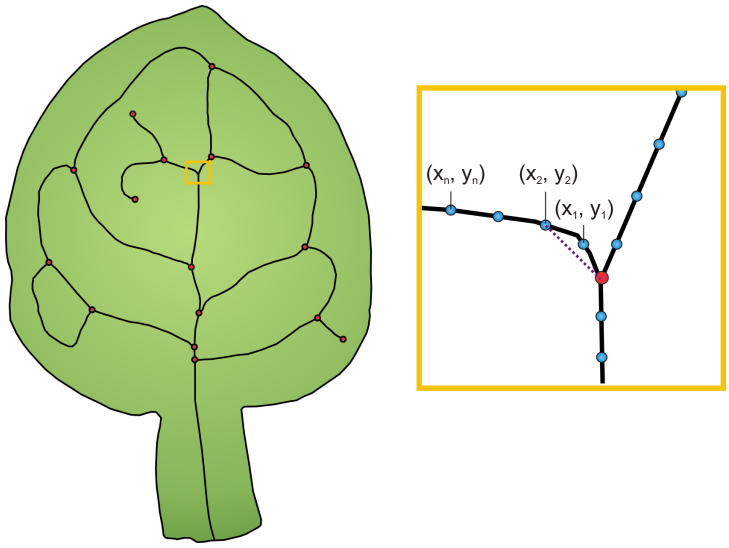

Figure 6: Solution for bent veins at branching points. To avoid inaccuracies in angle measurements, a line from the branching point to the third point (along the vein segment) is created.

type (small, intermediate or large), the branching point number at which the angles were calculated and whether this branching point was located along the midvein or somewhere on the leaf blade.

Appendix F - Statistical table of Mann-Whitney U test on relative angles data

Genotype grouping	DAS	Mann-Whitney U	Z	*P*-value
Col0 & *max4-1*	7	452	-.094	.925
	8	2738	-.173	.862
	9	5971	-.498	.618
	10	8340	-2.616	.009
	11	10916	-1.999	.046
	12	12192	-.542	.588
	13	10835	-1.671	.095
	14	13181.5	-.682	.496
	15	13114	-.072	.943
	16	10849	-.724	.469
	17	11553	-1.218	.223
Col0 & *max3-9*	7	1565	-1.272	.203
	8	2227	-1.032	.302
	9	5300	-3.797	.000
	10	9821	-1.317	.188
	11	11548	-2.465	.014
	12	11164	-2.385	.017
	13	11195	-2.879	.004
	14	12472	-1.842	.066
	15	13768	-.662	.508
	16	10210	-2.987	.003
	17	13706	-.173	.863
Col0 & *max2-1*	7	1766	-.494	.621
	8	5434	-1.026	.305
	9	7813	-2.259	.024
	10	11787	-1.115	.265
	11	12075	-1.421	.155
	12	11224	-1.635	.102
	13	10928	-1.003	.316
	14	12080	-1.033	.301
	15	11935	-.380	.704
	16	10633	-.629	.530
	17	12749	-.814	.416

Genotype grouping	DAS	Mann-Whitney U	Z	*P*-value
Col0 & *max1-1*	7	741	-.876	.381
	8	3563	-1.151	.250
	9	6766	-2.478	.013
	10	11148	-1.976	.048
	11	12838	-1.759	.078
	12	11441	-1.974	.048
	13	10015	-3.268	.001
	14	11736	-2.335	.020
	15	12901	-.807	.420
	16	11197	-1.450	.147
	17	11901	-.596	.551

Appendix G - Supplemental background information on the mechanical and chemical regulation of the cell

Contrary to animal cells, plant cells are immobile and develop in a constrained and rigid environment. Differences in solute concentrations between the interior and exterior milieu of the cell causes the cell to build up an internal hydrostatic pressure, known as turgor pressure, that exerts an outward isotropic force on the cell wall (Figure 7b) (Alberts et al. (2002)). At a certain point the cell reaches an equilibrium where the turgor pressure directed outwardly counter balances the restraining force of the cell wall. A deviation from this balance point (i.e. reduction in tensile stress) will allow the cell to enlarge through a process called stress wall relaxation (Figure 7c) (Cosgrove (1997)). More precisely, such loosening is caused by the action of auxin following the "acid growth hypothesis" first propounded by Hager and collegues (1971). Auxin stimulates a proton (H^+) pump located in the plasma membrane, directing H^+ into the cell wall and consequently increase its acidity (decrease in pH) (Figure 7c). This low pH activates a class of proteins, expansins, that loosen the bonding within cellulose microfibrils present in the cell wall. Breakage of these polymers allows the cell wall to become more elastic and yields (stretches) irreversibly to the forces generated by turgor. Only an infinitesimal expansion results in the reduction of cell turgor pressure and cell water potential therefore triggering water uptake which will in turn enable the cell to expand (Figure 7d).

During growth, the cell wall controls the direction of expansion through the arrangement of newly deposited cellulose microfibrils. Cells formed in the meristem acquire an isodiametric shape due to the randomly arranged microfibrils (Figure 7e). However, when most of these fiber-like strands have the same orientation (i.e. wound transversely around the cell preventing circumferential increases), the plant cell expands perpendicular to the direction in which the microfibrils are laid (Taiz & Zeiger (2006)). Also, attached to the inner face of the plasma membrane and present within the cell's cytoplasm are cortical microtubules (Figure 7e). In elongating cells, these polymers, are organized parallel to one another with overlapping ends and are oriented transversely as well to the cell's long axis. Moreover, the microtubule network contributes to the shaping of the cell by co-aligning with cellulose microfibrils on the opposite side of the plasma membrane (Baskin (2001)). There has been evidence that mechanical forces contribute to the regulation of cytoskeletal organization (Cleary & Hardham (1993); Wymer et al. (1996); Shi et al. (2011)). The increase of turgor pressure will induce wall stress and this will in turn affect the orientation of the cytoskeleton due to its attachment to the cell wall.

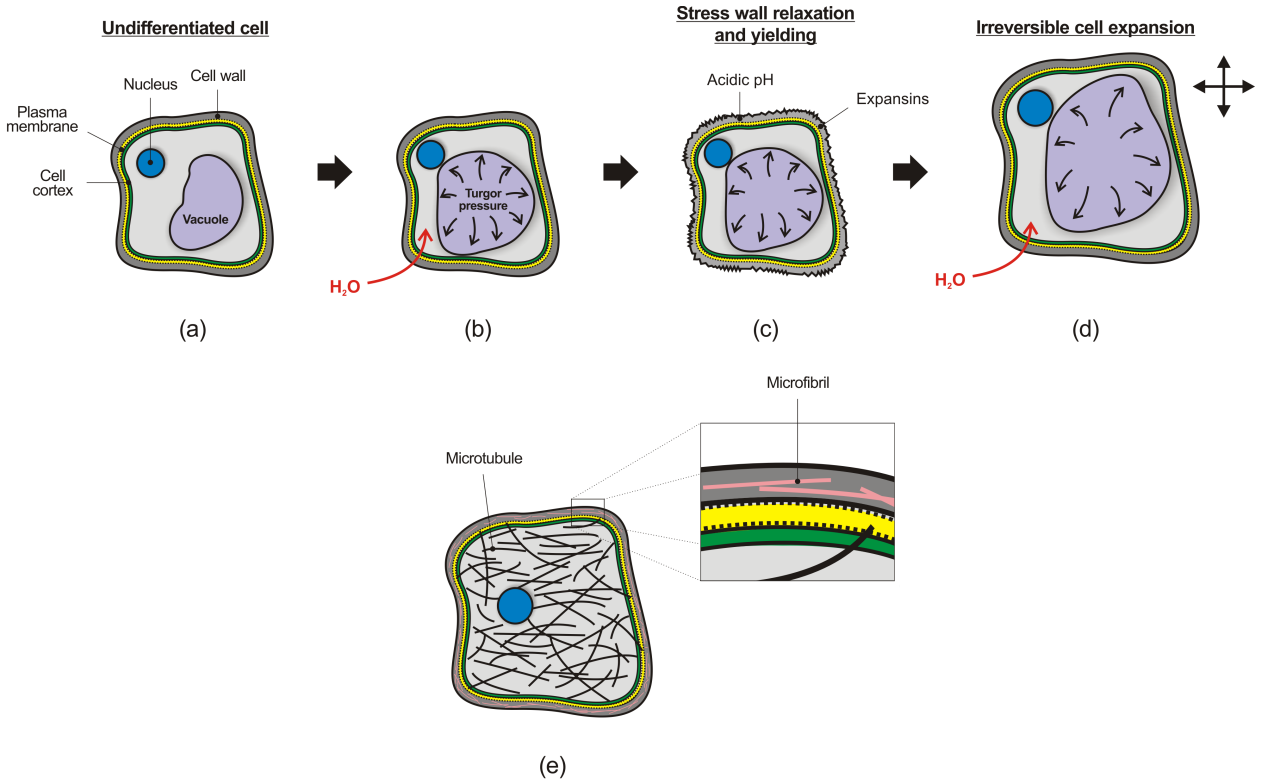

Figure 7: Generation of turgor pressure in plant cells and its effect on plant growth. (a) An undifferentiated cell (ground meristem) contains a nucleus (blue circle) and vacuole (light purple). Both organelles are enclosed the by cell cortex (green), the plasma membrane (yellow) and an outer layer, known as the cell wall (gray). (b) Water (H_2O) enters the cell via osmosis and accumulates in the vacuole placing pressure on the cell wall because of high turgor pressure. (c) The cell enlarges due to water uptake requiring the wall to loosen and release stress (stress relaxation) while still maintaining the same dimensions. With the help of expansins proteins, the cell wall is capable of adjusting to an acidic pH in order to extend and yield (irreversible stretching) much faster. (d) Due to equal and counterbalancing forces between the cell wall and cell turgor pressure, stress wall relaxation in consequence decreased the turgor pressure and water potential. More water is able to penetrate the cell and increase the volume, stretch the cell wall and restore cell wall stress. (e) In an isodiametric form, the microfibrils (in cell wall) as well as microtubules are randomly arranged. The orientation of these polymers are affected when the cell starts to elongate.